Master Thesis

ANALYSIS ON FACTORS AFFECTING THE DEMOLDING OF MICRO-STRUCTURED DEVICES IN THE INJECTION MOLDING PROCESS

by

Barbara Strohmayer

Montanuniversitaet Leoben
Department of Polymer Engineering and Science

Chair of Polymer Processing

Head: Prof. Dr. Clemens Holzer

May 2015 - printed: June 10, 2015

I declare in lieu of oath, that I wrote this thesis
and performed the associated research myself,
using only literature cited in this volume.

Ich erkläre an Eides statt,
dass ich diese Arbeit selbstständig verfasst,
andere als die angegebenen Quellen und Hilfsmittel nicht benutzt
und mich auch sonst keiner unerlaubten Hilfsmittel bedient habe.

June 10, 2015

Barbara Strohmayer

Kurzfassung

Mit der ständig steigenden Nachfrage nach patientennaher Labordiagnostik, steigen auch die Anforderungen an die Diagnostiksysteme und deren Herstellung. Bei der Massenproduktion solcher Systeme mit Spritzgießtechnologie ist der Entformungsprozess ausschlaggebend für die erfolgreiche Replikation, da während des Entformens die Gefahr der Verformung oder des Bruchs der Mikrostrukturen besonders hoch ist. Aus diesem Grund wurde ein Messsystem entwickelt, bei dem während des Produktionsprozesses die Entformungsenergie, die den Entformungsprozess quantitativ beschreibt, gemessen wird. Basierend auf einer Literaturstudie und entsprechenden theoretischen Überlegungen wurden vier Haupteinflussfaktoren auf den Entformungsprozess abgeleitet: Polymer, Maschinenparameter, Design der Mikrostrukturen und Werkzeugoberfläche. Jedem dieser Haupteinflussfaktoren wurden dann entsprechende Parameter zugeordnet und systematisch untersucht. Zusätzlich wurden Spritzgießsimulationen durchgeführt um den Einfluss der Schwindung auf die Entformungsenergie zu ermitteln.

Bei den Polymeren wurden ein semi-kristallines (PP) und zwei amorphe Materialien (COP und PMMA), sowie ein COC basiertes thermoplastisches Elastomer untersucht. Dabei wurde festgestellt, dass die Entformungsenergie zu einem größeren Teil von der Elastizität des Polymers als von der Schwindung abhängt. In Bezug auf die Maschinenparameter wurden die Werkzeugtemperatur und variotherme Prozessführung untersucht. Eine kritische Entformungstemperatur T_{dcr}, wie schon in anderen Arbeiten beobachtet, wurde für amorphe Polymere bestätigt. Zudem verringerte der Einsatz der variothermen Werkzeugheizung die Entformungskräfte um bis zu 50 %. Dieser Effekt wurde Relaxationsmechanismen aber auch einer Einschränkung des Messsystems zugeschrieben.

Für das Design der Mikrostrukturen wurde eine Platzierung nahe des Angusses und in Fließrichtung für vorteilhaft befunden, wobei der relativ geringe Einfluss des Designs wiederum auf den geringen Einfluss der Schwindung auf die Entformungsenergie hindeutet. Zudem mussten auch einige Defekte wie Bruch bei spröden Materialien sowie starke Deformationen (z.B. Durchbiegung) bei elastischen Materialien berücksichtigt werden. Eine TiN-Beschichtung, die einige Studien empfohlen hatten, wirkte sich im Vergleich zu Ni in einem eingeschränkten Temperaturbereich, vor allem aber bei höheren Werkzeugtemperaturen, vorteilhaft auf die Entformungsenergie aus. Trotzdem bleibt die Untersuchung der jeweiligen Polymer-Beschichtungs-Kombination notwendig. Alles in allem wurde die Entformungstemperatur aufgrund der starken Temperaturabhängigkeit der Eigenschaften von Kunststoffen als der größte Einflussfaktor auf die Entformungsenergie identifiziert.

Abstract

The increasing demand for disposable 'point-of-care' systems poses on-going challenges for health care industries to provide improvements in diagnosis and fabrication techniques. Regarding injection molding of thermoplastic polymers as one possible mass manufacturing process, the demolding stage is most critical for success, since the structures are prone to deformation or breakage during demolding. As a consequence, a concept for acquiring demolding energies in the fabrication process was developed to obtain a quantitative value that describes the demolding stage. Based on a literature study and theoretical considerations, regarding the demolding behavior of micro-structured devices in the injection molding process, the main influencing factors were grouped into four categories: polymer, machine parameters, micro-structure design and tool surface. Subsequently, a number of factors affecting the demolding energy were attributed to each of those categories and examined systematically. Additionally, injection molding simulations were conducted to analyze the impact of the shrinkage behavior on the demolding process.

In the category polymer a semi-crystalline material (PP), two amorphous materials (COP and PMMA) and a thermoplastic COC based elastomer were investigated. It was found that the demolding energies were rather determined by the elasticity of the polymer than the shrinkage. To investigate the machine parameters, the mold temperature and variothermal heating were analyzed. A critical demolding temperature T_{dcr}, which had been mentioned in other reports, was confirmed for amorphous polymers. When the variothermal heating was applied, the demolding energies were decreased by up to 50 %, which was most likely caused by relaxation mechanisms as well as limitations of the measurement system.

The investigation on the design of the micro-structures confirmed a favorable placement close to the gate and in flow direction. Still, the influence was very low, revealing a low impact of shrinkage on the demolding energy. However, a number of demolding effects had to be considered. These include part failure for rigid materials as well as strong deformation (eg. bending) of elastic materials during the demolding stage. In addition, since the efficiency of a TiN coating had been proven in other reports, it was found to lower demolding forces in a confined temperature range compared to the Ni surface. In general, TiN is advantageous at higher temperatures, although a thorough investigation for a specific polymer-coating-combination is necessary. Summing up, the demolding temperature was deduced to be the most important parameter affecting demolding energies, since polymer properties are strongly temperature dependent.

Acknowledgements

First and foremost, I offer my sincerest gratitude to my supervisor DI. Tobias Struklec, who supported me throughout my thesis with his encouragement and knowledge. He contributed considerably to the scientific quality whilst allowing me to work in my own way. He is the best AND friendliest supervisor one could wish for ;).

I am very grateful to Ass.Prof. Thomas Lucyshyn for his interest in my work. He provided valuable input, thoughtful remarks and offered guidance to improve my thesis. I would also like to thank Prof. Clemens Holzer for his efforts in reviewing my master thesis.

In my daily work I have been blessed with friendly and cheerful fellow students: Matthias Katschnig was a good advisor on the otherwise unsuccessful experiments on replication accuracy. Hannelore Mattausch and Bernd Haar kept me entertained during numerous coffee and lunch breaks. Michael Schmid and Bernhard Radler kept my spirits up while working on my experiments. I also thank all the staff of the Chair of Polymer Processing and the Chair of Injection Molding of Polymers for their willingness to help me in any situation.

Last but not least I would like to thank my family and friends, who have supported me throughout the entire process. Special thanks are due to my parents for supporting me throughout my studies at university.

Contents

Chapter 1

Introduction

Since global population is aging, ever more people need medical care. At the same time new markets evolve as health care systems improve in industrially developing countries such as India or China. Additionally, the demand for disposable 'point-of-care' applications for developing countries grows. This poses on-going challenges for health care systems and industries to provide improvements in diagnosis and treatments. To date microfluidic devices are already used in a multidisciplinary field intersecting engineering, physics, chemistry, medicine, pharmacy and biotechnology. Therefore, these factors will continue to drive research towards the development of innovative product design for even faster, safer and more compact analysis. To meet the requirements of modern diagnostics, future microfluidic devices will have to be applicable for high capacity diagnostics.

Since the introduction of 'lab-on-a-chip' devices in the early 1990s, glass has dominantly been used for their fabrication [30, 44]. The reason, among others, for the primary use of glass were well established processing and surface modification methods by the semiconductor industry. Furthermore, surface properties and derivatization methods were well characterized by the chromatography industry. Silicone based products display good surface quality but are poorly suited for low-cost mass production. As a consequence to the blossom of lab-on-a-chip devices in many areas the cost of producing microfluidic systems in glass caused commercial producers to seek other materials.

In contrast, polymers offer several advantages to substitute glass chips. A prominent example of successful replication in the field of micro-feature fabrication are compact discs (CD) and digital versatile discs (DVD), which are fabricated on industrial scale. As for CDs and DVDs the relatively expensive step of micro-fabrication is done once on a stamper, which can be replicated at low-cost. Thus, integrated microfluidic devices on mass-production

scale can be obtained. Since design complexity affects mold design only, the impact of the complexity of the design on overall costs is relatively low. Moreover, plastic materials offer the benefit of a wide range of characteristic material properties to meet the demand of a specific application. For mass-market application plastic devices can be used as disposables to avoid cross-contamination, maintenance costs and recalibration. On the other hand however, polymers have some disadvantages in comparison to glass, which are related to their temperature dependent properties and processing techniques.

Molding of thermoplastic polymers proved great potential for producing low-cost disposable microfluidic devices. Among different fabrication techniques, injection molding seems to be the most promising process. Hot embossing offers some advantages in comparison to injection molding such as relatively low cost for embossing tools, simple operation and low residual stresses. As the temperature variation range is smaller, reduced shrinkage during cooling results in lower friction forces that act on the micro-features. However, a constraint in the feasibility of hot embossing is the cycle time, which exceeds injection molding by approximately 10 times. Considering the low maintenance costs and large 'know-how' available from conventional injection molding as well as accurate shape replication and good dimensional control, injection molding leaves other techniques such as hot embossing or nanoimprint lithography behind. Furthermore, as indicated above, injection molding yields the shortest cycle time of all the fabrication methods mentioned so far.

Products manufactured by micro-injection molding are classified into two categories with regard to the part dimensions: One is the case, when part dimensions are lower than 1 mm. The other is the case, when overall part dimensions exceed 1 mm, but micro-sized structures are incorporated on the surface with sizes typically smaller than 200 µm. For both fields of application polymers contribute excellent replication fidelity if optimal processing conditions are applied. Small features can be completely filled and accurately replicated down to tens of nanometers if low viscosity during the filling stage was ensured.

With respect to accuracy the applicability of polymethyl methacrylate (PMMA) was analyzed, due to its importance in the so-called 'life-sciences' and its compatibility with cell culturing and cell growth. However, the replication accuracy of the micro-structures is a crucial constraint for the application of PMMA, which has not been solved so far. As a consequence, several processing parameters were investigated to obtain optimal feature accuracy, which was determined by AFM characterization.

Regardless of the replication quality, without successful demolding the structures will be ripped or sheared off and the technique fails. Once the

maximum stress during demolding exceeds the strength of the micro-features, breakage may occur. Therefore, demolding plays a key role for polymer replica and also the life time of the mold insert. Although injection molding has been used for several years to fabricate microfluidic devices, a comprehensive study on demolding is still lacking. Nevertheless, it is the demolding step that ultimately determines the part quality as most structural damages occur during this step. So far the micro-scale polymer processing technology remains in a trial and error stage in many areas.

To facilitate the investigation of the main factors affecting demolding force, they were grouped in 4 categories, which determine demolding force: polymer type and properties, processing parameters, micro-structure design and tool surface. The aim of this Master Thesis is to set up a general approach to reduce demolding force with respect to these factors, and thus the risk of feature damage. This requires in-depth understanding of thermal and deformation behavior of molded parts regarding general design recommendations as well as standardized methodology to test material properties in respect of applicability for microfluidic geometries and the optimal processing parameters. Furthermore, the interaction and interdependence among processing parameters, material properties and part geometry were investigated. A systematic study allowed for the determination of the parameters, that led to low stress and deformation in the polymer, thereby achieving successful demolding.

As the mold surface quality and anti-stiction coatings had been covered in literature, focus was put onto micro-structure design, the impact of the polymer and the processing parameters. Several works have been published on the performance of different polymers in injection molding of micro-structured devices. Unfortunately, the data was obtained from different processing conditions with different machines, materials and feature designs, since different work groups pursued different goals. Therefore, it is desirable to set a standard method to compare materials objectively for injection molding of these devices. Hence, thermoplastic polymeric materials, which include amorphous and semi-crystalline thermoplastics as well as thermoplastic elastomers, were investigated. In addition, the effect of feature design, feature placement and processing conditions on the demolding force were analyzed for 'isothermal' and variothermal processing conditions. To better understand the thermal expansion and contraction injection molding simulation was used to find a correlation between the shrinkage and the actual demolding force in the injection molding process.

Chapter 2

Applications

Modern microfluidic devices such as lab-on-a-chip applications or so-called miniaturized total analysis systems (µTAS) were first reported by Manz et al. in 1990 [43]. Starting from this, analysis and diagnostics have blossomed and branched off into several fields, which include biological and chemical analysis, point-of-care testing, clinical and forensic analysis and molecular and medical diagnostics [14]. Any of these integrated microfluidic devices incorporates many components and thereby combines the functionality of a typically room-sized laboratory on a small chip. Initially, the analytical improvements associated with the down-scaling were assumed to be the main advantage, but further research revealed more advantages, which include minimized consumption of reagents and increased automation in diagnostics [43, 44]. Moreover, with increasing demand and the concurrent change from silicon to polymeric materials as substrate, fabrication costs of microfluidic devices decreased considerably.

2.1 Theory

To understand the trend towards down-scaling in diagnostics, it is important to look at the behavior of physical parameters of a system being scaled down in size. Manz et al. (1990) analyzed these scaling-laws, which are based on the assumption that for a miniaturized system the transport phenomena are controlled by diffusion [43]. Subsequently, the flow regime in such a fluidic system is strictly laminar [20]. The transport phenomena cover the transport of individual molecules on the one hand and the transport of heat on the other hand. Thereby, the behavior of molecules in a static reaction vessel (e.g. a nanowell plate) is well explained. Fick's law describes the diffusion as can be seen in Equation 2.1 [4]:

$$\dot{n} = D \triangle n \tag{2.1}$$

Where:

n :	particle density or concentration.
D:	diffusion coefficient.
$\triangle$:	Laplace operator.

If Fick's Law is rewritten in terms of diffusion time t_D (Equation 2.2), it describes the time a molecule needs to travel the distance l by diffusive processes. In the case of heat diffusion it describes the time needed for a thermal gradient to equalize:

$$t_D = D^{-1} l^2 \tag{2.2}$$

Where:

t_D:	diffusion time.
D:	diffusion coefficient.
l :	distance in diffusive process.

Equation 2.2 implies, that the biggest advantage of downscaling lies in the quadratic decrease of equilibration time that accompanies the decrease of the linear dimensions of a system. Thus, typical time frames are reduced from hours to seconds. Recently, a trend towards high aspect ratios, which is the ratio of the height/length to the width of the micro structure [58], in these 'life-science' applications can be seen (compare Figure 2.1). Some reasons are:

- A higher active surface area per unit can be achieved, which is particularly important for chemical or biochemical applications like micro-reactors, micro-mixers, chromatographic columns or DNA concentrators.
- An increase in flow rate due to higher cross-sections per unit of the device area can be achieved.
- The packing density of micro-structural elements can be increased to parallelize MEMS (micro-electromechanical system) functions, eg. in DNA separation or nanowell-plates.

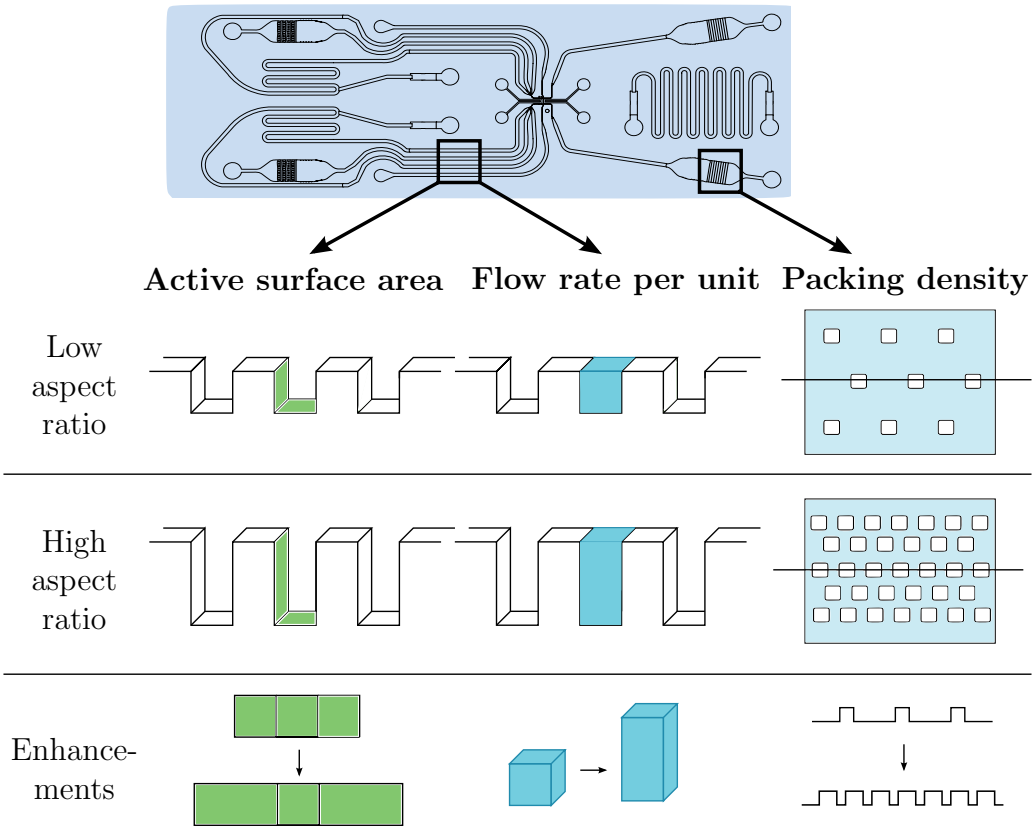

Figure 2.1. Increase of active surface area, flow rates per unit and packing density due to higher aspect ratios.

2.2 Example devices

Due to the rapid development resulting from down-scaling, microfluidic and nanofluidic devices gain importance in modern 'life-sciences'. Special types are applied in µTAS or in miniaturized drug delivery systems. Most of these miniaturized analysis systems are additionally equiped with passive components such as capillary micro-channel structures. Mostly they work as inlet or supply channels or as reaction or separation section. They may also contain integrated micro-components, which take over mixing or filter functions. In conventional micro-titer plates simple micro-depressions act as reservoir areas, the so-called wells. Thereby, precise sample transfer into and from the system can be achieved [26]. More complex µTAS include elements like small pumps or valves. In general, DNA analysis has produced the most highly integrated chips, as a consequence to the huge potential market [14]. To enhance the understanding of microfluidic technology, several polymer-based

devices were grouped by their specific application areas and listed below:

Flow cells: Geometrically simple micro-channel configurations of the order of 100 µm with networks or manifolds are successfully utilized in microfluidics. They can be used to extract a component with a high diffusion coefficient from a sample stream or to measure a sample concentration solely by using the diffusion properties of the substances involved. This concept is applied in a diffusion-based immunoassay, for example. Moreover, the different diffusion coefficients between smaller antibodies and larger antigens are utilized to create a color change of an indicator, that can be detected optically. Less complicated micro-channel networks, which encapsulate other functional elements such as DNA-arrays, fulfill simple tasks like metering, dosing or distribution [4, 29, 70].

Capillary electrophoresis (CE): One of the major applications of microfluidics technology is based on seperation by electro-kinetic processes. By means of CE, substance mixtures such as biomolecules (DNA, proteins, etc.) or inorganic ions can be seperated and split up into their components by applying a high voltage [4, 26, 41, 52].

Miniaturized polymerase chain reaction (PCR): PCR is commonly used in biotechnology for the amplification of specific DNA fragments and thereby constitutes a key stage in a complete DNA analysis. As the PCR process involves elevated temperatures (up to 95 °C), only polycarbonate (PC) and cyclic olefine copolymer (COC) can be utilized, due to their thermal stability [4, 72].

Clinical chemistry and diagnostics: Polymer devices are particularly suited for diagnostics since disposables avoid contamination. On commercial basis portable 'lab-on-a-chip' systems for blood diagnostics are produced. These include functions such as sample absorption, separation, mixing with reagent, analysis and waste absorption [4, 29, 52].

Cell handling: For biological applications the handling of (living) cells is of great interest. For example cell counting, flow cytometry or even manipulation is performed on these devices. With respect to handling of living cells, recent research proved the superior properties of PMMA for this application [1, 49, 55, 65].

Micro-reactors and containers: In contrast to the devices and applications described so far, many reactions can take place in a static environment in miniaturized reaction vessels. There is a number of micro-reactors which form an integral component of microfluidic applications. An example for these devices is the open micro-titer plate [4].

Chapter 3

State of the Art

Demolding is the process to overcome all levels of interaction between mold and polymer, which are formed by the process history and the properties of the materials involved. The forces observed during demolding involve physical (adhesion) and mechanical interaction (residual stress). Hence, it is necessary to obtain detailed information on the demolding process, since these forces are the main cause of defects resulting from the fabrication process. The following sections will summarize the theoretical background on surface adhesion and demolding forces. In addition, recent works on replication accuracy and demolding forces of micro-structured devices will be reviewed.

3.1 Replication accuracy

The replication quality of micro-features is a factor determining the reliability of the fabrication process of micro-structured devices. It depends on the size, aspect ratio and overall geometry of the part [61]. Hence, the replication quality is an important feasibility issue which is determined by the machine, the process and the material. As for conventional injection molding Greener et al. (2006) reported the dimensional integrity of molded parts to be determined by three main factors [21]:

- The thermal history of the polymer within the mold cavity,
- the ejection process and
- the cooling to room temperature after ejection.

The aspect ratio mainly determines the critical minimal dimensions, that can be replicated in good shape by injection molding. Special features of

'classic' micro-injection molding like evacuation and the variotherm mold heating, enable the fabrication of polymeric micro-structures with aspect ratios up to 20 [60]. High aspect-ratio patterns are favorable, since they improve sensitivity and increase detection limits of device components. However, as designs for injection molded micro-structures grow geometrically more complicated, the imprinted features may lose their accuracy. As a consequence, challenges in injection molding of micro-structured devices arise. These have to be addressed regarding process feasibility, since high surface-to-volume ratios (due to high aspect ratios) and feature complexity induce solidification of the polymer melt much faster than in conventional injection molding.

As anticipated intuitively structures with high aspect ratios are more difficult to replicate than wide ones. In accordance to this, Theilade and Hansen (2007) reported a linear correlation between feature width and replication quality [66]. Mönkkönen et al. (2002) investigated the effect of the angle between the sub-micron structure and the flow direction to influence the replication quality [50]. They concluded, that poor replication quality due to features arranged perpendicularly to the flow direction could be improved by an increase in melt temperature.

Subsequently, Lee et al. (2010) studied the injection molding process on a micro-rib pattern by simulation and verified their results experimentally [42]. The micro-rib patterns farther away from the gate were filled better in comparison to the ones near to the gate. This complicated flow pattern may be explained by the so-called 'hesitation' effect. This phenomenon describes the primary filling of the major part of the product, the so-called ground plate, whereas the structures at the surface are filled afterwards.

Figure 3.1 illustrates such a flow pattern, that is dominated by the 'hesitation' effect. The polymer melt fills the ground plate and at the same time gradually starts filling the micro-ribs. As the cross-section of the ribs is relatively small compared to the ground plate, the filling of the ribs slows down due to the rapid cooling of the material. When the ground plate is filled completely, the melt far from the gate is still hot enough to fill the unfilled portion at the flow path-end. Hence, replication was found to be better at the end of the flow path.

Since the process parameters are of significant importance for replication capability and accuracy they have been studied extensively in many works [40, 50, 61]. The main factors mentioned in these reports are melt and mold temperature, injection velocity and packing pressure because of their direct impact on the melt flow properties. Experimental observations proved, that the viscosity of polymer melt and the pressure in the cavity affect the replication accuracy. For that purpose, Chien (2006) investigated the effects of mold temperature, melt temperature, injection velocity and

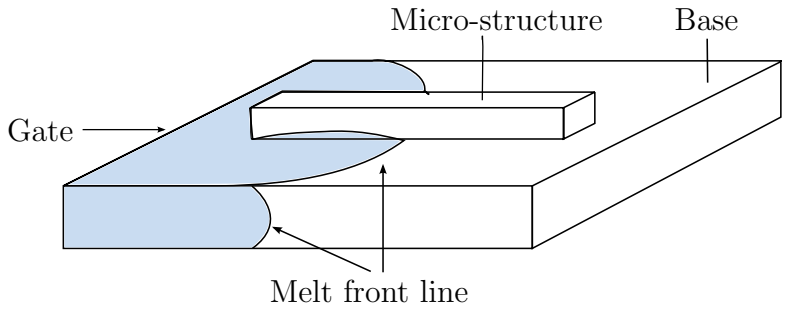

Figure 3.1. Typical filling pattern of a micro-rib [42].

packing pressure on the replication accuracy of PMMA for injection molding of micro-structured parts [10]. He found that higher melt temperature improves the melt flow to fill the micro-channels and high injection velocity assists the melt in doing so, thus increasing accuracy. The width of the replicated micro-channels decreases and the depth increases with increasing melt and mold temperature. Thus, the higher melt and mold temperatures are, the closer the widths and depths come to the true dimension.

In fact, Yoon et al. (2010) identified the mold temperature to be the most influential parameter for good replication [73]. In addition, an increase in holding pressure reduced the subsequent shrinkage during cooling. An increase in injection velocity leads to better replication accuracy for two reasons: First, higher injection velocity decreases melt viscosity by viscous heating. Secondly, the melt-mold contact time is reduced and thereby the temperature drop during filling is lowered.

However, discrepancies appeared with respect to the most influential factors and the magnitude of their influence. Sha et al. (2007) concluded, that this discrepancy could be explained by different test settings, such as different polymers and test structures [61]. In accordance to the conclusions drawn from a literature review, they conducted a systematical study to ascertain the combined effects of the most important factors. They identified the size of the micro-features and their position relative to the gate as most influential, whereas the accuracy proved to be insensitive to the distance between the features. In general high settings within the usual processing ranges are considered a good strategy for producing accurate parts. However, there are some limitations with regard to mold temperatures such as poor surface quality and inferior edge definition of micro-features [61].

This is in accordance with Chen et al. (2010), who investigated the influence of the polymeric material (cyclic olefine copolymer (COC), polycarbonate (PC), polymethyl methacrylate (PMMA) and polystyrene (PS)) on the

replication accuracy [7]. Due to intermolecular forces polymer devices tend to develop a flat surface, which leads to larger width and smaller depth of the micro-channel compared to those of the stamper. The comparison of replication accuracy of micro-channels for COC, PC, PMMA and PS identified COC as the best material, due to its good flowability and low shrinkage during demolding. Also, PS exhibited acceptable replication accuracy whereas PC and PMMA showed the worst results. In addition, Sha et al. (2007) found that process parameter adaptation exhibited a major impact on accuracy on POM, but not on PP and ABS, which were also studied in their work [61].

Another issue when considering replication quality is flatness and thickness distribution to ensure the device functionality. There are a number of techniques available for sealing of the device to provide an enclosed microfluidic path. Bonding techniques such as adhesive bonding, thermal fusion bonding, solvent bonding or ultrasonic welding may be applied [68]. Marson et al. (2011) investigated the flatness optimization of a PMMA microfluidic component. The cooling time was identified as the only statistically significant parameter affecting the part flatness, as plastic deformation decreases with increased cooling time, due to the increase in relaxation time [45].

3.2 Theoretical analysis of demolding

In injection molding, demolding describes the stage, when the part is ejected from the mold. This happens after the polymer cools down and thus solidifies. When analyzing the demolding behavior of an injection molded microstructured device several aspects have to be considered. These include the demolding of a single micro-structure as well as effects which occur from demolding of an array. These demolding phenomena result from the surface interaction between the polymer and the stamper. Consequently, they cause stress and deformation of the part.

3.2.1 Demolding a single micro-structure

There are two main aspects, which influence the demolding force of a single micro-structure: On the one hand, the polymer follows its pvT-curve regarding the changes of specific volume due to the variation of pressure and temperature during the molding cycle. During the cooling phase volumetric expansion due to cavity pressure decrement and volumetric contraction due to cooling can occur. First of all, the molded part follows the pvT-curve of the polymer, which means that the part contracts due to the temperature de-

crease. On the other hand, the specific volume increases due to the pressure drop at the end of the processing cycle [15, 18].

Figure 3.2 illustrates the influence of the demolding temperature (T_d) and the holding pressure on the diameter of the micro-structure (d_d). At one point a balance between expansion and contraction is struck, which means that the size of the part equals the mold cavity. This is described by the critical demolding temperature (T_{dcr}). At temperatures below T_{dcr} the diameter of the micro-structure is smaller than that of the micro-cavity. Whereas at temperatures higher than T_{dcr} its diameter would theoretically exceed the diameter of the micro-cavity, if it was not constrained by it.

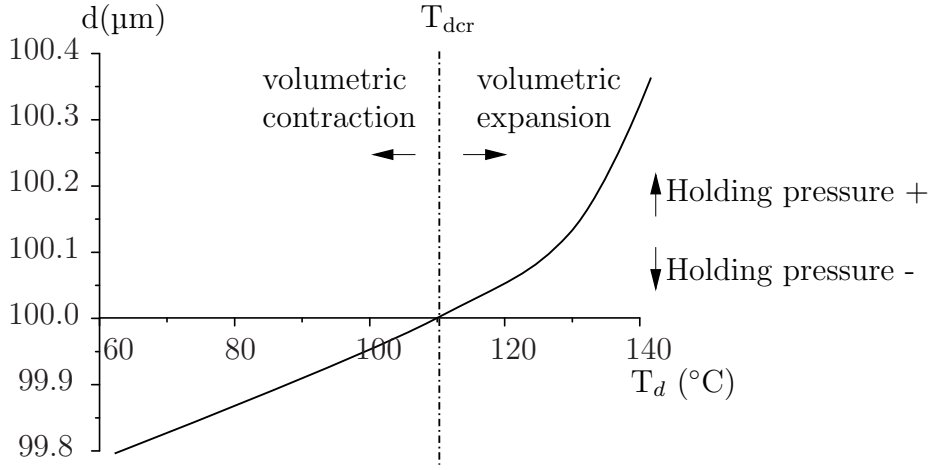

Figure 3.2. Diameter (d_d) of the micro-structure at the demolding temperature T_d [18].

To separate the polymer from the mold the friction and adhesion between the surface of the micro-cavity and the molded micro-structure have to be overcome. Thus, a specific demolding force is required. Consequently, the demolding force of a single micro-structure is influenced by several factors, such as dimensions of the micro-structure, aspect ratio, demolding temperature and holding pressure [15]. This is illustrated in Figure 3.3, where the total release force (F_D) to eject a single feature is depicted. This correlation is also shown in Equation 3.1 [15].

At the onset of demolding, before the part starts to move, the coefficient of friction (μ_{static}) determines the force needed to initiate movement. It is the adhesive coefficient that is characteristic for the interface between the mold and the polymer. μ_{static} is determined by surface roughness, interface temperature as well as processing parameters [46, 57]. Subsequently, when the part starts to move, from the onset of demolding until ejection the sliding

coefficient μ_{slide} applies. In the latter case, the demolding speed and the time at which the demolding force is calculated influence the total outcome of the demolding force.

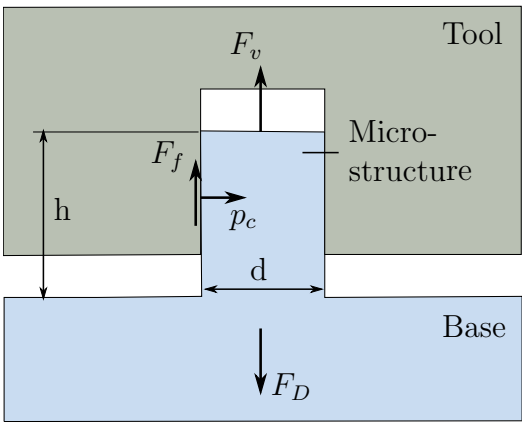

Figure 3.3. Model of forces acting when demolding a single micro-structure [15].

$$F_D = F_f + F_v = \mu \cdot A_c \cdot p_c + S \cdot p_v, \tag{3.1}$$

Where:

F_D:	total release force.
F_f:	release force required for ejection.
F_v:	additional release force due to the vacuum effect.
μ_{static}:	static coefficient of friction between the micro-structure and the tool surface.
μ_{slide}:	sliding coefficient of friction between the micro-structure and the tool surface.
p_c:	contact pressure.
A_c:	area of contact.
p_v:	negative pressure, due to evacuation of the micro-cavity before injection.
S:	cross-sectional area of the micro-cavity.

3.2.2 Demolding an array

When demolding an array of micro-structures, the shrinkage of the ground-plate or base during cooling, but before demolding, has to be considered. According to the specific volume based on pvT-properties and molding conditions, the ground plate shrinks towards its center line. As a consequence

the micro-features also move towards the center line of the molded part as is illustrated in Figure 3.4. Since the movement is hindered by the micro-cavity, the transition area from the micro-structure to the base experiences thermally induced stress, which will be discussed in detail in Section 3.2.4.

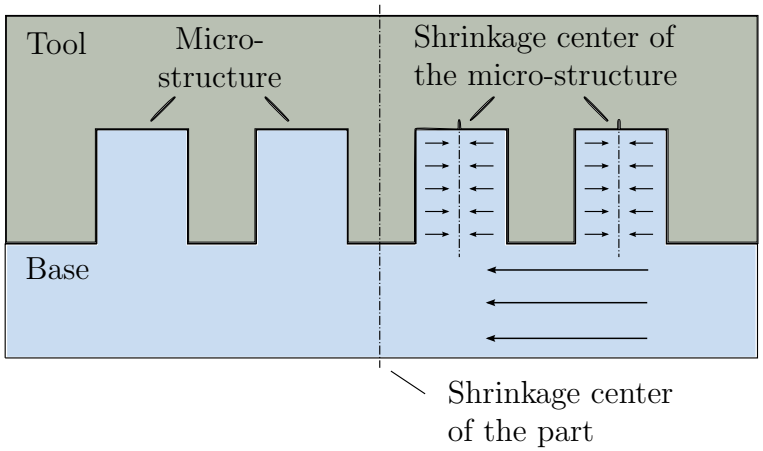

Figure 3.4. Shrinking behavior of molded part and micro-structures [15].

Fu et al. (2008) analyzed the demolding behavior of a 24 x 24 array in metal micro-injection molding [18]. For their report on the demolding forces they chose some representative micro-structures to reflect the demolding behavior of their array. By comparing different packing pressures and different demolding temperatures, they investigated the influence of the contraction and expansion behavior of the feedstock. Their theoretical and experimental analysis showed the so-called critical demolding temperature (T_{dcr}), where the volume of the part equals the mold cavity. At this temperature, which is packing pressure dependent, a balance between contraction and expansion is struck, as is depicted in Figure 3.5.

Below T_{dcr} the specific volume of the part decreases due to thermally induced shrinkage. Hence, the part contracts towards its centerline. This movement is hindered by the mold-cavity, which exhibits a lower thermal expansion coefficient in comparison to the part. As the part volume declines the demolding force increases since the contraction causes larger contact pressure between the micro-structure and the mold cavity. On the other hand above T_{dcr} the specific volume grows due to the pressure decrement. As the part becomes blocked into the mold cavity, the demolding forces increase as well. Nevertheless, it has to be noted, that demolding forces due to volumetric expansion remain significantly below those due to volumetric contraction. Thus, demolding temperatures at T_{dcr} or slightly above are most favorable to obtain minimum demolding stress.

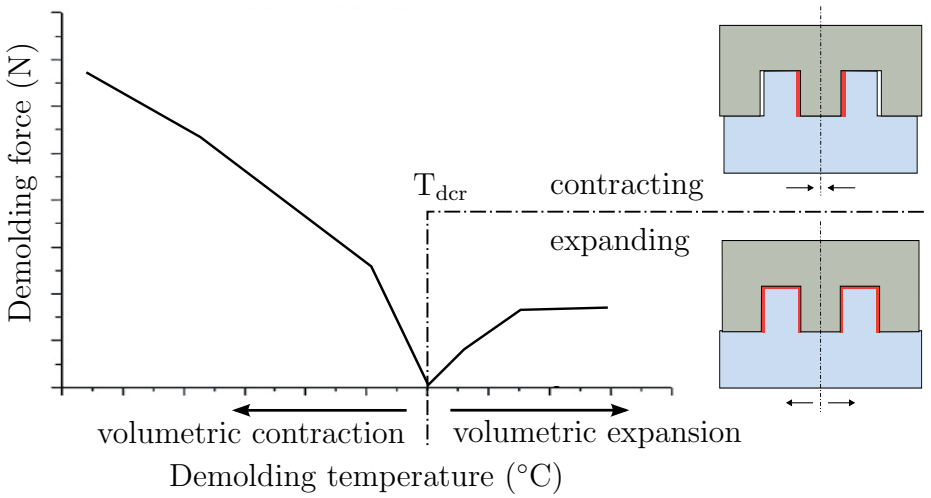

Figure 3.5. Demolding force at different demolding temperatures for an array of 576 micro-structures [18].

3.2.3 Surface interaction

There are two main causes for demolding forces: the friction force at the side walls, which is caused by surface adhesion and thermal stresses due to shrinkage, and the adhesive force at the top and the sidewalls of the cavity (see Figure 3.6). Considering the whole contact area, surface adhesion cannot be ignored. In this context van der Waals and electrostatic forces are the main factors causing stiction between two adjacent surfaces [39].

Friction is encountered when two surfaces are in contrary motion while in contact. They endure a resistance that results in a shearing force. This kind of shearing force F_f is called friction force and defined in accordance to Equation 3.2. By lowering the coefficient of friction or the adhesive force the friction force can consequently be reduced.

$$F_f = \mu \cdot F_n, \tag{3.2}$$

Where:

F_f:	friction-force acting along the contact surface.
μ_{static}:	static coefficient of friction.
μ_{slide}:	sliding coefficient of friction.
F_n:	normal force on the contact surfaces.

The adhesive force is determined by an empirical formula according to Equation 3.3 [56]. For that formula, the work of adhesion is specified in

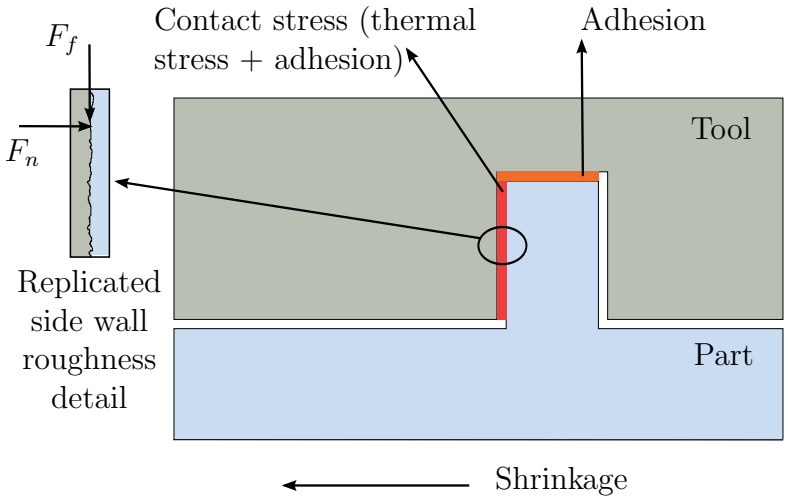

Figure 3.6. Main forces determining demolding force in micro-molding [28].

Equation 3.4 [56] and the composition Young's modulus is given in Equation 3.5 [56]. It is apparent that the frictional force will decrease with a decrease in γ, thus a material with lower surface energy is favorable. Also, the demolding force correlates with the Young's modulus of the two materials. From Equation 3.5 it is obvious, that a decrease in the Young's modulus lowers K. As a consequence F_n and thereby F_f will decrease.

$$F_n = (\frac{3}{2}\pi\gamma K R^3)^{\frac{1}{2}}, \tag{3.3}$$

Where:

F_n: normal force on the contact surfaces.
γ: work of adhesion (compare 3.4).
K: composition Young's modulus (compare 3.5).
R: effective radius of interface.

In Equation 3.3 R is the radius of the contact circle, which results from the surface contact. In practice, the roughness apexes of two solid materials are simplified to the contact between a sphere and a plane [27]. Hence, R indicates the radius of a polymer apex which is in contact with the plane (mold cavity).

$$\gamma = \gamma_1 + \gamma_2 - \gamma_{12}, \tag{3.4}$$

Where:

γ_1: surface energy of the polymer.
γ_2: surface energy of the mold.
γ_{12}: interface energy of contact surfaces.

$$\frac{1}{K} = 0.75 \cdot \left[\frac{(1 - {\nu_1}^2)}{E_1} + \frac{(1 - {\nu_2}^2)}{E_2} \right], \tag{3.5}$$

Where:
E_1: Young's modulus of the polymer.
E_2: Young's modulus of the mold.
ν_1: Poisson's ratio of polymer.
ν_2: Poisson's ratio of mold.

3.2.4 Stress and deformation

During demolding the polymer part and the stamper both experience friction and adhesion forces, which result in locally concentrated stress as the demolding proceeds. Considering the high Young's modulus of the stamp structures, deformation occurs in the polymer only. Structural damages occur depending on the maximal local stress with respect to the yield stress of the polymer [62]. The stress distribution during cooling and demolding was studied in several works. Most results were obtained from a theoretical approach, but were verified experimentally.

Fu et al. (2006) investigated the stress and deformation of an array of 24 x 24 micro-pillars [15]. They conducted finite element analyses (FEM) in the field of metal micro-injection molding [15]. In their analysis they calculated the stress distribution during cooling and demolding for the array. Figure 3.7 displays a cross-sectional plane of 12 micro-structures along the diagonal starting from the center to the features farthest from the centerline [18]. Due to the complex three-dimensional stress distribution equivalent von Mises stress was used, which gives an overall estimation of the magnitude of the stress components of the tensor.

Accordingly, they reported that the structures were prone to failure at the onset of demolding, when the maximum stress was observed (see Figure 3.7 b). At this point the thermally induced stress due to the cooling of the part and the shear stress due to friction between the polymer and the micro-cavity added up. Moreover, the structure farthest from the shrinking center displayed the maximum stress level. The arrows indicate the area of the maximum stress for each micro-structure, which occurs at the transition zone to the base. This is in accordance with the theoretical considerations

regarding the shrinking behavior of the ground plate, as discussed in Section 3.2.2.

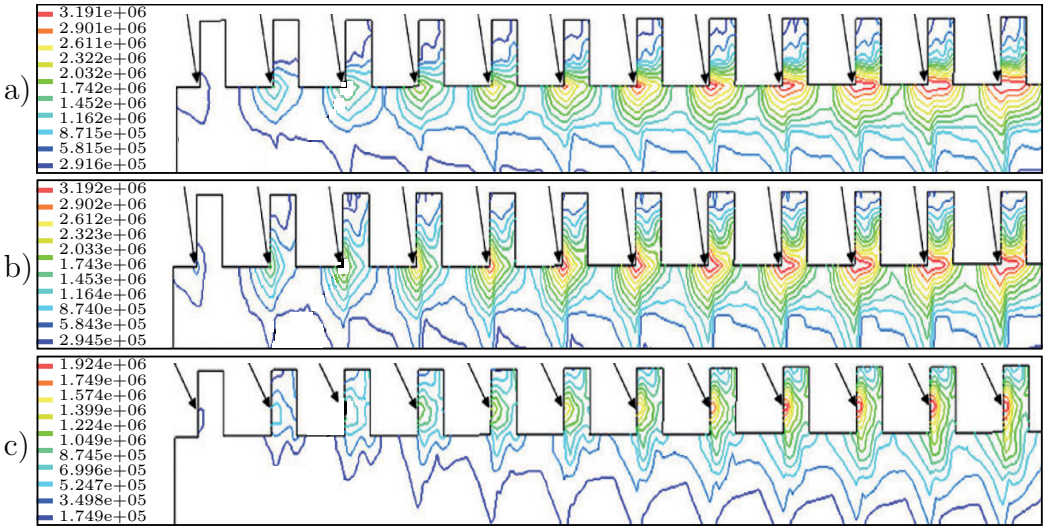

Figure 3.7. Equivalent von Mises stress (MPa) distribution of a PIM feedstock at temperatures below T_{dcr}. a) just before demolding, b) at the onset of demolding, c) at displacement 80 µm [18].

Song et al. (2008) analyzed the demolding stress (von Mises stress) in thermal imprint lithography for PMMA and a Si stamp via FEM simulations [62]. They concluded that the stress concentrates at two locations in the part. The first location was found to be the transition zone between the micro-structure and the ground layer, which is in accordance with Fu et al. (2006) [18]. The second stress concentration was observed near the contact point with the moving stamp edge [62]. This was attributed to the thermal stress generated during cooling, since PMMA will not relax immediately, but follows multi-relaxation mechanisms, each dependent on a relaxation time on its own. As a consequence the residual stress between the edge of the stamp and the polymer remains high throughout the entire demolding process. Figure 3.7 c) displays this change in the location of the maximum stress, with reference to the progression in demolding.

Figure 3.8 shows a more detailed 3D plot of the von Mises stress along the vertical PMMA feature as a function of demolding time. At the onset of demolding the local stress concentration along the vertical sidewall of the micro-structure increases rapidly (first maximum stress) and in this case thereby exceeds the yield stress of PMMA at 70 °C. Afterwards it decays rapidly and is kept at a constant level until the end of the demolding process is reached. Then the second maximum stress occurs, just before the demolding

is completed. It appears due to the strong geometrical confinement against the relaxation of PMMA. The stress along path '1', which equals the contact point with the moving stamp edge in Figure 3.8 is slightly higher than the average stress within the feature.

Due to the highest local stress at the beginning of demolding, local deformation is expected to occur at this point. However, care must be taken with respect to the prediction of failure, as the high stress is confined to a small area. Nevertheless, the results indicate, that the higher the aspect-ratio (or the smaller the width of the structure) becomes, the higher the relative contribution of the zones with stress concentration to the polymer is.

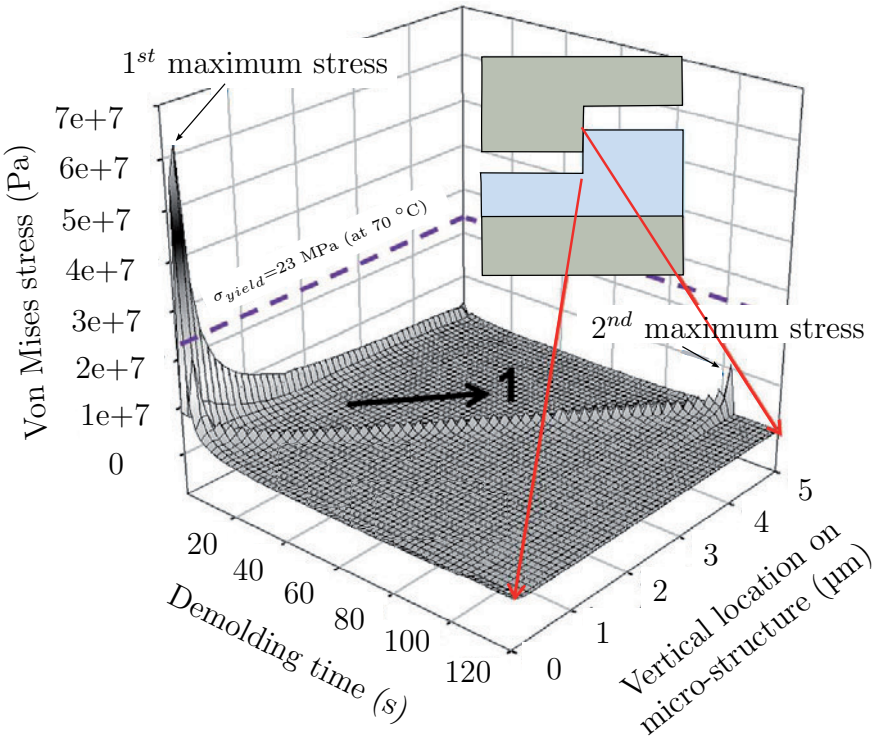

Figure 3.8. Von Mises stress evolution as a function of demolding time at the vertical sidewall of a PMMA single structure [62].

As explained earlier, the polymer expands at temperatures higher than T_{dcr}. Hence, a contact pressure establishes between the micro-structures and the micro-cavity, but also between the base and the surrounding mold cavity wall. Since the ground plate is constrained in radial direction the part can only move along the demolding direction. The resulting stress distribution is shown in Figure 3.9 [18]. Each feature displays the same stress distribution during demolding, since the assumption of isotropic expansion applies.

At the edge of the micro-cavity entrance the maximum shear stress, due to the maximum contact area, and the maximum compressive stress, due to the expanding tendency, occur. As with temperatures below T_{dcr} the von Mises stress decreases with the progression of the ejection as well. Additionally, above T_{dcr} the gradient of the demolding force curve decreases with increasing demolding temperature [18].

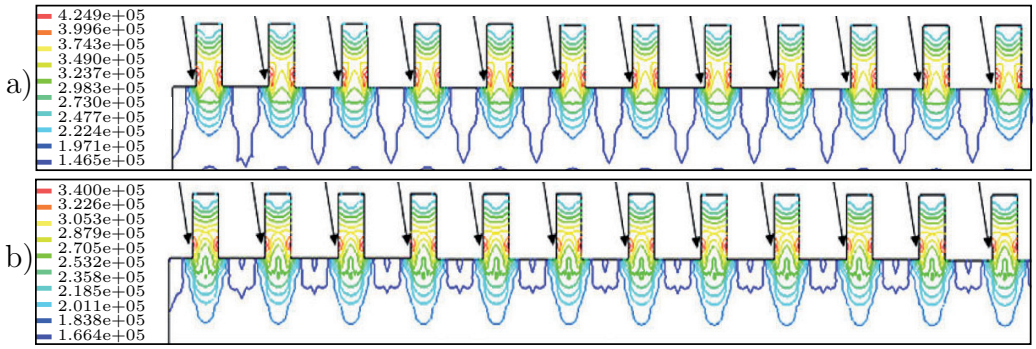

Figure 3.9. Equivalent Mises stress (MPa) distribution of a PIM feedstock at temperatures above T_{dcr}. a) at the onset of demolding, b) displacement 40 µm [18].

3.3 Main factors influencing demolding force

There are several factors determining the demolding force of injection molded micro-structured devices. The smaller the feature sizes are, the more problematic demolding becomes due to attracting surface forces and friction between the side walls. As size decreases and aspect-ratios increase the identification of the main influencing factors on demolding force becomes more and more important. Otherwise demolding defects, which form due to adhesion, intensive shearing or a combination of both effects, will occur.

Figure 3.10 shows the impact of adhesion and shearing on two simple micro-structures. Figure 3.10a displays defects due to adhesion of a single micro-structure at the top of the micro-structures, whereas Figure 3.10b displays damage due to shear forces resulting from contact stress. To prevent identify the main causes of such demolding defects the main influencing factors on the demolding process were grouped into four categories, which will be discussed in the following:

- Polymer
- Machine parameters

- Micro-structure design
- Tool surface

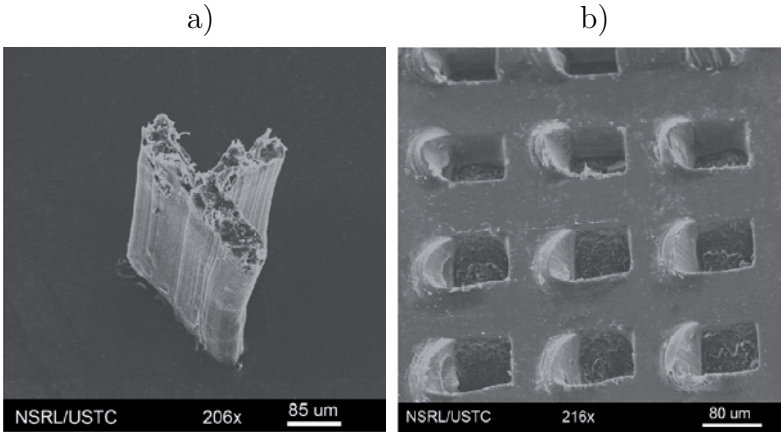

Figure 3.10. Typical defects of polymer micro-structures: a) surface adhesion at the top of the microstructures; b) defects due to shear forces resulting from contact stress [28].

3.3.1 Polymer

Material selection is one of the most challenging tasks in process design for parts with micro-features. Several aspects, which include costs, achievable part tolerance and material property requirements, must be taken into account. Furthermore, with respect to demolding the tendency to shrinkage and warpage should be considered. High mechanical strength is also desirable in order to resist mechanical stresses acting during the demolding process.

Guo et al. (2007) identified the friction force, which is caused by interface adhesion and thermal stresses due to shrinkage between the polymer and the mold, as the main factor affecting demolding forces in metal-micro injection molding [27]. Their analysis also showed, that friction contributed more severely to deformation than thermal stresses. Thus, it would be beneficial to use materials with low thermally induced shrinkage, to minimize contact forces.

Apart from the analysis of the demolding forces in metal micro-injection molding [15, 16, 17, 18], the effect of several polymer materials on demolding force has been investigated experimentally and by simulation. Nevertheless, to date these reports are limited (compare Table 3.1) compared to the wide range of materials, like ABS, COC, PC, PMMA, POM and PS, that have

Table 3.1. Polymeric materials investigated regarding demolding force: an overview.

Class	Polymer	Work
Amorphous	PMMA	Song et al. (2008) [62]; Guo et al. (2007) [28]; Griffiths et al. (2007) [25]; Kawata et al. (2009) [37]
Amorphous	COC	De Grave et al. (2007) [19]
Amorphous	PC	De Grave et al. (2007) [19]; Griffiths et al. (2008) [23]
Amorphous	ABS	Griffiths et al. (2008) [23]
TPE	TPU	Yoon et al. (2010) [73]

been investigated regarding their impact on replication accuracy [3, 7, 8, 9, 10, 34, 50, 61, 66].

Moreover, it is almost impossible to compare the results on demolding force let alone to draw conclusions from them. Most works concentrated on PMMA, as it is commonly used in injection molding of micro-structured devices. De Grave et al. (2007) concentrated on the effect of demolding angles when comparing COC and PC [19]. Griffiths et al. (2008) found that from their set of experiments, there was no unique setting as far as demolding forces are concerned for each type of polymer [23]. In addition, Guo et al. (2007) concentrated on friction forces but also on the effect of anti-stiction coatings [27]. Yoon et al. (2010) employed TPU for injection molding on silicon tooling [73]. Apart from good replication quality due to an anti-stiction coating based on fluorinated silanes, the flexibility of the TPU provided superior demolding behavior in comparison to PC or other thermoplastic polymers. In addition, polymer residue on the stamper was reduced.

3.3.2 Machine parameters

As with polymers, little has been reported on how processing parameters influence demolding force. Most works concentrated on replication accuracy, which should always be as good as possible, when measuring demolding force. Processing parameters such as mold temperature, injection speed, holding pressure and cooling time are crucial in conventional injection molding. Still, polymer melt might flow differently in micro-cavities. Several works reported mold temperature and holding pressure to be most influential on demolding

force, as these factors strongly impact the specific volume of the molded part at ejection [15, 18, 66].

Fu et al. (2006) investigated the effect of temperature on the stress during demolding [15]. Their simulations on the stress distribution of the microstructure farthest from the center line at different temperatures are shown in Figure 3.11. As the temperature of the mold decreases, the thermally induced stress in the part increases. On the other hand the strength of the polymer but also thermally induced stress increase with decreasing mold temperature, the demolding temperature has to be investigated thoroughly, to prevent damage or failure.

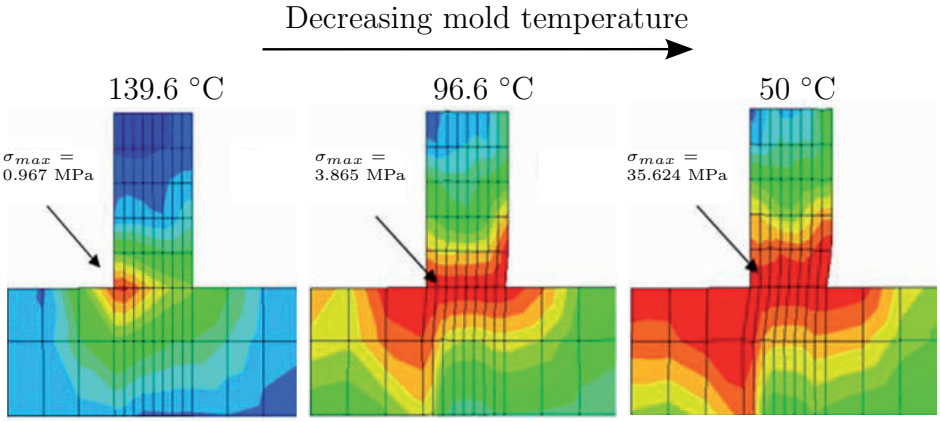

Figure 3.11. Thermal stress distribution of a PIM feedstock of the farthest structure from the center line [15].

In another study Fu et al. (2008) reported the effect of the temperature and packing pressure dependent part volume on the demolding force for metal injection molding [18]. Their comparison of different packing pressures (80 to 120 bar) and different demolding temperatures (60 to 140 °C) is displayed in Figure 3.12. Furthermore, the results from the experimental analysis were compared with the data obtained from simulation. They found the experimental verification of T_{dcr} for powder micro-injection molding. Also they found, that T_{dcr} is depending on both the packing pressure as well as material properties.

With increasing packing pressure T_{dcr} decreased, which is in accordance with the hypothesis posted from theoretical considerations. A limitation to their results is that the isotropic shrinkage assumption is only applicable for a variotherm mold or a conventional mold with small part size. When using a variotherm mold, demolding temperature should meet the critical demolding temperature to ensure minimum demolding forces. The existence of a critical

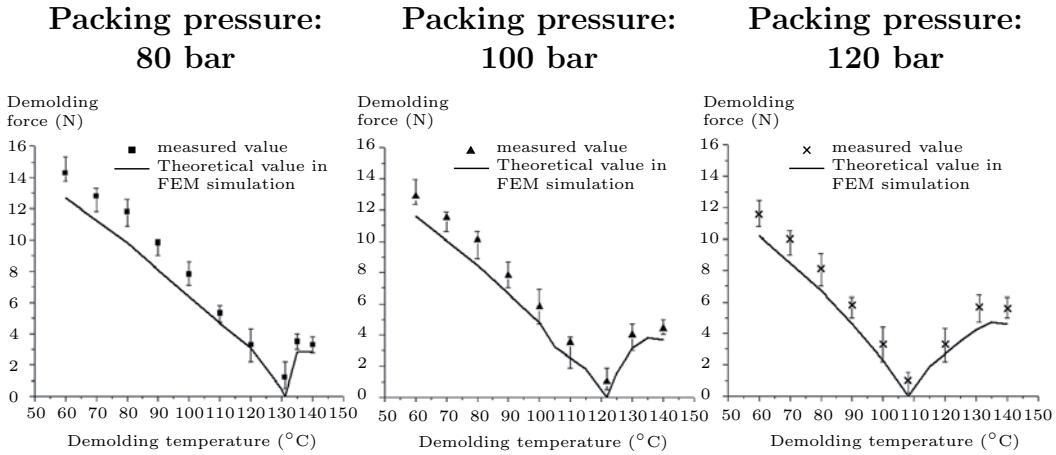

Figure 3.12. Simulated and measured demolding force of a PIM feedstock at different packing pressures and demolding temperatures [18].

demolding temperature for PMMA in hot embossing has also been proven experimentally by Trabadelo et al. (2008) (compare Figure 3.13) [67]. In addition, the demolding force was affected by the demolding velocity as well. They found, that slower demolding velocity also reduced demolding forces.

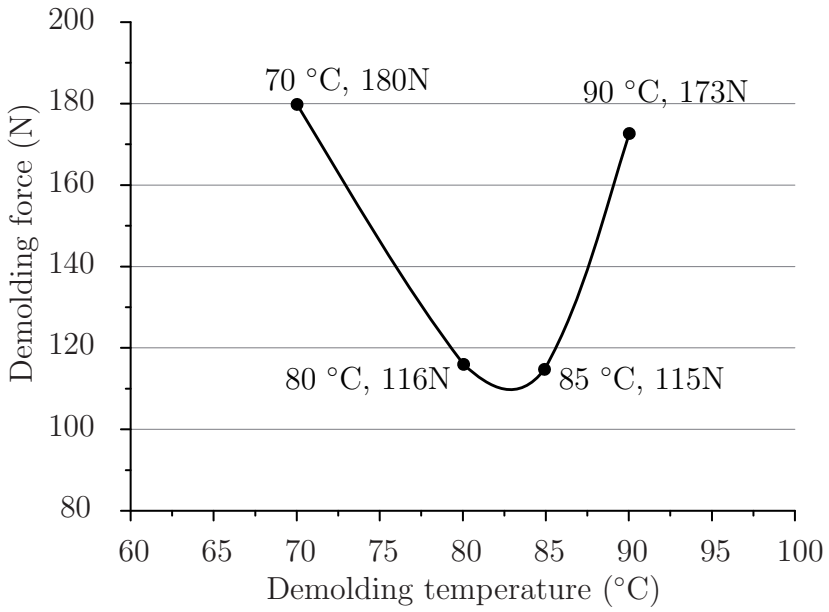

Figure 3.13. Demolding force as a function of demolding temperature for PMMA [67].

These findings are in accordance with the theoretical considerations of Pollock and Yan (1978) [56]. Higher temperatures imply a lower Young's modulus in the material and thus lower stress levels are induced due to demolding. As a consequence, the strength of the part exceeds the maximum demolding stress and risk of part failure is reduced.

3.3.3 Micro-structure design

During the injection molding process different forms of thermally induced shape changes take place. As a consequence volume changes due to part shrinkage and shape distortions due to warpage are common. Thus, feature placement relative to the gate will impact demolding as shrinkage is the main cause of friction forces between the polymer and the cavity wall. Moreover, orientation of the injected polymer must be considered, because it affects the predominant direction of shrinkage. According to Heckele and Schomburg (2004) the farther the features from the shrinking center are, the harder the demolding becomes [32].

Apart from that little is mentioned in literature about designing microfluidic devices for manufacturability in injection molding. Most design considerations focus on designing for functionality rather than criteria associated with the demolding force of the molded part. Worgull et al. (2005) suggested a few modifications based on simulations on large-scale hot embossing to reduce the shrinkage of the parts [71]. Regarding demolding, they suggested to use a 'frame' around the micro-structures, which levels the pressure distribution in the melt and subsequently reduces shrinkage and even warpage. Additionally, they suggest to add micro-structures at the edges, that may be torn off, but would reduce stress in the outermost micro-structure, where the largest strain due to the contraction of the base occurs.

This is in accordance with FEM calculations for the hot embossing process conducted by Guo et al. (2007), who concluded that the thermal stress is a function of the orientation of the micro-structures relative to the shrinkage direction [28]. They drew the same conclusions as Worgull et al. (2005) [71] and proposed the introduction of an auxiliary structure as a thermal stress barrier. In practice, the orientations of structures and stress barrier should be kept coincident with the shrinkage center, e.g. circular.

Figure 3.14 illustrates the stress distribution achieved by the introduction of such a stress barrier. The maximum stress of the adjacent micro-structure at the transition area from the micro-structure to the base was reduced by 60 %. Further simulations revealed, that the position of the auxiliary structure relative to the micro-structure (marked as ρ in Figure 3.14) did not influence its efficiency critically, although higher values of ρ proved to be

more effective [27]. Thus, the stress barriers could be placed far from the field of micro-structure, so as not to interfere with functionality of the micro-structures. Nevertheless, in practice difficulties could arise from placing stress barriers coincident to the shrinkage center on asymmetric devices.

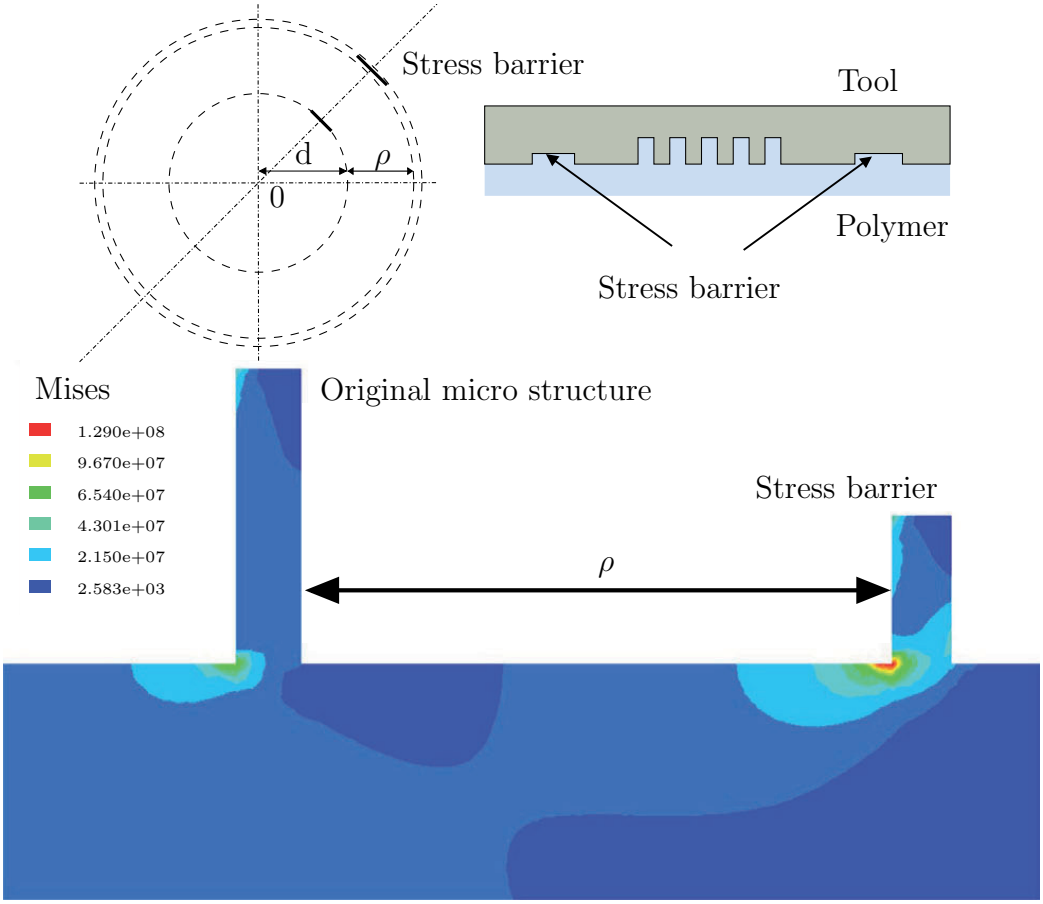

Figure 3.14. Thermal stress distribution of the PMMA micro-structure after introduction of a stress barrier [27].

For high aspect-ratios Heckele and Schomburg (2004) observed that the large contact area between polymer and mold imposes higher frictional resistance during demolding [32]. Regarding demolding, draft angles and side-wall roughness need to be considered to ensure that the plastic part is demolded without damage or destruction. Small inclination angles of at least 1/4 ° are desirable for the ability to demold. Still, functionality of the micro-structures has to be maintained despite changes in design.

3.3.4 Tool surface

Polymer properties become an even more important factor, when considering surface treatment. Quality and topography of the mold surface have significant influence on the replication capability. As scale decreases, interfacial effects such as wall slip and surface tension become more dominant [13]. Griffiths et al. (2010) investigated the demolding forces of a representative microfluidic chip utilizing two polymers (PC and ABS) and different surface treatments (uncoated, DLC coating and SiOC coating) in combination with four process parameters (barrel temperature, mold temperature, cooling time, ejection time) [24]. They found that the average demolding force was clearly reduced by both surface coatings compared to the uncoated tool, although the decrease appeared to be much more prominent in ABS than in PC.

At the same time part quality improved with the use of surface treated tools. From the set of experiments, that could be employed for other polymers as well, no unique selection of parameters could be deduced. Hence, it is impossible to draw conclusions for other materials. Instead, according to the authors, systematic experimental studies should be carried out to cover new combinations of tool surface and polymers [24].

Section 3.2.3 highlights the theoretical background on adhesion. For steel molds Dearney (1999) found that polished surfaces caused less surface interaction and thus lower friction forces than spark erosion finish [12]. Kawata et al. (2009) examined several Si templates varying in surface roughness (achieved by KOH treatment) and vertical or tapered sidewalls for the thermal imprint process [37]. It was found, that the dominant impact on demolding force was the friction due to sidewall roughness, rather than adhesion between Si template and PMMA. Their investigation determined that the demolding force for a template with tapered sidewalls was half the value of the demolding force of the vertical structure. In addition, smooth sidewalls reduced roughness by a quarter. Hence especially tapered and smooth sidewalls reduced demolding forces considerably.

The effect of coatings and various surface treatment techniques has been covered extensively in literature. These investigations showed that surface treatment significantly reduced demolding forces. In particular, good demolding behavior can be achieved by low material affinity between the coating and the polymer. The main contributing factors are the 'surface composition' and 'surface energy', which is defined as the interaction between the forces of cohesion and adhesion [63]. Nevertheless, care must be taken when applying these results to uncharacterized polymer-coating combinations, as various factors such as mold temperature and injection velocity affect inter-

actions.

To lower the adhesion and friction between molding insert and polymer, transition metal nitrides have been widely applied in conventional injection molding, to enhance wear resistance and decrease release forces. Especially techniques like physical or chemical vapor deposition of titanium nitride (TiN) and chromium nitride (CrN) reduce part-mold forces and thereby improve surface quality of the molded parts [11, 33, 48]. Miikkulainen et al. (2008) deposited thin films of molybdenum nitride and tungsten nitride as tribological coatings by atomic layer deposition [47]. Molybdenum displayed particularly good resistance to contamination in the injection molding process.

Additionally, diamond like carbon (DLC) was reported to be another anti-stiction coating [24]. It is an amorphous material, that displays some of the unique properties of natural diamond when applied as a coating on tool surfaces. From the mean values of PC and ABS Griffiths et al. (2010) concluded that parts fabricated with such coatings were subjected to a lower stress level compared to uncoated tools [24].

Recently, PTFE-based materials have been suggested to promote anti-adhesive properties. Several methods such as electrochemical [51] and plasma polymerization [35] and phosphoric acid precursors [38] have been applied in an attempt to deposit PTFE films on mold surfaces. Peng et al. (2005) found that Ni-PTFE compound inserts performed better in hot embossing than a Ni stamper [54]. The authors concluded that Ni-PTFE yields lower frictional coefficients and lower average surface energy compared to Ni, although De Grave et al. (2007) doubt that PTFE could be deposited uniformly [19]. Furthermore, PTFE wears significantly faster than Ni proving it impractical for industrial production. Chen et al. (2009) found that a more thermally insulating material, such as PTFE, could delay the heat transfer from the part surface to the mold, if applied as coating for injection molding [8]. Thus, the surface temperature of the part remains higher, compared to metal surfaces throughout the filling cycle.

A complementary approach to hard wear coatings are organosilicon-based coatings. They offer low surface energy, which is likely to minimize adhesion of molded parts to the surface coating. Short-chain fluorinated silanes for example self-assemble on the mold surface and form relatively thin layers compared to the dimensions of the mold features. Moreover, they rather adhere to the mold than to the molded parts. Commonly, hexamethyldisiloxane, tetramethyldisiloxane or tetraexthoxysilane are used as precursors. They are mixed with oxidants (O_2) and/or noble gases (Ar, He) and applied onto the surface via plasma-enhanced chemical vapor deposition (PECVD) to obtain silicone oxide thin films [24]. They can be applied on top of a

wear-resistant coating like Diamond Like Carbon (DLC), to achieve initial low gliding and consequent contact with an underlying hard and low friction material.

Although advanced coatings like Ti-DLC coatings have been developed for enhanced interfacial adhesion between the tool surface and the deposited material, interfacial interactions remain the main issue that slows advancement in the field of coatings. There are several adhesion mechanisms at hand, which include mechanical locking of irregular surfaces, physical absorption (Van der Waals forces), chemical bonding (covalent, ionic or hydrogen bonds) and diffusion (interdiffusion of polymer chains). Nevertheless, at deposition layers thicker than 1 µm, cracking and delamination can occur, due to the contact pressure from the injection molding process [24]. Moreover, polymer-based coatings pose problems for mass production due to their poor wear resistance, diffusion into the molded polymer and their sensitivity to heat induced degradation [35, 54, 59], which would not be compatible with regulations for medical applications.

Summing up, frictional force will decrease with a decrease in the surface energy of the mold or coating material, respectively. A reduction in friction force along the sidewalls lowers the risk of excessively shearing the microstructures during demolding. As a consequence, high stress areas can be minimized to reduce damage to the features.

3.4 Measuring demolding force

To improve demolding, a prerequisite is to measure the demolding force during the fabrication process. To achieve this, several measuring set-ups with varying mechanisms and goals were designed [18, 22, 67]. Trabadelo et al. (2008) suggested a method for full wafer thermal nano-imprinting [67]. The stamp was designed with a homogenous pattern consisting of a 4 µm periodical orthogonal array with 2 µm square holes or pillars. Furthermore, all stamps were coated using silane based anti-adhesives.

For the embossing of the features into PMMA the force history curves were recorded. The analysis showed that for different structural depths the demolding force can be deduced from discontinuities of the force at $F < 0$. The sudden release of the polymer from the stamp results in a characteristic 'kink' in the force curve, which represents the force in an instantaneous parallel demolding process. According to the authors, a lack of such a 'kink' indicates peeling movement. In this case, the polymer bends upwards and subsequently demolds from the edges to the center. Concluding, they found, that the value of the demolding force correlates to the 'kink' in the recorded

force curve, which is indicated in Figure 3.15. In addition, they stated that the demolding force depends strongly on the total surface of adhesion, meaning that the additional surface area of the side walls of a highly structured stamper adds up to the surface of an unstructured wafer. Hence, microstructures with higher aspect ratios are expected to contribute more severely to demolding forces.

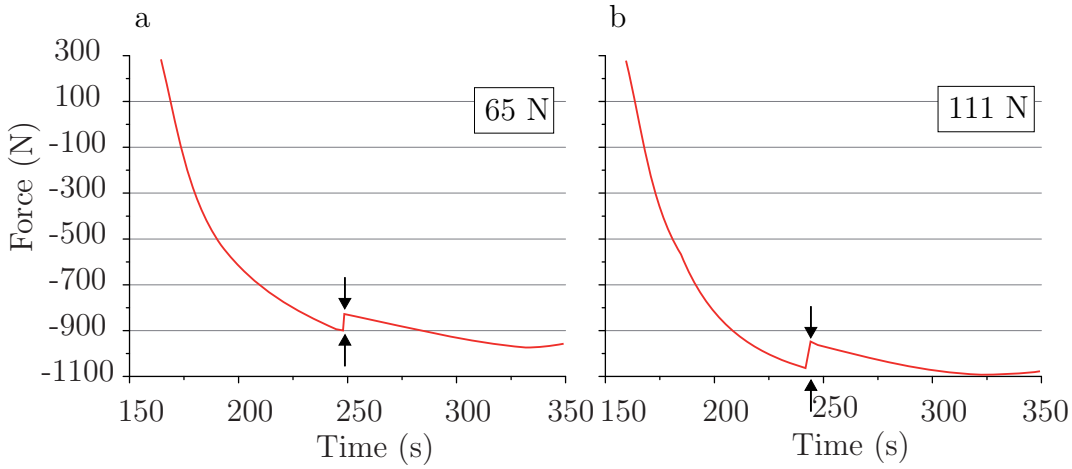

Figure 3.15. Detail of the force curve of PMMA for an unstructured stamper (a) and 500 nm high pillars (b) at 80 °C [67].

To verify the results obtained from simulation, Fu et al. (2008) conducted indirect measurements of the demolding force of metal micro-injection molded parts [18]. For that purpose they removed the mold half with the ejection system and the green part after injection molding. Until it was placed in a tensile testing machine the mold was kept at ejection temperature similar to the injection molding process. While the part was 'ejected' at the same speed as was used in the injection molding process, the demolding force was measured. These measurements were conducted for two stampers, since the demolding force could not be measured directly due to the frictional and adhesive force. The forces obtained from the stamper without micro-structures were used as a reference and then compared to the results of the stamper with micro-cavities. For comparison they chose the maximum demolding force, which occured at the onset of movement of the part. Thereby, an increase in the demolding force due to the micro-structures could be proven.

In addition, Griffiths et al. (2010) conducted force measurements in the micro-injection molding process, which were assessed with an ejector sub-assembly [24]. Four ejector pins were connected to a force transducer, which was subjected to a mechanical load upon ejection. This sub-assembly was

fitted to the main ejector plate positioning the transducer in the middle of the ejector plate. The force that was measured by the transducer was then calculated from the measured output voltage, which resulted from the removal of the part from the cavity.

3.5 Summarizing literature review

Several constraints influence the fabrication of micro-structured devices. On the one hand, good replication quality has to be obtained to guarantee high functionality. On the other hand, successful demolding is crucial, for the micro-structures are easily deformed or destroyed during demolding. Therefore, it is important to address both issues. As a consequence various research groups investigated the replication accuracy for injection molding of micro-structured devices [6, 42, 50, 61, 66, 73]. Although the process parameters were investigated thoroughly, high replication accuracy for PMMA has not been reported so far. As PMMA exhibits desirable surface properties for cell culturing [31], achieving high replication quality is of importance.

Regarding the processing parameters various authors reported melt and mold temperature, injection velocity and packing pressure to be most influential on replication quality [40, 50, 61]. Especially the mold temperature seemed to influence the replication quality strongly. This occurred due to its impact on the flow behavior and the tendency of the polymer to freeze while filling the micro-cavities. Due to that, higher mold temperature was expected to yield a higher degree of replication, since the flowability of the polymer was maintained for a longer period of time.

After successfully replicating micro-structures into a polymeric material, demolding without damaging the micro-features is crucial. The demolding force, which is widely used to quantify the demolding step, is influenced by a number of factors, which were categorized into 4 groups: polymer, machine parameters, micro-structure design and tool surface (compare Section 3.3). These factors cause either friction or adhesion between polymer and tool surface. A study on all of these factors is still lacking, since each research group covered one or two influencing factors at most [15, 18, 19, 23, 27, 32, 71, 73]. Furthermore, all factors occur to be interdependent, which deems an independent investigation of only one factor impossible.

So far, most applications and reports on hot embossing or injection molding of micro-structured devices included PMMA as polymeric material [7, 10, 42], but COP is receiving increasing attention, due to its promising properties [52]. For applications where no optical transparency is required commodity plastics such as PP would yield considerable advantages for low cost

production. Its chemical resistance against organic solvents provides for a good carrier material, although its limited thermal stability might hinder applications where sterilization or other treatments, which demand elevated temperatures are required. The only general recommendation with respect to material properties is to use polymeric material with low shrinkage. According to this, amorphous polymers would be favorable compared to semi-crystalline due to the higher shrinkage of the latter when crystallizing. Apart from that no approach on material selection for low demolding forces has been determined.

Therefore, there is a number of factors affecting the demolding behavior of polymers (compare Figure 3.16), which have not been investigated so far. The Young's modulus and the thermal expansion coefficient as well as surface energy influence the demolding behavior. Moreover, the specific volume, which is temperature and pressure dependent, impacts the demolding behavior. At T_{dcr} the volume of the part equals the mold and subsequently marks the ideal demolding temperature (compare Section 4.3.1). Nevertheless, care must be taken, as T_{dcr} is also dependent on the processing parameters such as switch-over volume and packing pressure. According to the literature study demolding at temperatures slightly higher than T_{dcr} would be favorable [17]. However, the temperature dependent strength of the polymer and the induced stress during demolding have to be considered as well to find a suitable demolding temperature. If the stresses resulting from demolding exceed the strength of the polymer with the given dimensions at the demolding temperature, damage or failure of the micro-structures can occur.

At lower demolding temperatures than T_{dcr}, where the strength of the polymer increases, the elasticity of the polymer affects the demolding process and thereby determines the demolding forces [73]. As indicated above, the higher the elasticity of the polymer is, the lower the frictional forces and the resulting demolding force. Since the specific volume, the shrinkage and the strength of the polymer but also the elasticity (or Young's Modulus) of polymers are strongly temperature dependent, a suitable demolding temperature has to be determined. Since all relevant properties of polymers and their relative impact are temperature dependent, their interdependence has to be considered when examining and selecting a material for microfluidic devices as well. In addition, several processing parameters as injection velocity, barrel temperature, switch-over volume and packing pressure affect these properties as well. Apart from the properties discussed so far, they influence the thermally induced stresses as well as the orientation which in turn impact the anisotropic shrinkage.

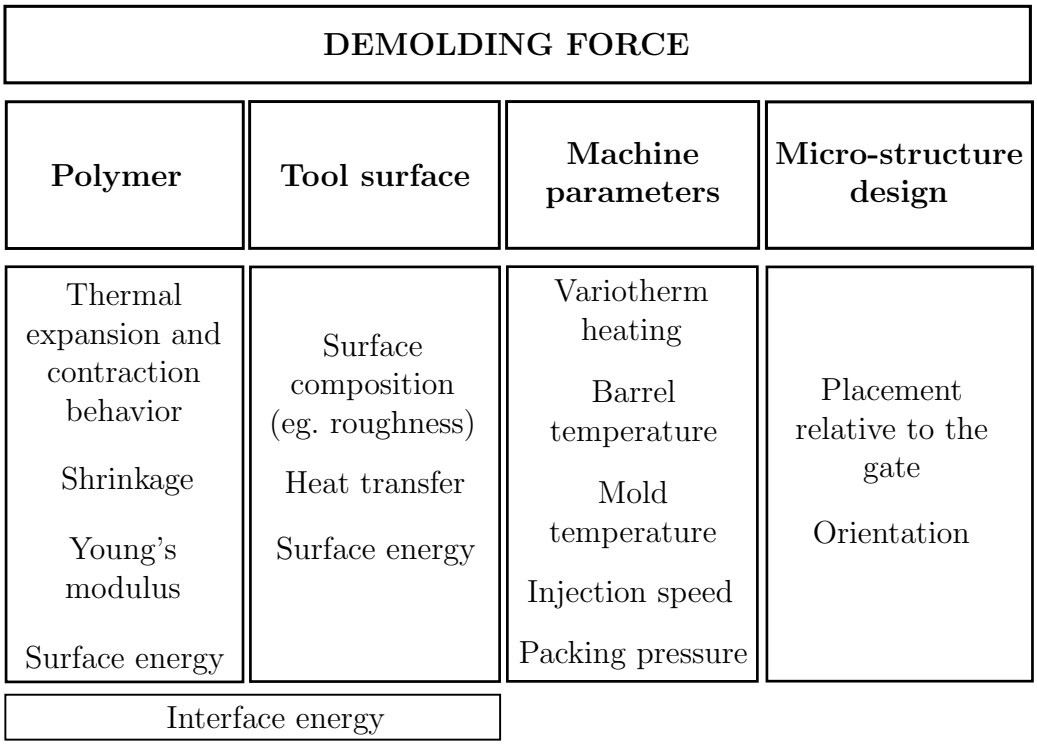

Figure 3.16. Summary of potential factors affecting demolding forces.

Chapter 4

Experimental work

This section provides information on the experimental details of this work. All injection molding experiments were conducted on a fully electric Arburg Allrounder 470 A (Arburg GmbH + Co KG, Lossburg, Germany) with clamping force of up to 1000 kN. Moreover, the experimental work was based on a micro-slide format (MS) (75 x 25 x 1 mm^3), because it is one of the most commonly used formats for medical or diagnostics applications. Initially, the experiment design, which was set up in accordance to the literature study and the corresponding review, is explained. Moreover, the concept of acquiring the demolding force is discussed in detail, although the tool design, measurement system and evaluation procedure were provided by Struklec [64]. Furthermore, the experiments on replication accuracy and the injection molding simulation are summarized. The 4 factors affecting demolding energies are explained for the set of experiments as well as the prerequisites of measuring demolding energies. Finally, a glossary explains the nomenclature chosen for the description of the results.

4.1 Experiment design

In compliance with the information obtained from the literature review experiments were specified for this thesis. These aimed at setting a standard method to identify the impact of polymer, process parameters, design and tool surface on replication accuracy, demolding forces and deformation of micro-structured devices. The experiments, which were performed in this work, were grouped into 7 case studies with regard to their aim. For better understanding, Table 4.1 gives a summary on nomenclature and a short introduction into the investigations conducted in each of them.

First of all, the replication accuracy of PMMA was analyzed and com-

Table 4.1. Summary of case studies and conducted experiments.

Case study	Description
1	Replication accuracy of COP and PMMA
2	Injection molding simulation on deformation behavior
3	Impact of amorphous and semi-crystalline polymer on demolding force
4	Impact of thermoplastic elastomer on demolding force
5	Impact of demolding temperature on demolding force
6	Impact of micro-structure placement on demolding force
7	Impact of tool surface on demolding force

pared to COP for a specific life science application, which included a micro-structured chip for in vitro culturing and differentiation of stem cells. Haubenwallner et al. (2014) reported plasma treated COP and PMMA as optimal polymers for primary neuronal cell culturing and propagation [31]. Furthermore, certain cell characteristics seemed to be enhanced when cultured on oxygen-plasma treated PMMA. Hence, these two polymers were chosen to compare their suitability regarding replication. However, Chen et al. (2010) reported poor replication quality for PMMA compared to COP, which showed excellent replication due to its low viscosity and low, isotropic shrinkage [7]. This constraint was adressed with a Design of Experiment (DoE) approach to identify the optimum processing parameters for high replication accuracy of PMMA.

In various reviews on factors affecting replication accuracy [40,50,61], the authors reported melt and mold temperature, injection velocity and packing pressure to be most influential. In accordance to this, melt temperature, mold temperature and injection speed were selected for the analysis conducted in this work as well. The impact of packing pressure was not included, since the packing pressure profile was set as a standard. In addition, the design of the film gate limited the impact of the packing pressure on the actual part.

Secondly, the deformation behavior of micro-structured devices, which resulted from the process parameters, was assessed. Hence, simulations on the injection molding process were conducted within case study 2. Several reports had dealt with the implementation of a FEM model to calculate the stress level and deformation at different locations in the micro-features, which resulted from thermally induced stresses and the demolding process [15, 18, 27, 32, 71]. On the contrary, the investigations in this thesis were conducted with SIGMASOFT® software. Thereby, the impact of the injection molding

conditions on the shrinkage behavior were analyzed to obtain information on the deformation of the device, during cooling within the mold. As the shrinkage of the ground plate is the main cause of contact forces between the micro-features and the tool surface, simulations were performed without micro-structures. The shrinkage of the ground plate was then compared to the shrinkage of the parts which were obtained from the fabrication process to support the results from the simulation. The aim was to deduce predictions on the demolding forces, which resulted from processing.

Subsequently, a comparative study was set up, which covers all four factors affecting demolding forces. As a consequence, several case studies dealt with the analysis of factors affecting demolding forces in injection molding of micro-structured devices. The 4 main factors, which were deduced from the literature study (see Section 3.3), were analyzed systematically. The tool surface and coatings, which were already covered by [64], were treated marginally with a comparison of nickel and titanium nitride coated tool surface. Hence, experiments on the influence of the micro-structure design, the polymer (amorphous, semi-crystalline and thermoplastic elastomer) and the processing parameters (demolding temperature) were performed.

Due to this, case study 3 aimed at testing the effect of amorphous and semi-crystalline polymers on the demolding force. Therefore, a semi-crystalline material (PP) and two amorphous materials (COP and PMMA) were investigated. PP was selected, as it is commonly used in injection molding. Due to the focus on micro-structured devices for medical applications, COP and PMMA were chosen, since they are used commercially in such systems [26, 41] and comply with standards regarding their use in medical applications. Thus, a standard setting within the usual processing scope was defined for each polymer to investigate the influence of the morphology of the polymer on the demolding forces.

In addition, to the analysis on amorphous and semi-crystalline polymer a thermoplastic COC-elastomer (TPE) was investigated in case study 4. On the one hand, this material was processed independently to obtain further information on the impact of morphology on the demolding forces. On the other hand, it was used as an additive for COP, since its Young's Modulus (44 MPa) and its T_g at 6 ° promised to increase the elasticity of COP. It was expected to lower the Young's Modulus compared to native COP and thereby decrease demolding forces. To achieve this, 10 and 40 wt % of COC-TPE were added to COP to examine its impact on the demolding behavior.

Since Theilade et al. (2007) identified the demolding temperature as the most influential parameter parameter on demolding force [66], case study 5 investigated the impact of the demolding temperature on the demolding forces. It aimed at deducing T_{dcr}, where the demolding forces reached their minimum

value. This temperature results from the interaction and interdependence of several factors: In particular the temperature dependent Young's Modulus, the thermally induced stresses during cooling and the expansion and contraction of the polymer in accordance with the pvT-curves as well as the in-mold shrinkage had to be considered. Because of that, the demolding temperature was varied in a range of at least 30 °C to deduce its impact on the demolding force of each polymer.

For case study 6 a simple micro-rib pattern was used to analyze the impact of feature placement relative to the gate. In addition, these micro-features were arranged in flow or perpendicularly to flow to identify the impact of orientation relative to the flow direction on the demolding force. It was anticipated from the theoretical study, that a micro-structure arranged perpendicular to the flow direction and placed far from the gate would yield the highest demolding forces within case study 5 [32]; whereas an arrangement in flow direction and close to the gate would cause considerably lower demolding forces. The aim of these tests was to derive design recommendations for ideal feature placement and orientation with respect to demolding forces.

Although the effect of tool coatings has already been covered in literature [11, 24, 26, 28, 33, 37, 47, 48, 54, 73] and by Struklec [64], the effect of a titanium nitride (TiN) coating on the demolding force was investigated. TiN was chosen due to the findings of the literature study, where several authors suggested transition metal nitrides for anti-stiction coatings [11,33,48]. Since Griffiths et al. (2010) had found that the interaction of polymer and tool surface depended strongly on the polymer-coating-combination [24], Ni and TiN were tested for all materials to examine the impact of demolding temperature on the efficiency of these two.

4.2 Concept of acquiring demolding force

Section 3.4 summarized several concepts which had been reported for acquiring the demolding forces. Another approach for obtaining demolding force measurements was developed for this work, which was then implemented in the tool design. Moreover, the original signal had to be processed to interpret and compare these measurements in order to obtain a quantifiable result. As a consequence, this section deals with the tool design, measuring, recording and consecutive signal processing, which converted the recorded displacement and force measurements into a value that described the demoldability of the polymer part.

4.2.1 Tool design and measurement device

The injection molding tool, which was used to conduct all experiments, was designed and built to perform demolding force measurements for state of the art lab-on-a-chip manufacturing. Therefore, a measurement system that enables the measurement of the acting demolding forces and operates in a production environment was developed by Burgsteiner and Struklec [5]. For that purpose Struklec (2015) drafted and evaluated demolding concepts, the measuring mode, conducted pre-testings of the available equipment and designed the mold unit [64]. Some constraints, which were addressed, included the fitting of the measuring equipment into the mold unit as well as the level of the dominating forces that were to be measured, since demolding forces of micro-structured devices act on a different level than those of conventional injection molding.

Figure 4.1 shows the concept of the mold and the measuring device. It consists of basic components such as cooling channels or ejector pins but also incorporates a variotherm heating as well as air venting (not included in Figure 4.1) to achieve vacuum in the mold cavity. The variotherm heating and vacuum are necessary to achieve proper replication of the micro-structures [9]. Since it is impossible, to vent the micro-structures, the air inside the cavity has to be removed before injection. Therefore, the entire mold is sealed air tight with a sealing ring. The evacuation system is directed next to the cavity into the parting plane to ensure a pressure in the cavity below 600 mbar. The part includes a 0.5 mm thick film gate, which ensured a balanced melt front advancement in the cavity. However, this film gate set the smallest physical dimensions of the part.

To guarantee the propagation of the vacuum into the cavity, the process was adapted as follows: In the first step the mold closes until the moveable half is in contact with the sealing ring and the pressure drops. With the cavity evacuated, the mold closes completely. Afterwards the pressure sensor, which is located close to the cavity, triggers the injection step once the vacuum input signal is activated. Subsequently, the evacuation is maintained as long as the mold remains closed. To enable air flow with acting clamping force, a 4 µm gap was inserted into the parting plane between the cavity and the vacuum channel.

As mentioned above, the mold also incorporated a variotherm heating system, which consists of the ceramic heating unit (Watlow Plasmatech GmbH, Scheffau, Austria) that is specified in Table 4.2. These ceramic heating elements are arranged right behind the cavity surface, to provide heating of the stamper. Furthermore, a power output of over 1000 W (compare Table 4.3) can be achieved. This set-up facilitates the investigation of the effect of

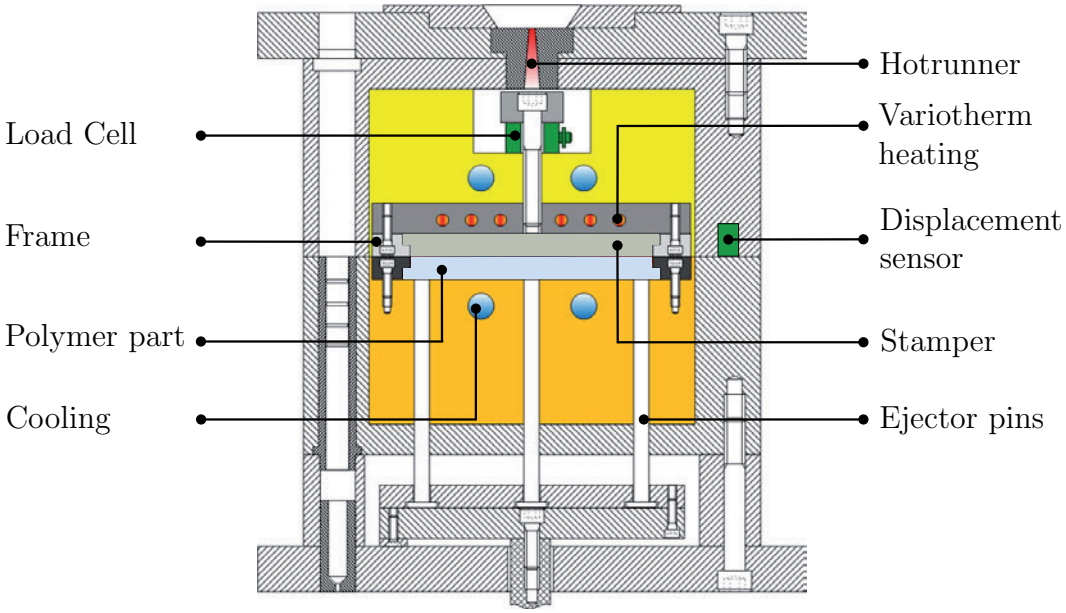

Figure 4.1. Schematic overview of the design of the injection mold for demolding force measurements [64].

the variotherm process on the demolding forces. In addition, as the variotherm heating is controlled separately from the injection molding machine, the starting signal of the injection stage was chosen to regulate the heating unit.

Table 4.2. Specifications of the AIN ceramic heating element [69].

Ceramic heating element	
Voltage	240 V
Power	1455 W
Resistance	39.6 ± 9.9 Ohm
Max. heating temperature	400 °C
Temperature sensor type	Type K thermocouple

Additionally, the injection tool was designed to fit independently replaceable mold inserts into the tool main body. Therefore, the tool contained a frame where these stampers could be placed and exchanged easily. The frame can be removed, while the mold is mounted on the injection molding machine as long as the mold is in an open position. The frame itself is directly con-

nected to the load cell, which is located behind it. Due to that, all forces acting on the micro-structured stamper, that is placed in the frame, can be measured. The Kistler load cell 9001A (Kistler Instrumente AG, Winterthur, Switzerland) provides a range of 0 - 750 N, with further specifications to be seen in Table 4.3.

Furthermore, a displacement sensor, which is placed in the parting plane of the tool to record the mold opening motion, forms part of the measurement system. This sensor was inserted additionally to assign the necessary distance information to the demolding force and the demolding point, as the machine movement exhibited inappropriately low resolution of 0.01 mm. The µ-epsilon displacement sensor CSH1-CAm1.4 (Micro-Epsilon Messtechnik GmbH & Co. KG, Ortenburg, Germany) is also specified in Table 4.3. It is calibrated accurately to the range of 0–1 mm, defining anything over 1 mm an open mold position. Moreover, an assembly offset of approximately 0.16 mm from the parting plane was included for safety reasons, since the mold opening and closing motion could damage the sensor otherwise.

Table 4.3. Specifications of the sensors used for the demolding force and displacement measurements.

Load cell		**Displacement sensor**	
Range	0 – 750 N	Range	0 – 1 mm
Resolution	1 N	Resolution	0.38 nm
Linearity	0.5 %	Linearity	0.05 %
Calibrated range 10 %	0 – 600 N	Temperature stability	-12 ppm/°C
Max. temperature	+200 °C	Max. temperature	+200 °C

The load cell was preloaded in accordance to the specifications of the manufacturer, to provide the necessary clamping when operating. Due to the assembly of the load cell, a negative force amplitude indicates 'pushing', whereas positive excitation signifies 'pulling'. An example of such a signal, which was obtained from the force and displacement measurements is displayed in Figure 4.2. When the mold is closing, the measured force will drop below 0 N because the clamping force exerts pressure onto the frame. This drop seems rather small compared to the clamping force of 600 kN, because most of the forces act on the tool main body as intended by the design. The consecutive large drop in force indicates the injection stage when the polymer melt hits the cavity. At the same time this causes a slight change in the displacement signal, which occurs due to elastic deformation of the

mold. As soon as the part is solidified the demolding stage starts with the mold opening movement. With this set-up the force, which is acting on the stamper when the part is pulled off, is directly transferred to the load cell. The force, which results from this pulling motion, correlates to the demolding force. This is recorded up to a 1 mm gap in the parting plane, since the demolding process of the micro-structures has been terminated at this mold opening position.

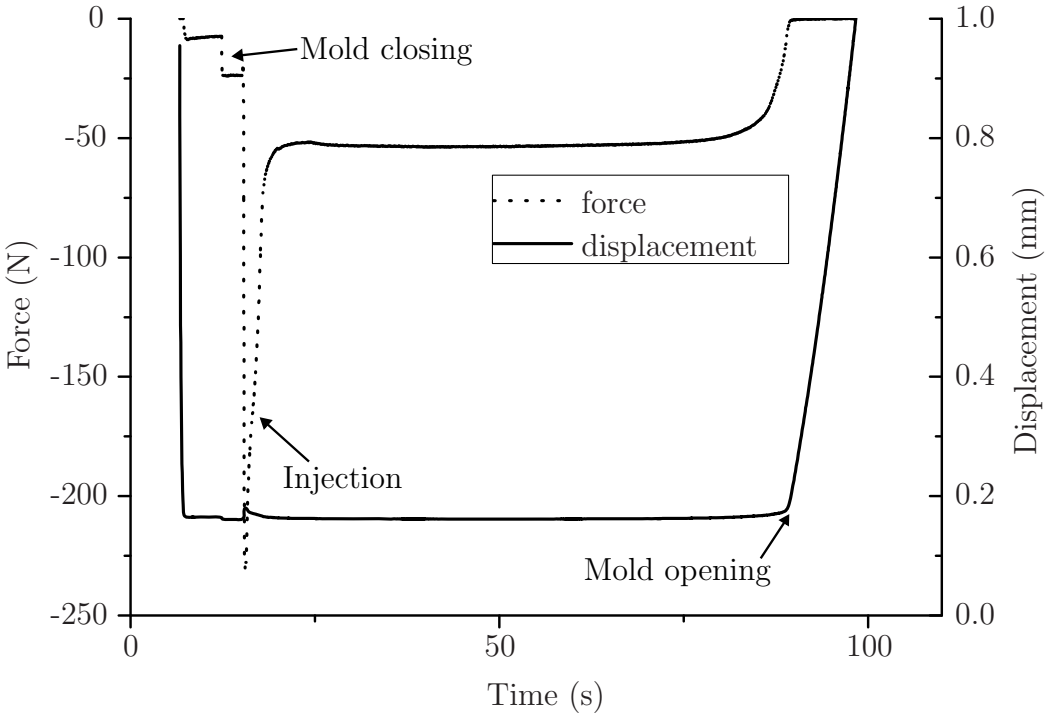

Figure 4.2. Force and displacement measurement over time [64].

Moreover, the load cell and the displacement sensor were externally attached to a charge amplifier, which was a µ-epsilon capaNCDT 6100 (Micro-Epsilon Messtechnik GmbH & Co. KG, Ortenburg, Germany) for the displacement sensor and a Kistler 5073A4 (Kistler Instrumente AG, Winterthur, Switzerland) for the load cell. The signals were then transmitted to an A-D-converter and subsequently to the data acquisition software catman (HBM, Darmstadt, Germany). This way the data was acquired, processed and stored systematically for further processing.

4.2.2 Data acquisition

The force and displacement signals were both recorded at the maximum frequency for this configuration of charge amplifiers and sensors at a sampling rate of 1400 Hz. Therefore the mold opening was carried out slowly, to obtain as much information as possible without affecting the measurement. Force and displacement were recorded simultaneously and were thus considered one measurement. Both signals were synchronized with a time measurement that was also applied during the measurement (compare Figure 4.2). Afterwards the signal had to be processed in order to evaluate the measurements. For that purpose the following measures were taken:

First of all, the mold opening stage was extracted, since this included the relevant information for further analysis. The rest of the signal that depicted the whole injection molding cycle and thus superfluous information was discarded to speed up the succeeding calculations on the extracted section. This step decreased the number of data points per measurement and sensor from 200.000 to approximately 20.000. In the following step, a smoothing function based on Sawitzky-Golai base polynomials was applied to reduce the noise of the original measurement. For that purpose second degree polynomials over a span of 200 points were used, which provided good results without altering the original signal [53].

Finally, the measurements, which all had a different number of measurement points due to the high recording frequency, were standardized. Therefore, a displacement vector, which ranged from 0 mm to 0.9 mm with a resolution of 0.001 mm, was created. The measurement points were tailored to the same length and then fitted to the displacement vector as can be seen in Figure 4.3. This interpolation step ensures for each measurement to have the same length and the same step size, whereas redundant data is dropped. This step created a signal that describes the measured demolding force at any displacement. With this, results can be compared for all measurements.

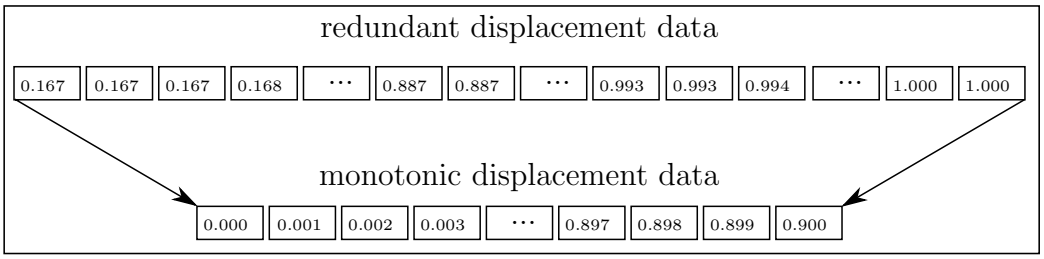

Figure 4.3. Fitting of reduntant data to a monotonic increasing vector [64].

4.2.3 Evaluation of demolding force

In literature the separation of polymer and stamper is recorded to result in a discrete demolding peak in the force measurement, which coincides with the release of the polymer from the tool [67]. However, this peak could not be detected for most set-ups, which were investigated within this work. Therefore, another approach was chosen and implemented by Struklec (2015) [64]: the demolding energy was calculated from the demolding force of each set of experiments to evaluate the demolding stage. The demolding energy was defined as the energy needed to seperate the polymer from the tool surface. Thus, the demolding energy was calculated according to Equation 4.1 where the demolding energy results from the integral of the force over the displacement [64]. Due to the evenly distributed step height from the normalized signal the integral becomes a sum for numerical evaluation (compare 4.2), which was implemented with trapezoidal rule.

$$\int_0^E \mathrm{d}E = \int_0^1 F \,\mathrm{d}s \tag{4.1}$$

$$E = \sum_0^1 F \Delta s \tag{4.2}$$

Where:

- E: demolding energy.
- F: acting demolding force.
- s: displacement while demolding from 0 to 0.9 mm.

For each configuration 10 measurements were performed, which were then evaluated to obtain their mean curve and standard deviation. This mean integral was then used to compare different configurations. However, due to differences in slope and shape comparing these curves proved almost impossible. Therefore, the demolding energy at a certain displacement had to be chosen, to establish a method for comparing configurations. To illustrate differences among curves from different measurements, the demolding energy at a displacement of 0.1 mm was compared. This single value was determined empirically, since the demolding process had been finished at displacements smaller than 0.1 mm.

4.3 Replication accuracy

In accordance to 4.1 a comparison of the replication capabilities of COP and PMMA was performed. For that purpose, both materials were used to fabricate replications of features commonly used for cell cultivation. As a consequence, a Design of Experiment approach was chosen to evaluate the effect of the processing conditions on the replication accuracy. Due to that, the materials and machine parameters, the design of experiment and the part design are specified in the following sections.

4.3.1 Materials and machine parameters

The materials compared in case study 1 were COP and PMMA. The COP (Zeonor 1060R) was provided by Zeon Chemicals LP (Luisville, USA) and the PMMA (Delpet 70NH) was provided by Asahi Kasei Chemicals Corporation (Chiyoda, Japan). Both comply to standards regarding the application for medical products. Furthermore, they exhibit relatively low mold shrinkage of 0.1 – 0.3 % and 0.2 – 0.6 %, respectively.

Initially, a standard process setting was established for the injection molding process (compare Table 4.6). To provide similar conditions, both materials were dried prior to processing for at least 4 hours at 70 °C (COP) and 80 °C (PMMA). Findings from other reports, which recommended high barrel temperature within the usual processing parameters to obtain high replication accuracy were taken into account [10, 73]. Due to that the barrel temperature (T_b) was chosen at the upper limit of the recommended process parameters for both materials. The mold temperature (T_m), back pressure and injection speed (v_i) were set in accordance to recommendations of the suppliers. In addition, the switch-over volume was determined with a filling study and set accordingly. The cooling time was selected to provide sufficient solidification of the part to prevent deformation or failure during the demolding stage.

The packing pressure for COP and PMMA was applied unaltered for all test runs. Its time dependent values are displayed in Table 4.5 and Figure 4.4. Furthermore, the set values after the respective cooling time are noted in the upper section. The high initial value was set this way to level the decline from injection pressure to packing pressure. Only this early in the cooling stage (up to 0.45 s) additional mass flow into the part could be achieved. As the film gate of the part solidified quickly, the packing pressure was deemed ineffective on the part. After 0.45 s the packing pressure was maintained at 200 bar for 4 s for both materials. In total packing pressure was applied for 4.55 s.

Table 4.4. Standard molding conditions of COP and PMMA.

Polymer	T_b	T_m	Back pressure	Injection speed	Switch-over volume	Cooling time
	°C	°C	bar	cm^3/s	cm^3	s
COP	260	80	100	50	14.0	30
PMMA	280	80	100	35	14.7	30

Table 4.5. Time dependent settings of packing pressure.

Polymer	Packing pressure set-value					Unit
	0	0.25	0.45	4.45	4.55	s
COP	600	300	200	200	100	bar
PMMA	750	400	200	200	100	bar

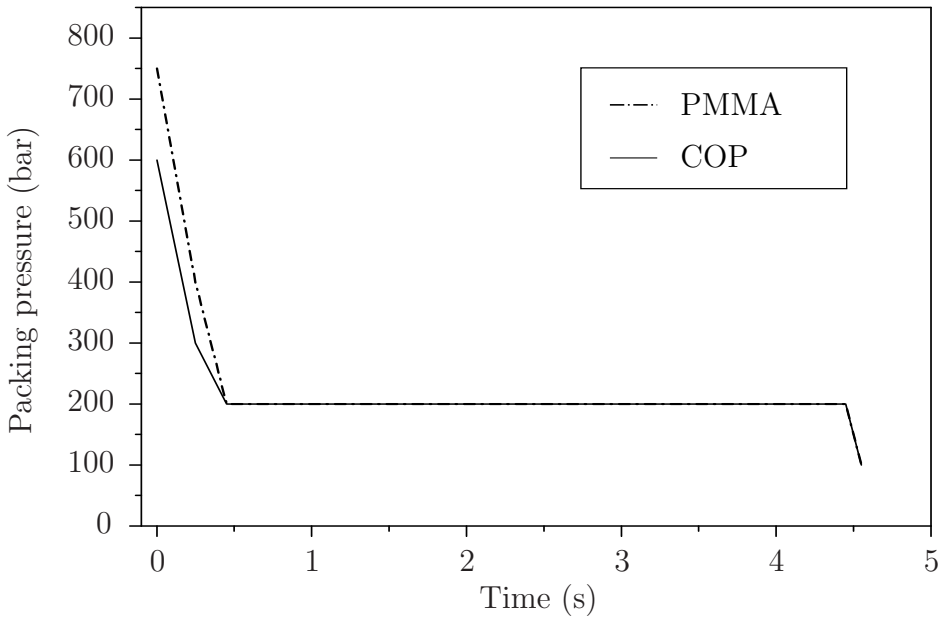

Figure 4.4. Time dependent packing pressure.

4.3.2 Design of experiment

To evaluate the effect of processing conditions on the replication accuracy of this application a design of experiment (DoE) approach was chosen. When the standard settings had been established, preliminary tests on the boundaries of T_b, T_m and v_i were conducted. The machine parameters for COP and PMMA in Table 4.6 were chosen as standard settings. Subsequently, each processing condition was then varied within the recommended parameters. As Yoon et al. (2010) had identified T_m to be the most influential machine parameter its window was chosen as wide as possible [73].

During this analysis two constraints had to be considered: On the one hand complete filling of the mold cavity had to be ensured. On the other hand, maximum injection pressure at the die had to be kept below 1800 bar, due to the load cell incorporated in the mold. The former aimed at avoiding short shots during the implementation of the DoE. The latter was set-up, to avoid any damage to the measuring system. Especially with PMMA several constraints occurred simultaneously, which resulted in a narrow processing window as summarized in the following:

		$\mathbf{T_b}$		
pressure exceeds 1800 bar	$\leftarrow$	$\mathbf{275 - 280\ °C}$	$\rightarrow$	degradation of polymer
		$\mathbf{T_m}$		
part failure	$\leftarrow$	$\mathbf{75 - 90\ °C}$	$\rightarrow$	boiling point of cooling agent (water)
		$\mathbf{v_i}$		
partial filling of the device	$\leftarrow$	$\mathbf{30 - 50\ cm^3/s}$	$\rightarrow$	pressure exceeds 1800 bar

In addition to the factors mentioned so far, part failure had to be considered. Thus, the lower limit of T_m was established at 75 °C for PMMA to ensure successful demolding of the device. The upper limit was confined by the boiling point of the cooling agent (water) as any further increase of temperature and hence an increase of gas pressure would have caused severe risk of leakage of the cooling system. Also, the maximum recommended processing temperature of 280 °C for PMMA was complied with, to prevent material degradation.

Consequently, a two level, full-factorial (2^3) approach was planned to investigate the influence of individual processing conditions on the selected

response, the replication accuracy of the micro-structures. This meant a total of 8 trials was needed, where each configuration was repeated 5 times. Each processing condition was set to 2 different levels as summarized in Table 4.6.

Table 4.6. Molding conditions of COP and PMMA for the DoE approach.

Polymer	T_b	Injection speed	T_m
	°C	cm^3/s	°C
COP	255 – 260	40 – 70	70 – 90
PMMA	275 – 280	30 – 50	75 – 90

The experimental design was established with 5 repetitions of each configuration and randomized except for the barrel temperature. T_b was blocked, since changing it in accordance to a fully randomized experimental design would have been very time consuming and hence inefficient. For that purpose the experiments for the lower barrel temperature limit were conducted at first and afterwards for the higher limit. When stable process conditions were reached after at least 10 shots, 5 parts were molded from each configuration and used for testing of the replication accuracy.

4.3.3 Part design

The part design used in this case study was a 70 x 25 x 1 mm^3 micro-structured plate, which is shown schematically in Figure 4.5. It includes features commonly used for cell culturing applications. In this case the aim was to investigate the impact of micro-structure design on cell culturing. Therefore, it is very important to achieve high replication accuracy of the micro-structures, as they would be useless for cell culturing otherwise. The properties of the micro-structures are defined by their shape, height and pitch. The pitch describes the distance between 2 corresponding micro-structures. It is defined from the initiation of the ascent of the first to the same point at the next feature, as is indicated in Figure 4.5 for field D1. Thus, the pitch indicates the displacement of one micro-pillar or micro-rib relative to another.

Concerning the micro-structures two fields with micro-pillars and two fields with a micro-rib pattern were reproduced into the polymer. To acquire knowledge on the exact dimensions of the stamper, it was inspected with an atomic force microscope (AFM) before molding. As for the micro-pillars,

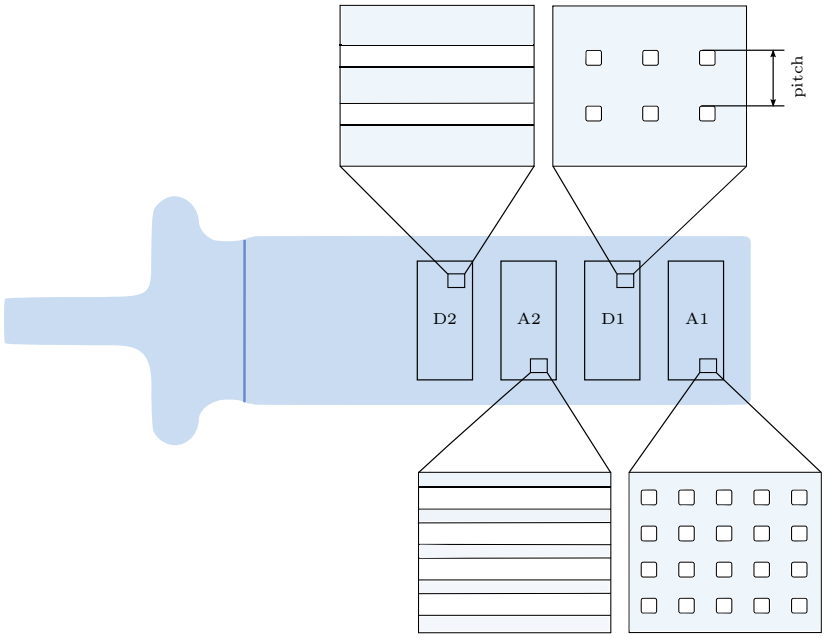

Figure 4.5. Part design with details on pillars (field A1 and D1) and micro-ribs (field A2 and D2).

field A1 consists of micro-pillars with a square base and a height of 1.218 µm. The pitch was measured to be 1.969 µm along the x-axis and y-axis. Field D1 differed only slightly from A1 regarding the height, which is 1.204 µm, but strongly regarding the pitch, which is 6.142 µm and 5.909 µm, respectively. In addition, the micro-ribs in field A2 displayed a height of 1.259 µm and a pitch of 2.047 µm. In contrast to that, field D2 was made of ribs of 1.215 µm height and 6.221 µm pitch.

4.4 Deformation

The deformation of polymer micro-structures occurs due to thermally induced stresses, which result from the shrinkage of the ground plate and the dimensional restrictions of the tool. To reduce those stresses and the demolding forces resulting from them, the shrinkage behavior, which develops due to the processing parameters, has to be understood and controlled. Therefore, case study 2 investigated the shrinkage behavior of the ground plate using simulation, regardless of the design of micro-structures. Furthermore, the findings from the simulations were compared to dimensional measurements of molded parts right after demolding.

4.4.1 Injection molding simulations

Since most research groups, who included simulations on the demolding behavior in their works, only conducted structural mechanics simulations [15, 18, 62], the impact of processing parameters on the demolding behavior has not been included in these simulations so far. Therefore all simulations within this work were conducted with SIGMASOFT® software (SIGMA Engineering GmbH, Aachen, Germany), since the SIGMA-stress package provided the tools to simulate and subsequently evaluate the shrinkage behavior resulting from the processing conditions. To obtain accurate information, the mold was modeled to closely resemble the genuine mold. Figure 4.6 illustrates the mold, which was prepared for the simulations. It contained the fixed and moveable half, which incorporate the part, the ceramic heating and the cooling system. Additionally, the hot runner system as well as the ejector pins were copied from the genuine mold. To reduce the number of cells of the mesh and hence the simulation duration, the hot runner was modified to a less complex geometry. Therefore, the insulation was subtracted from the hot runner and at the same time a cylindrical linkage to the part was added, to ensure connection between hot runner and part. These changes to the geometry are displayed in Figure 4.6. Consequently, the mesh was scaled to ensure at least 5 elements through the thickness direction of the part.

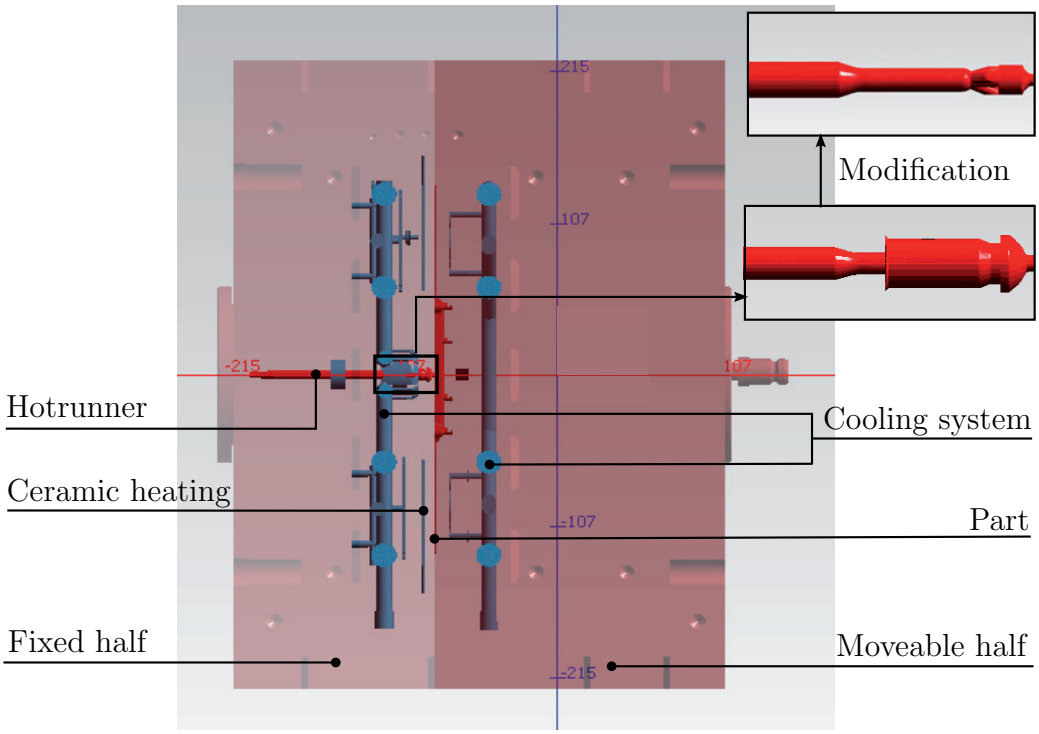

Figure 4.6. Mold design for injection molding simulations.

The materials for the simulations are summarized in Table 4.7. The aim was to use the same polymers in the simulations as were used for the experimental part. Thus, data from in-house characterization of DOW PP C7069-100NA was implemented into SIGMASOFT®. Since the SIGMASOFT® database provided only limited material datasets, material data on COP and PMMA was used from the Autodesk® Simulation Moldflow® (Autodesk. Inc., San Rafael, California, U.S.) database. Hence, the material data of Zeonor 1060 R was exported from Moldflow® database and imported into SigmaSoft®. The same procedure was applied for PMMA with DELPET 80N from Asai Kasei Chemicals Coorporation. This material closely resembles DELPET 70NH which was used for the experiments.

Table 4.7. Overview on trade names and data export for simulation.

Class	Trade name	Data exported from
PP	DOW PP C7069-100NA	in-house characterization
COP	Zeonor 1060R	Autodesk Moldflow® database
PMMA	DELPET 80N	Autodesk Moldflow® database

The process settings were modeled from the injection molding process (compare Table 4.8). All parameters were chosen in accordance to a standard process setting except for the mold temperature, whose impact on the shrinkage behavior was analyzed. This means the mold temperature was varied in the range of 30 to 70 °C for PP, 60 to 90 °C for COP and 70 to 90 °C for PMMA. The packing pressure was set in accordance to the description in Section 4.3.1, where the five values given below describe the level of the packing pressure at 0, 0.25, 0.45, 4.45 and 4.55 seconds of the cooling time.

Table 4.8. Molding conditions defined in simulation.

Polymer	T_b	T_m	Injection speed	Packing pressure	Cooling time
	°C	°C	cm^3/s	bar	s
PP	220	30 – 70	35	370-300-200-100-100	40
COP	260	60 – 90	50	600-300-200-200-100	30
PMMA	270	70 – 90	35	750-400-200-200-100	30

Also, the variothermal and hot runner heating were implemented with 'Heatmed' material from the SIGMASOFT® database. The variothermal heating was then set to 180 °C and implemented into the cycle by inserting a delay time of 10 s at the beginning. For this duration, the ceramic element was heating the stamper with 1000 W, which approached the heating capacity of the real heating element. Moreover; the cooling time was also set to the actual cooling time.

4.4.2 Experimental verification of simulation results

To evaluate the simulations, deformation in flow direction of the part at the initiation of the demolding stage was deduced from the results. For that purpose, the results for displacement in flow direction were evaluated as displayed in Figure 4.7. Since SIGMASOFT® calculates the shrinkage results and fits them to the part afterwards, the difference between the displacement at the end of the film gate (indicated as 'starting point') and the respective position on the part was used for comparison as depicted schematically in Figure 4.7. Hence, 10 approximately equidistant measuring points were picked with the cursor control and analyzed regarding the overall shrinkage and the change over the part length.

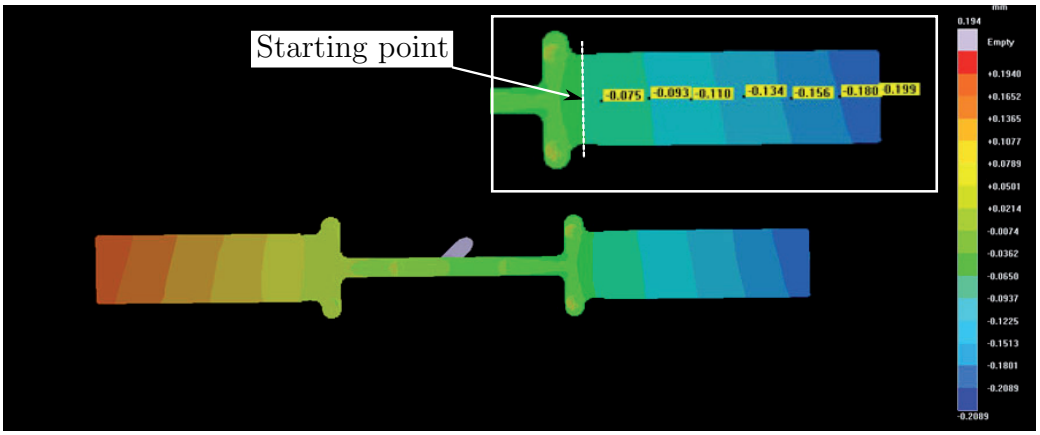

Figure 4.7. Evaluation of displacement in injection molding simulation.

In addition, the results obtained from injection molding simulations were verified experimentally by measuring the dimensions of the slides right after processing with a sliding caliper. For that purpose, the length, width and thickness of 3 slides per configuration were determined. For each dimension 5 checkpoints were selected (compare Figure 4.8), which summed up to a total of 15 values per dimension for each configuration. From these the mean value

and standard deviation were calculated and utilized for comparison with the results from the injection molding simulation.

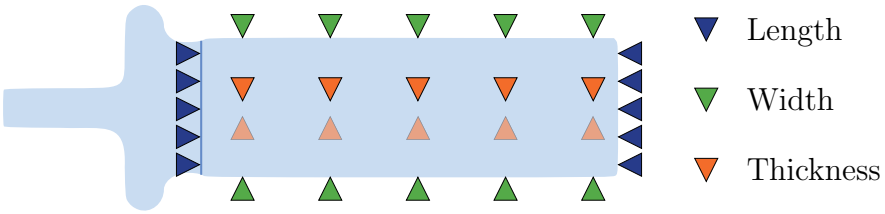

Figure 4.8. Checkpoints for dimensional measurements.

4.5 Factors affecting demolding energy

In addition to the analysis with injection molding simulations, several factors affecting demolding forces were investigated experimentally. First of all, the number of shots until constant conditions were reached was determined from the machine protocol. As shown in Table 4.9 the electric injection molding machine reached constant values after 5 shots. Using this information a standard method was specified as follows: For each configuration, at least 10 shots were discarded before measurements were performed. The demolding force measurements, which were conducted afterwards, included 10 shots per configuration and were obtained from constant process conditions.

Regarding the stampers, two standard inserts, which are depicted in Figure 4.9, were used for all case studies except for case study 6. The testchip included a micro-rib pattern with the smallest dimension of 55 µm. Moreover, these ribs were arranged in flow and perpendicularly to it and were then placed on a groundplate, which was fitted into an adapter, as is indicated by the circle in Figure 4.9. Due to that, only the micro-structures and the surrounding support area were fabricated from nickel. The rest of the mold area was made of steel without surface polish. As a consequence mechanical interlocking could occur, which has to be considered when comparing the testchip to the medical application.

The design of the medical application, which was used for the investigations, was derived from a filter application. Therefore it incorporated a number of micro-channels and reservoirs with channel depths of 25 and 50 µm and reservoir dimensions up to 500 µm, but also areas with even smaller dimensions, which serve as filters. In this case the whole stamper was made from nickel, as the micro-features were distributed all over the device.

Table 4.9. Machine protocol of the first 30 COP shots after starting the machine.

Protocol cycle counter	Injection time	Maximum injection pressure	Switch-over pressure	Switch-over volume	Cycle time
	s	bar	bar	cm^3	s
1	0.26	159	104	13.988	35.73
2	0.35	1383	1139	13.979	35.83
3	0.40	1334	1110	13.985	35.86
4	0.33	1424	1122	13.985	34.04
5	0.27	1139	1139	13.994	84.05
6	0.27	1143	1143	13.991	84.08
7	0.27	1146	1146	13.979	84.16
			...		
11	0.27	1152	1152	13.997	84.05
12	0.27	1164	1164	13.982	84.06
13	0.27	1144	1144	14.000	84.06
			...		
17	0.27	1142	1142	14.000	84.06
18	0.27	1148	1148	13.979	84.06
19	0.27	1145	1145	13.985	84.06
			...		
23	0.27	1144	1144	13.988	84.06
24	0.27	1147	1147	13.988	84.06
25	0.27	1148	1148	13.979	84.06
			...		
29	0.27	1146	1146	13.991	84.06
30	0.27	1152	1152	13.976	84.06

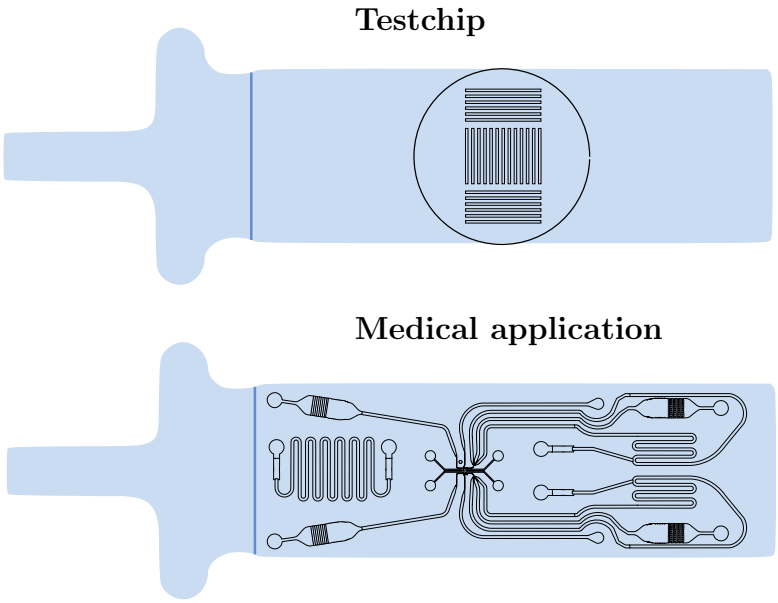

Figure 4.9. Stamper design of the medical application and testchip.

4.5.1 Polymer

The polymer class, trade name and suppliers of all polymers which were used in this work are shown in Table 4.10. These were used in all experimental case studies. As the investigations concentrated on applications in the medical field, no mold release agents or other processing aids were added in order to avoid contamination. Moreover, the mentioned COP and COC-TPE were not only processed independently, but also blended. For that purpose 10 and 40 wt% COC-TPE were added to COP to alter its properties and hence change demolding behavior.

Table 4.10. Overview on trade names and suppliers of polymers.

Class	Trade name	Supplier
PP	C7069-100NA	DOW Chemical Company, Midland, USA
COP	Zeonor 1060R	Zeon Chemicals LP, Luisville, USA
PMMA	Delpet 70NH	Asahi Kasei Chemicals Corporation, Chiyoda, Japan
COC-TPE	COC-elastomer E-140	Topas Advanced Polymers Inc., Florence, USA

4.5.2 Machine parameters

To ensure comparability within test runs but also among the case studies a standard process setting was determined for each material. These standards are summarized in Table 4.11 and were applied for all case studies included in this thesis, unless marked differently. PP was processed as provided, whereas all other materials were pre-dried in compliance to the recommendations of the suppliers for at least 4 hours prior to processing. This meant 70 °C for COP, 80 °C for PMMA and 60 °C for TPE.

Table 4.11. Standard process settings.

Polymer	T_b	T_m	Back pressure	Injection speed	Switch-over volume	Cooling time
	°C	°C	bar	cm^3/s	cm^3	s
PP	220	40	60	35	14.7	25
COP	260	80	100	50	14.0	10
PMMA	280	80	100	35	14.7	10
COC-TPE	240	60	130	50	11.6	10

All settings were established within the processing ranges recommended by the suppliers. The dosage volume and the temperature of the variotherm heating were the same for all polymers and due to this not included in Table 4.11. For all polymers the dosage volume was 25 cm^3 and the variotherm heating was set to 200 °C nominally, which resulted in heating to 110 °C at the cavity surface of the stamper. For PP this temperature approaches the melting temperature, whereas for COP and PMMA this is just above their T_g to support filling of the micro-structures. Therefore, the ceramic heating element was triggered at the onset of the mold closing motion and kept at 200 °C until the initiation of the cooling time. Due to the delay at the initiation of each cycle to guarantee the propagation of the vacuum the variotherm heating was maintained for approximately 10 s. Regarding the switch-over volume, a filling study was conducted for each polymer, to ensure optimum filling conditions.

The barrel temperatures (T_b) and mold temperatures (T_m) were set at high levels within the usual processing ranges to ensure high replication accuracy and low thermally induced stresses in the polymer. The mold opening

proceeded at 0.1 mm/s, which was as slow as possible with regard to machine capabilities to ensure precise measurements of the demolding forces. To avoid unwanted acceleration at the beginning of the mold opening stage, the injection molding machine automatically reduced the clamping force from 600 N to 0 N slowly. Only afterwards did the actual opening motion start. This means the cooling time of COP, PMMA and TPE added up to approximately 30 seconds, although the remaining cooling time was set to 10 seconds only. This was not the case for PP, as the first measurements with this material had been conducted before considerations regarding the cycle time were made.

For processing of the TPE blends and COC-TPE the parameters were derived from COP but changed in accordance to the processing recommendations of the COC-TPE. First of all, the barrel temperature and mold temperature were reduced by 20 °C, since COC-TPE exhibited better flowability compared to COP. The back pressure for the TPE and the COC-TPE was increased to 130 bar as the patches of COP with 10 or 40 wt% TPE required better mixing. In addition, the switch-over volume was reduced to 11.6 cm^3 for COC-TPE, as its density deviated strongly from COP at elevated temperatures.

For the tests on the process parameters the demolding temperature was chosen for a detailed investigation. Accordingly the mold temperature was varied in a range of at least 30 K for each polymer to examine its impact on the demolding forces. For that purpose PP was investigated in a range from 30 to 70 °C, COP from 60 to 90 °C and PMMA from 70 to 90 °C. Furthermore, the behavior of COC-TPE and the COP-TPE blends was analyzed in a range from 40 to 70 °C and 40 to 90 °C, respectively. Due to the slow opening motion of the mold, the mold temperature was found to equal the demolding temperature for all experiments. This was verified by means of a temperature sensor installed in the tool and contact measuring at an open mold position right after part fabrication.

4.5.3 Micro-structure design

For the experimental investigation of the impact of micro-structure design (case study 6) on the demolding energies two mold inserts were fabricated, as depicted in Figure 4.10. These were named 'Designchip' and included similar micro-rib patterns, which were arranged parallelly to the flow direction (insert (a) in Figure 4.10) or perpendicularly to it (insert (b) in Figure 4.10). The micro-structures themselves displayed a width of 100 µm and a height of 50 µm, at a pitch of 200 µm. Both inserts could be installed in two different directions, to place the structures either close to the gate or far from it.

Depending on the installed insert and its orientation four different settings were achieved:

- In flow direction and close to the gate,
- in flow direction and far from the gate,
- perpendicular to flow and close to gate or
- perpendicular to flow and far from gate.

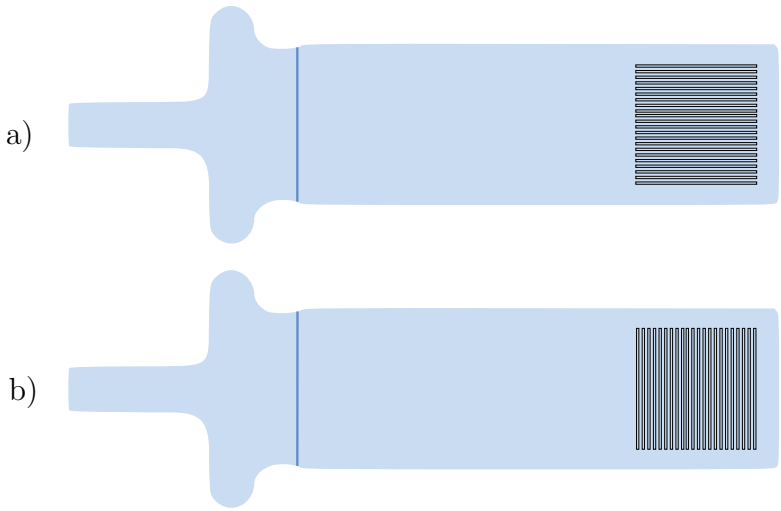

Figure 4.10. Stamper design for the Designchip (case study 6) on the impact of micro-structure arrangement in flow direction (a) and perpendicular to it (b).

Since a standard setting proved impractical for the comparison of the polymers, as their demolding behavior was strongly influenced by the processing conditions, the behavior over a temperature range was investigated. Therefore, PP was investigated in a range from 40 to 60 °C, COP from 60 to 90 °C and PMMA from 70 to 90 °C for each configuration.

4.5.4 Tool surface

For the analysis of the impact of tool coatings a nickel stamper identical to the testchip described in Figure 4.9 was fabricated. Afterwards the micro-structured areas were coated with TiN and fitted into the adapter. Each

polymer was then processed with varying mold temperature settings, to deduce the combined impact of TiN coating, polymer and demolding temperature on the demolding energies. The high and low temperature settings which were used for evaluation are summarized in Table 4.12.

Table 4.12. High and low settings of T_m for the analysis of the influence of TiN on demolding forces.

Polymer	Low setting	High setting
	°C	°C
PP	40	60
COP	70	90
PMMA	75	90
COP10TPE	40	60
COP40TPE	40	60
COC-TPE	40	60

4.6 Stability and reliability of measurements

To investigate the stability and reliability of the measurements, some experiments were performed repeatedly. For that purpose COP was repeated at random with the medical application at T_m 70 °C with and without variothermal heating. In addition, certain prerequisites have to be met, to allow for these comparisons to be made. As stated earlier, good replication quality is an important feasibility factor for experiments concerning demolding forces. Good replication of the micro-structures has to be ensured, to compare results from demolding force measurements correctly. Otherwise different degrees of filling of the micro-structure would result in varying surface interaction. Hence, due to changes in friction and surface adhesion variations in the demolding force would occur. As a consequence, all case studies on demolding force (case studies 3 to 7) were verified with an FRT MicroProf® confocal microscope (Fries Research & Technology GmbH, Bergisch, Germany).

Depending on the stamper, three representative lines were chosen, to examine the channel depth that was achieved in the fabrication process (compare Figure 4.11). In the first test run, three samples of each configuration

were analyzed. From the results the reproducibility of the characterization method could be deduced, which allowed for a smaller number of samples to be investigated in the next run. Subsequently, one sample per configuration was analyzed. The depth of the micro-channels along each line was evaluated at six different locations to obtain mean value and standard deviation for each given configuration.

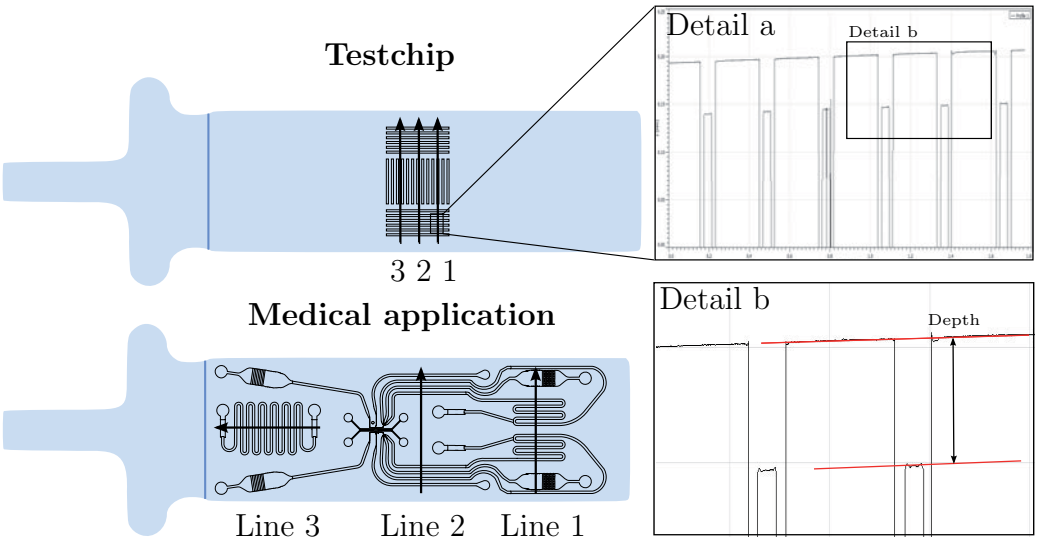

Figure 4.11. Lines, topography measurements using FRT and evaluation of channel depth.

Detail (a) in Figure 4.11 displays the profile that was obtained from one line. As the resolution of these measurements was 1 µm, the drops in intensity formed due to the tapering of the side walls, which could not be recorded with this measuring rate. Detail (b) specifies the evaluation of the depth, which was performed by measuring the distance between the top of the microstructures and the respective bottom. Two lines (one at the top and one at the bottom) were inserted to minimize the impact of the surface roughness on the results.

4.7 Glossary of measurements

To facilitate labeling of materials and measurements, Table 4.13 defines the terms and nomenclature, which were used in Section 5. Nomenclature of the stampers was performed according to their application (like medical application) or to the main goal of the investigations performed (like testchip or designchip). For the testchip information on the coating (either nickel (Ni)or

titanium nitride (TiN)) is included, whereas the designchip is specified by information on the orientation (either in-flow (I) or perpendicular (P) to it) of the micro-channels. The corresponding abbreviations, which are given in brackets, will be applied in Section 5.

The labeling of the polymers follows their class and includes information on the composition. PP, COP, PMMA and COC-TPE are used to describe the corresponding native materials. For blends of COP with 10 or 40 wt% COC-TPE COP10TPE and COP40TPE will be used. Regarding the processing parameters, the application of variotherm mold heating will be indicated with a V, whereas non-variotherm (NV) process setting indicated the default value, which will not be added to the label. Moreover, the label of each measurement includes the demolding temperature and the melt temperature, if two melt temperatures were investigated for the same set of parameters. This applies for PMMA, which was investigated at barrel temperatures of 270 and 280 °C, and for COP-COC-TPE blends, which were investigated at 240 and 260 °C.

Table 4.13. Summary of nomenclature of design/coating, material and machine parameters used for labeling measurements.

Design/Coating	**Material**	**Machine parameters**		
		T_m	V	T_b
Medical application (MedA)	PP		V	
Testchip Ni (Ni)	COP		NV	
Testchip TiN (TiN)	PMMA			
Designchip inflow (I)	COP10TPE			
Designchip Perflow (P)	COP40TPE			
	COC-TPE			

MedAPMMA80V270, for example, would specify a sample, which was fabricated from PMMA with the medical applications stamper (MedA) and variotherm heating (V). The polymer was processed at a barrel temperature of 270 °C and the part was demolded at 80 °C.

Chapter 5

Results

5.1 Replication accuracy

Case study 1 aimed at determining optimum processing parameters to achieve high replication accuracy for PMMA. Therefore, preliminary tests were performed to obtain the boundaries for the DoE approach. In addition to these the systematic testing plan was set up and executed for COP. However, during the first PMMA setting, the replication failed despite prior success. Figure 5.1 illustrates the part failure which deemed demolding of PMMA unsuccessful. During the demolding stage part breakage occurred, since the areas with micro-pillars stuck to the stamper (compare marked areas in Figure 5.1). This occured due to several reasons: On the one hand the polymer experienced higher displacement at the end of the flow path, due to shrinkage. On the other hand, the cooling system was not inserted symmetrically in the fixed half compared to the moveable half. Due to that, thermally induced stresses resulted from the locally unbalanced temperature distribution. During demolding, the parts were peeled off the stamper until the bending reached a critical value, where the induced stresses exceeded the strength of the polymer with the given dimensions and therefore broke.

To identify the potential causes of the part failure during the implementation of the DoE an Ishikawa diagram was compiled, as a common quality management tool. The categories, which were selected to deduce the source of variation in the demolding behavior between the preliminary experiments and the performance of the DoE, are displayed in Figure 5.2. These included all factors contributing to a particular effect like part failure. This is machine, tool, process, personnel, polymer and environment. To begin with, human error could be excluded, since all experiments were conducted by the same operator and have been redone several times. However, a number of

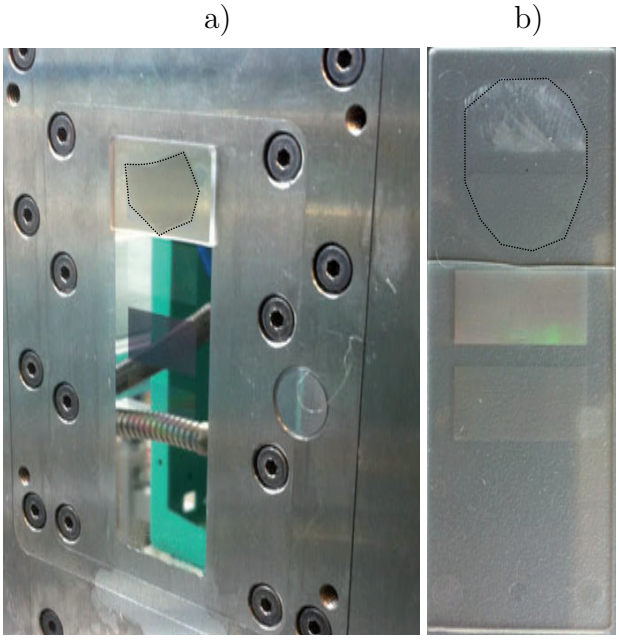

Figure 5.1. Part failure of PMMA during demolding: micro-structured areas sticking to the stamper (a) and after removal (b).

technical factors remained to be investigated.

Beginning with the machine, the plastification unit was expected to pose problems with regard to the necessary accuracy of the movements. Especially the non-return valve seemed to work inaccurately for such small volumes, which could cause uncontrollable changes of the switch-over volume. This in turn could influence the residual stresses and hence the critical stresses, which could be endured during demolding. This issue was investigated with the machine data recordings obtained from a series of test runs. Although the maximum injection pressure varied from 1300 to 1900 bar within 40 shots, no fluctuations were observed from switch-over pressure and switch-over volume. Due to that, the fluctuations in the maximum injection pressure were attributed to the material and might have originated from moisture, whereas the functionality of the non-return valve was not limited.

Several factors concerning the polymer were addressed. First of all, factors affecting the rigidity of the polymer were considered. These included ageing of the polymer, the impact of contact with oxygen and degradation during the process, which were dismissed after conducting a literature research on their impact. Secondly, the humidity of the polymer was taken into account. However, a residual moisture content after drying would have enhanced flexibility due to the plasticizing effect of water rather than increasing rigidity. Furthermore, the air moisture during the performance of

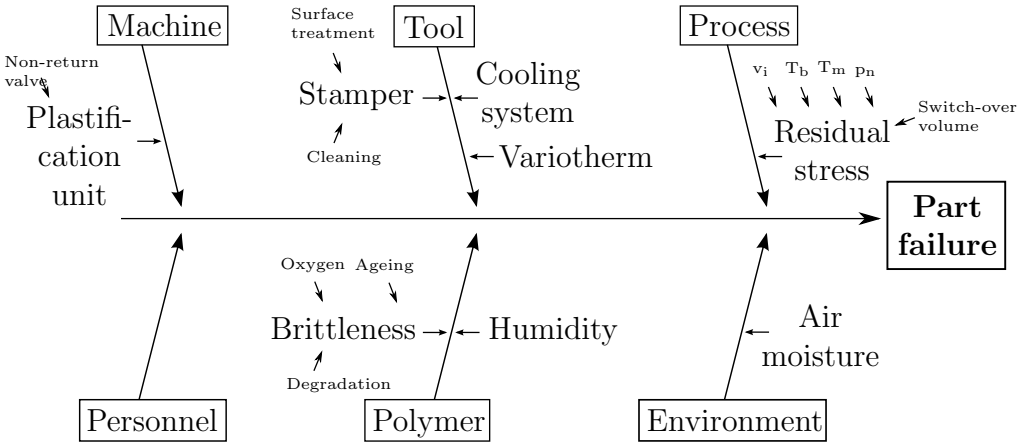

Figure 5.2. Ishikawa diagram to identify the source of variation which caused part failure during the implementation of the DoE.

the experimental work was kept in mind, because the water could have condensed inside the tool. Nevertheless, it was concluded, that condensation was unlikely to occur at such high mold temperatures (75 to 90 °C) and with the evacuation preceding each cycle. Hence, humidity for both, the polymer and the air, was excluded as the factor causing part failure as well.

All in all, tool and process were expected to be most influential on successful demolding. The variotherm heating and cooling system as well as the process parameters were considered, as these mainly influence the residual stresses in the polymer. Due to that the injection speed (v_i), T_b and T_m were compared to settings which had been used in other reports. A summary of this comparison is given in Table 5.1. Unfortunately all these settings were based on different PMMA grades which require different processing parameters. As a consequence the settings below differed strongly from the parameters used in this thesis. Thus, a comparison among the reports and the parameters applied in this work is impossible. Additionally, those reports did not mention part failure as a feasibility constraint. The packing pressure (p_n) was not included as it was ineffective on the part, as explained before. Finally, the influence of the residual stresses due to the tool construction and process parameters was dismissed as well, since the process parameters had been determined in preliminary experiments, where successful demolding had been achieved.

At last, the stamper surface was reassessed, because the stamper was cleaned with isopropanol to remove polymer residue from the preliminary tests before starting the DoE. A likely explanation for the part failure could be that the nickel stamper had been coated with an organic layer. The composition however, was not revealed by the supplier. With regard to the-

Table 5.1. Comparison of processing parameters applied for PMMA in different reports.

Work	Grade of PMMA	T_b	v_i	T_m
-	-	°C	mm/s *cm^3/s	°C
Attia (2010) [2]	N.N.	230 – 250	200 – 300	72 – 80
Chen et al. (2010) [7]	CM205, Chi-Mei	220 – 250	40 – 80	60 – 80
Chien (2006) [10]	CM205, Chi-Mei	240 – 260	300 – 400	60 – 80
Lee et al. (2010) [42]	IF870S, LG MMA	210 – 250	5 – 15*	40 – 75
Marson et al. (2011) [45]	N.N.	240 – 255	200 – 300	70 – 81

oretical considerations, lower surface energies result in a decrease in adhesive forces between polymer and mold. Thus, Guo et al. (2007) [28] reported surface energies of PMMA and Ni to be 0.04 and 1.7 J m^{-2}, respectively, while the interface energy is approximately zero. Therefore, the application of PTFE as a coating with surface energy of 0.018 J m^{-2} will lower the adhesion and thus the adhesive force. This was also confirmed by Peng et al. (2005) who had reported the low surface energy resulting from such a coating [54]. Presumably this organic coating had lowered the surface adhesion during the preliminary experiments considerably, thus facilitating demolding of PMMA.However, it was removed either from the cleansing agent or wore off during the performance of the DoE for COP.

Furthermore, these thermally more insulating materials affected the temperature balance between polymer and mold. In general, an organic surface layer displays lower thermal conductivity than metals. As a consequence a higher temperature is maintained within the mold, which facilitated relaxation mechanisms and the reduction of residual stresses. As mentioned above, this coating was either based on PTFE or on an organo-silicone compound, which are both disadvantageous due to their poor wear resistance. With hindsight though it appeared impossible to determine whether the or-

ganic coating was dissolved by the isopropanol or worn by the performance of the DoE for COP. Certainly, this coating would not be applicable on industrial scale. As the coating could not be recovered, the fabrication of parts from PMMA and hence comparison to COP was impossible. The main goal of case study 1 was to successfully replicate the micro-pillars on PMMA. Thus, the parts of COP were not evaluated, since they were merely meant for comparison.

5.2 Injection molding simulation

To obtain information on the impact of processing parameters on the demolding behavior, injection molding simulations with SIGMASOFT® software were conducted. In contrast to the structural mechanics simulations, which were performed in other reports, the thermal stresses in the polymer were not calculated. Instead, as the tendency to shrink has been reported to be the most important factor affecting demolding forces, the temperature dependence of the in-mold shrinkage was investigated. Figure 5.3 shows the impact of the demolding temperature on the shrinkage behavior of PP, COP and PMMA. The displacement in longitudinal direction of the part describes the displacement of the part at the starting point of the demolding stage compared to the initial length of 75.6 mm, which equals the dimensions of the mold.

All three materials showed a linear correlation between the lengthwise shrinkage and the distance from the gate. This means the lengthwise displacement due to shrinkage increased with increasing distance from the gate. Due to the higher mold shrinkage of 1.5 to 3 % of PP [36] compared to 0.1 to 0.3 % of COP and 0.2 to 0.6 % of PMMA the increment is stronger for PP. Moreover it was confirmed, that the shrinkage increases with decreasing mold temperature as well, as illustrated for PP. Thus, the shrinkage in longitudinal direction also correlates with the demolding temperature. As a consequence, high demolding temperatures are favorable with regard to minimized shrinkage and thereby reduced friction between polymer and stamper.

In addition, the results obtained from the simulations were compared to the actual part dimensions after demolding of an unstructured part and the medical application. Figures 5.4 and 5.5 show the correlation of the alternation of length with the demolding temperature for PP and for COP, respectively. For both materials a linear correlation of the shrinkage and the demolding temperature is suggested by the results of the injection molding simulations. Nevertheless, the measurements of the COP parts after fabrication reveal considerably lower shrinkage and even expansion at higher

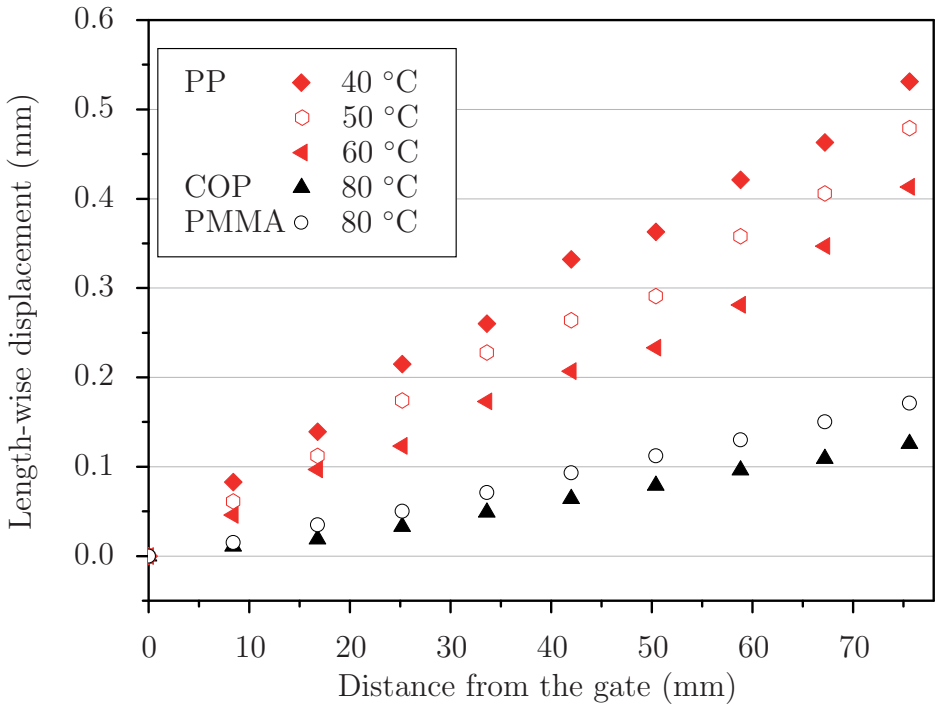

Figure 5.3. Simulation of in-mold shrinkage for COP and PMMA and for varying demolding temperatures of PP.

mold temperatures. In case of the medical application, this phenomenon is attributed to the micro-structures, which are confined in the micro-cavities and, as a consequence, hinder shrinkage of the ground plate as well. Still, the unstructured stamper displays the same trend. In this case, the unpolished steel surface seems to favor physical attraction between the polymer and the stamper, which in turn hinders the shrinkage of the ground plate. This was attributed to the larger contact area due to the higher surface roughness.

Since PP exhibits higher mold shrinkage than COP, the part length decreases stronger with decreasing mold temperature. However, the measurements after the fabrication process reveal different behavior than suggested by the simulations. At 30 °C the results coincide, whereas the effective shrinkage exceeds the predictions from simulation at 60 °C by approximately 40 %. This means, acoording to the injection molding simulations, shrinkage is the main factor determining part dimensions of PP. However, other factors such as crystallinity seem to influence the shrinkage behavior as well. Due to that, to date injection molding simulations are insufficient to predict the demolding behavior. Nevertheless, the information on the shrinkage of amorphous polymers due to the processing parameters can be applied to improve predictions from mechanical (FEM) simulations.

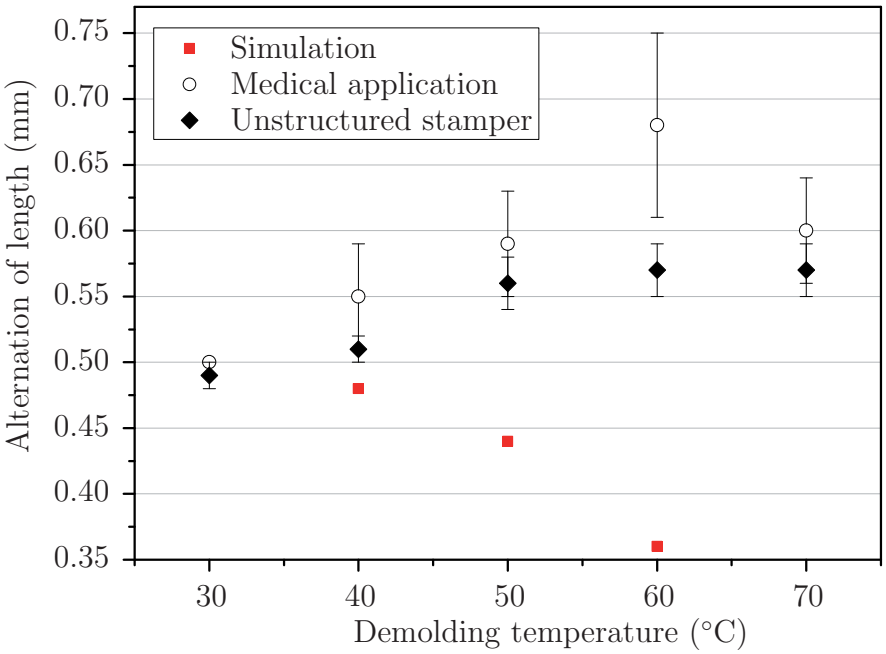

Figure 5.4. Comparison of shrinkage deduced from simulation and actual values from the fabrication process of PP.

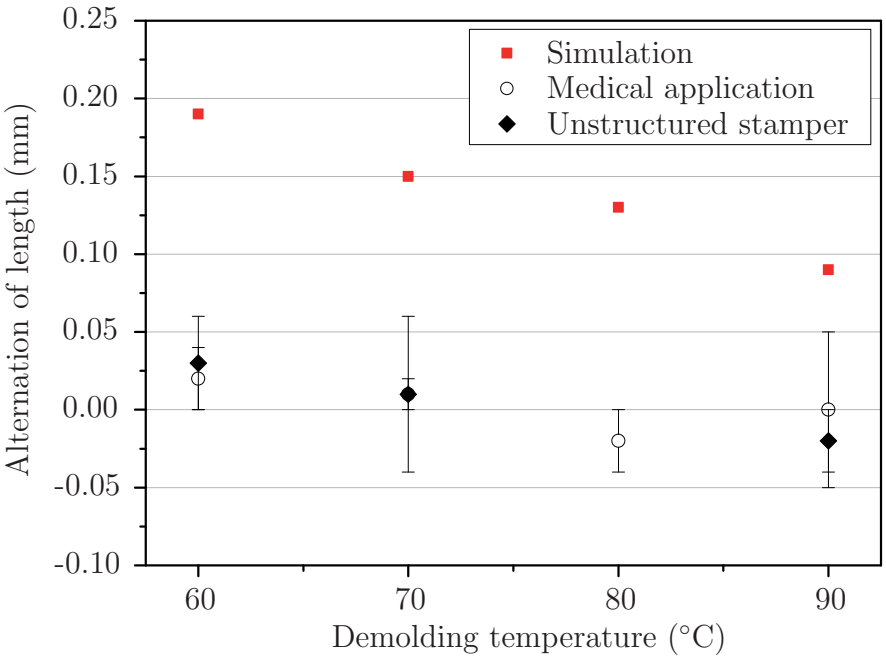

Figure 5.5. Comparison of shrinkage deduced from simulation and actual values from the fabrication process of COP.

5.3 Factors affecting demolding energy

This section deals with the main factors affecting demolding energies as defined in Section 3.3. First of all, the comparability of different settings was ensured by determining the replication accuracy for different settings. In addition, the impact of polymer, process settings, micro-structure design and tool surface were investigated. Hence, semi-crystalline and amorphous morphology as well as thermoplastic elastomer, T_m and the influence of variothermal heating were compared. Furthermore, tests on the influence of the orientation of the micro-structures were conducted. Regarding the tool coating, titanium nitride was disposed on a nickel stamper to examine its impact on demolding forces.

5.3.1 Prerequisites for demolding energy measurements

In addition to the analysis on the replication quality of COP and PMMA, certain standards regarding replication accuracy had to be met for all configurations. This is a crucial issue with regard to the comparability of the demolding force measurements. Good replication accuracy had to be ensured as a prerequisite for comparing demolding energies among different polymers, process settings, designs and coatings. First of all, the reproducibility of the measurements was confirmed. For that purpose three parts of NiCOCTPE60V and MedACOC10TPE70V were investigated. Table 5.2 summarizes the mean value (MV) and standard deviation (SD) for each slide and shows that neither measurements from the same setting nor measurements with different settings have a significant deviation regarding the replication accuracy. The same result was encountered for the effect of polymer and stamper coating on the replication quality. Table 5.3 illustrates the fact, that there was no significant deviation among PP, COP and PMMA. Additionally, the coating of the testchip with TiN did not affect the replication quality either.

Subsequently, the effect of processing parameters on the replication accuracy was investigated. Table 5.4 depicts the influence of barrel and mold temperature. For that purpose two barrel temperatures (270 and 280 °C) and three mold temperatures (ranging from 70 to 90 °C) were examined for PMMA. Table 5.4 shows that these two process parameters did not impact on replication quality either. At last, the impact of variothermal heating of the stamper was investigated (compare Table 5.5). For that purpose, the replication qualities with and without variothermal heating for COP blends and COC-TPE were examined at the same barrel and mold temperatures. As with all other configurations, no significant deviation could be detected.

Table 5.2. Reproducibility and replication accuracy of different polymer and stamper configurations (V=ON).

Nr.	Stamper	Polymer	T_b	T_m	MV	SD
-	-	-	°C	°C	µm	µm
1	Ni	COC-TPE	240	60	53.73	0.77
2	Ni	COC-TPE	240	60	53.69	0.49
3	Ni	COC-TPE	240	60	53.81	0.92
1	MedA	COP10TPE	240	70	54.01	0.67
2	MedA	COP10TPE	240	70	53.99	0.35
3	MedA	COP10TPE	240	70	54.04	0.19

Nevertheless, the high standard deviations of COP40TPE and COC-TPE have to be regarded.

Table 5.3. Effect of polymer and coating on replication quality (V=OFF).

Stamper	Polymer	T_b	T_m	MV	SD
-	-	°C	°C	µm	µm
Ni	PP	220	40	54.76	0.86
TiN	PP	220	40	54.56	0.69
Ni	COP	260	70	54.85	0.72
TiN	COP	260	70	54.82	0.71
Ni	PMMA	270	80	54.66	0.43
TiN	PMMA	270	80	54.42	0.90

These findings were essential for the evaluation and comparison of demolding force measurements. If the micro-cavities were not filled completely the contact surface between polymer and tool surface would have differed among configurations. Hence, it would have been ineligible to compare demolding energies obtained from different polymers, process settings, designs and coatings. On the contrary, due to the confirmation of replication quality, an important quality prerequisite with regard to comparability was met. Thus, demolding energies which derive from varying configurations can be compared.

Additionally, the reliability of the measurements was investigated by repeating a measurement with COP at 70 °C. It was found that COP yielded a

Table 5.4. Effect of barrel and mold temperature without variothermal heating on replication quality of the medical application (V=OFF).

Polymer	T_b	T_m	MV	SD
-	°C	°C	µm	µm
PMMA	270	70	54.51	0.62
PMMA	270	80	54.42	0.90
PMMA	270	90	53.97	0.67
PMMA	280	70	54.27	0.18
PMMA	280	80	54.58	0.59
PMMA	280	90	54.12	0.66

Table 5.5. Effect of variothermal heating on replication quality of COP-TPE-blends and COC-TPE with the medical application.

Polymer	T_b	T_m	V	MV	SD
-	°C	°C	-	µm	µm
COC10TPE	240	60	NV	54.01	0.21
COC10TPE	240	60	V	54.10	0.10
COC40TPE	240	60	NV	54.35	1.12
COC40TPE	240	60	V	54.31	1.15
COC-TPE	240	60	NV	53.56	0.34
COC-TPE	240	60	V	54.63	1.47

demolding energy of 0.34955 ± 0.02009 Nmm in the first test run and 0.38169 ± 0.05680 Nmm in the second without variothermal heating.

When the variothermal heating was applied the demolding energies were 0.12698 ± 0,00833 Nmm and 0.20168 ± 0.00456 Nmm, respectively. This means, that different measurements of the same configuration with variothermal heating were inaccurate. This finding was attributed to the fact, that the variothermal heating impacts the clamping of the load cell due to thermally induced stresses. These might apply additional loading, which distorts the demolding force measurements and the results. Nevertheless, the repetition without variothermal heating proved to be adequate.

5.3.2 Polymer

The impact of different polymers was examined in case study 3. Griffiths et al. (2010) had already confirmed for PC and ABS, that the average demolding force was influenced differently by different polymers [22]. There are a number of factors, which were identified to account for the demolding behavior of the polymers. Apart from the processing parameters, the morphology, the thermal expansion and mold shrinkage, Young's modulus and surface energy as well as the interface energy between polymer and mold influenced demolding critically. For the polymer involved it was anticipated that morphology (amorphous and semi-crystalline) would yield different behavior when demolded.

On the one hand, amorphous polymers were expected to cause high friction due to their rigid nature, whereas the chosen semi-crystalline polymers tend to be more flexible which should facilitate demolding. On the other hand, the formation of crystals in semi-crystalline polymer leads inevitably to higher shrinkage and subsequently causes higher contact forces between the polymer and the cavity surface. Nevertheless, these could be overcome more easily, due to the elasticity of PP. In practice, PP displays relatively high mold shrinkage of 1.5 to 3 % [36] compared to 0.1 to 0.3 % of COP and 0.2 to 0.6 % of PMMA. Guo et al. (2007) concluded, that materials with low shrinkage, in this case COP and PMMA, would minimize contact forces and hence demolding forces.

Figure 5.6 illustrates the demolding energies of PP, COP and PMMA with the nickel testchip and the medical application. Therefore it is clear that a single (standard) setting can not be selected to compare the demolding behavior of these polymers. Although PP exhibits the lowest demolding energy in configuration with the medical application stamper, the nickel stamper yields considerably higher values. Additionally, PP and COP do show a deviation between the demolding energies from the nickel testchip and the medical application, whereas very small changes are detected for PMMA. Furthermore, this deviation appears in the opposite way for COP compared to PP. This means no unequivocal conclusion could be drawn from this study.

Different demolding behavior was also expected due to the coefficient of thermal expansion: According to the supplier COP exhibits thermal expansion of 7 x 10^{-5} K^{-1}, which is approximately the same as for PMMA (7 to 8 x 10^{-5} K^{-1} [36]). PP, on the contrary, has a significantly higher thermal expansion coefficient of 12 to 15 x 10^{-5} K^{-1} [36], which implies higher changes of specific volume between the melt and the solid state. In addition to that, surface adhesion engages in demolding forces as well. Section 3.2.3 dealt

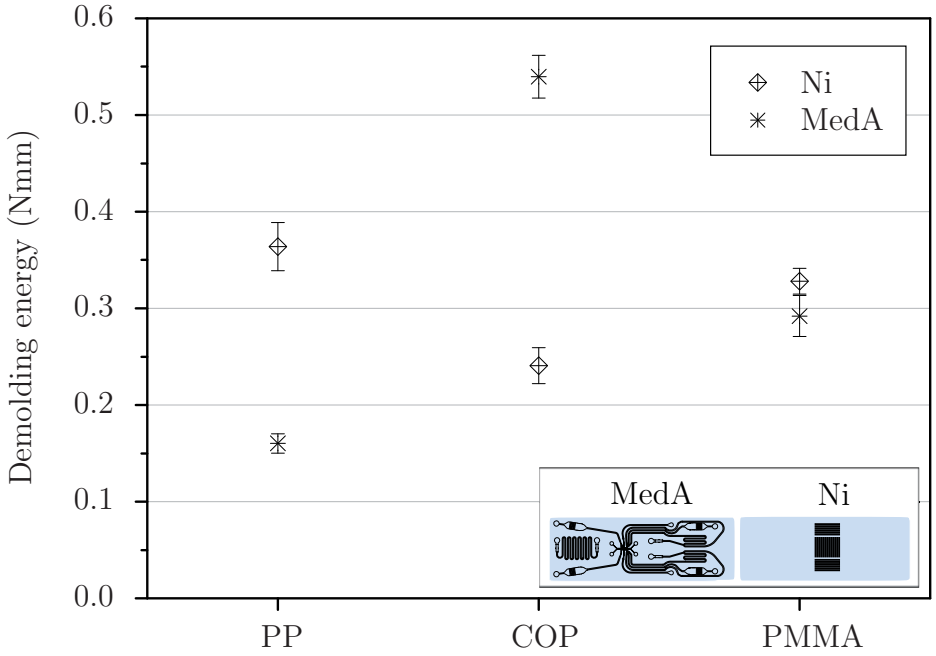

Figure 5.6. Comparison of PP, COP and PMMA at a standard setting for nickel testchip (Ni) and the medical application (MedA).

with the theoretical background on these facts. From Equation 3.3 it was concluded, that a decrease in F_n is directly proportional to a decrease in surface adhesion. As a consequence low surface energies or an increase in the interface energy of the polymer and the stamper surface would be favorable. Additionally, a decrease in F_n could also be achieved by a decrease in the composition Young's modulus K (see Equation 3.5). However, care must be taken as the tensile modulus, decreases with increasing temperature. All in all, because of the importance of processing parameters on the properties of the polymer, no explicit difference in demolding energies resulting from the morphology was found. This might be caused by the strong dependence of the relevant material properties on the processing temperatures (eg. mold temperature).

Also, the impact of an increase in elasticity was investigated in case study 4. Figure 5.7 displays the impact of blending COP with 10 and 40 wt% COC-TPE, when processed at 260 °C barrel temperature. The blending with 10 wt% COC-TPE lowers demolding forces by 75 %. Nevertheless, a higher share of COC-TPE (40 wt%) does not continue the decrement towards lower demolding energies. In fact, demolding energies of COP40TPE approached those of native COP at higher demolding temperatures, due to the increase of surface adhesion at elevated temperatures.

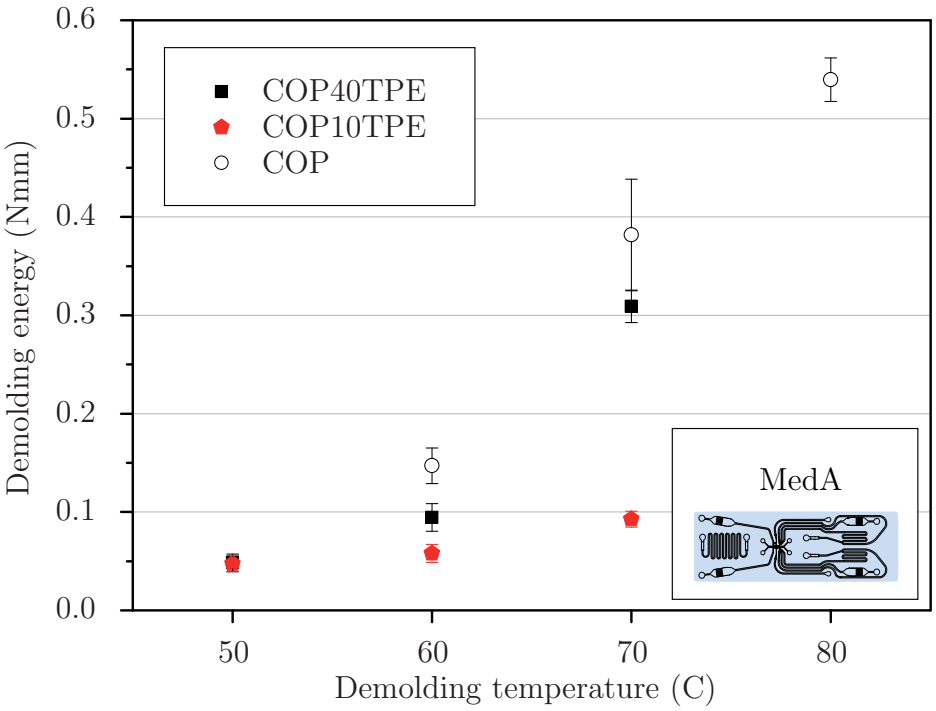

Figure 5.7. Comparison among COP, COP plus 10 wt% TPE (COP10TPE) and COP plus 40 wt% TPE (COP40TPE) for T_b = 260 °C and different demolding temperatures with the medical application (MedA).

When looking at COP with 10 and 40 wt% COC-TPE and COC-TPE (compare Figure 5.8), which were all processed at 240 °C barrel temperature, COP10TPE shows temperature dependent behavior for demolding temperatures ranging from 40 to 70 °C. At high demolding temperatures (60 and 70 °C) the demolding energies appear to be considerably lower, than at 40 and 50 °C. This is in accordance with the conclusions drawn from other works, which reported a critical demolding temperature (T_{dcr}) and a strong increase of demolding forces at temperatures below this critical point [18,67]. At higher COC-TPE concentrations this temperature dependence seems to be suppressed. COP40TPE still shows a slight dependence of the demolding energy on the demolding temperature, especially at 70 °C. Accordingly, native COC-TPE showed the lowest temperature dependence in comparison to the blends. This is attributed to the low Young's modulus of the polymer even at lower demolding temperatures. This means the polymer exerts low contact forces on the micro-structure. Subsequently low frictional forces occur due to the elasticity of the polymer.

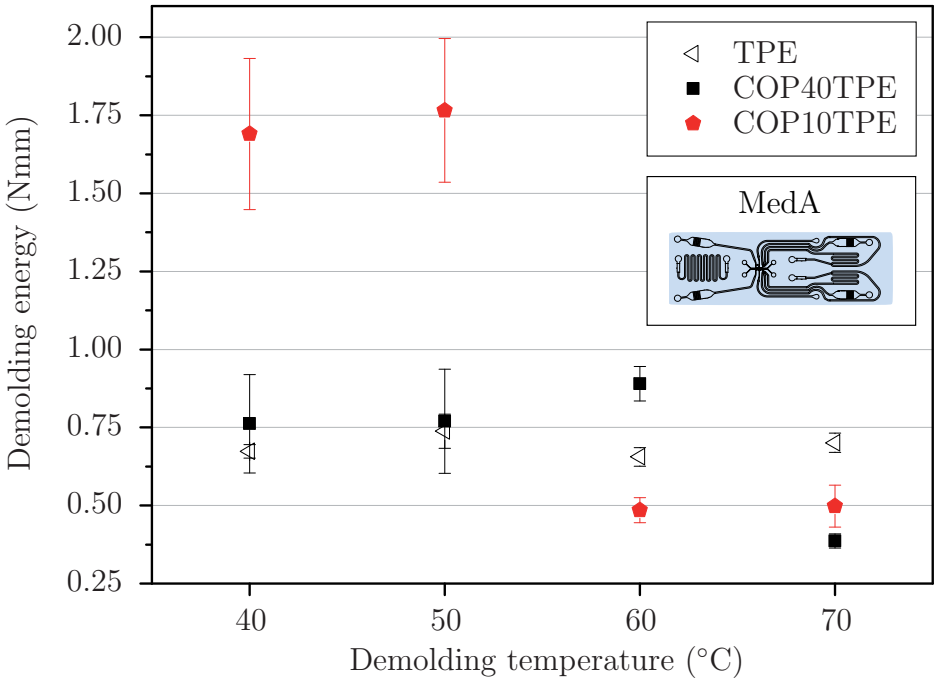

Figure 5.8. Comparison among COP plus 10 wt% and 40 wt% COC-TPE and COC-TPE for different demolding temperatures with the medical application (MedA).

5.3.3 Process parameters

Regarding the process parameters two main factors were analyzed within case study 5 with respect to their impact on the demolding energies. First of all, the demolding temperature was deduced to be the main factor affecting demolding energies from the literature study [15, 17, 18, 67]. Consequently, the demolding behavior of each polymer was investigated in a range of at least 30 K. In addition, the impact of the variothermal heating on the demolding energies was examined. As the replication quality turned out to be equally good for all designs involved in the case studies, the influence of the variothermal process could be traced back to process and material parameters.

The impact of the mold temperature (T_m) on the demolding energies of PP, COP and PMMA was examined. From the literature study a optimum demolding temperature was expected to be found. Theoretical considerations in accordance to Section 4.3.1 involving the specific volume as a function of pressure and temperature suggested a critical demolding temperature (T_{dcr}), where minimum demolding energies for each polymer were expected to be found [15, 17, 18, 67].

Initially, the impact of the demolding temperature on the demolding energies of PP with the medical application and testchip design was examined. Figure 5.9 displays the testchip design that shows significantly higher demolding energies compared to the medical application design. The same behavior is observed for both stampers at different levels. In general, both stampers exhibit the lowest values at 30 and 70 °C. These relatively low values at low and very high demolding temperatures and the higher values from 40 to 60 °C disagree with the findings from other reports [18, 67]. However, so far no investigations on the demolding behavior as a function of temperature of semi-crystalline polymers have been conducted. In fact, the works published so far, dealt with metal micro-injection molding or the demolding forces of PMMA.

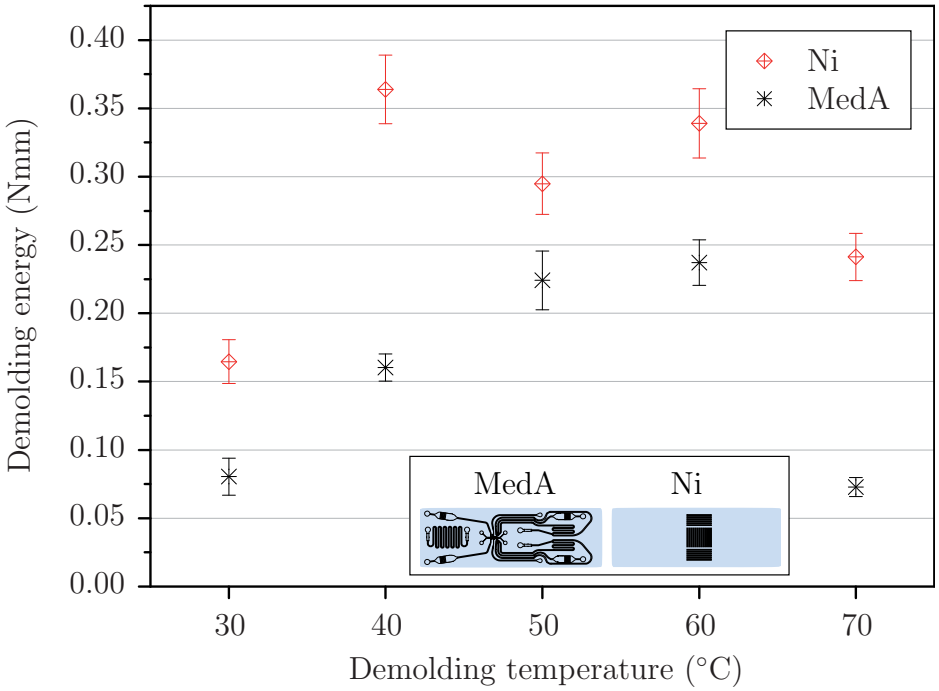

Figure 5.9. Impact of demolding temperature on demolding energy of PP with the medical application (MedA) and nickel testchip (Ni).

The behavior depicted in Figure 5.9 is possibly explained as follows: at 30 and 40 °C for the medical application and at 30 °C for the nickel testchip relatively low demolding energies are obtained. This is attributed to the crystallization behavior of PP, which is decelerated with decreasing mold temperatures. When the melt fills the mold cavity at lower mold temperatures, the polymer cools down rapidly, freezing large portions of the amorphous morphology and small crystallites in place. Due to the different crystallite

size the polymer maintains high elasticity with decreasing mold temperature. Adversely, the size of the crystallites increases with increasing mold temperature since the polymer chains remain flexible for a longer period of time, which enhances crystallite formation. At the same time increasing mold temperatures cause a decrease of the Young's modulus of the material. This means at 70 °C the the mechanical properties had regressed to such an extent, that the demolding was facilitated by the increase in elasticity.

Figure 5.10 compares the demolding behavior of COP and COP with 10 wt% TPE (COP10TPE) for two micro-structures (medical application and nickel testchip). Since the standard barrel temperature for all COP-TPE-blends was chosen to be 240 °C compared to 260 °C for native COP, the demolding energies of COP10TPE exceed those of the native material. This implies that the higher melt temperature enhances relaxation in the material, which consequently loweres frictional forces between polymer and tool surface. Nevertheless, trends in demolding energies remain the same for the native material and for the blend.

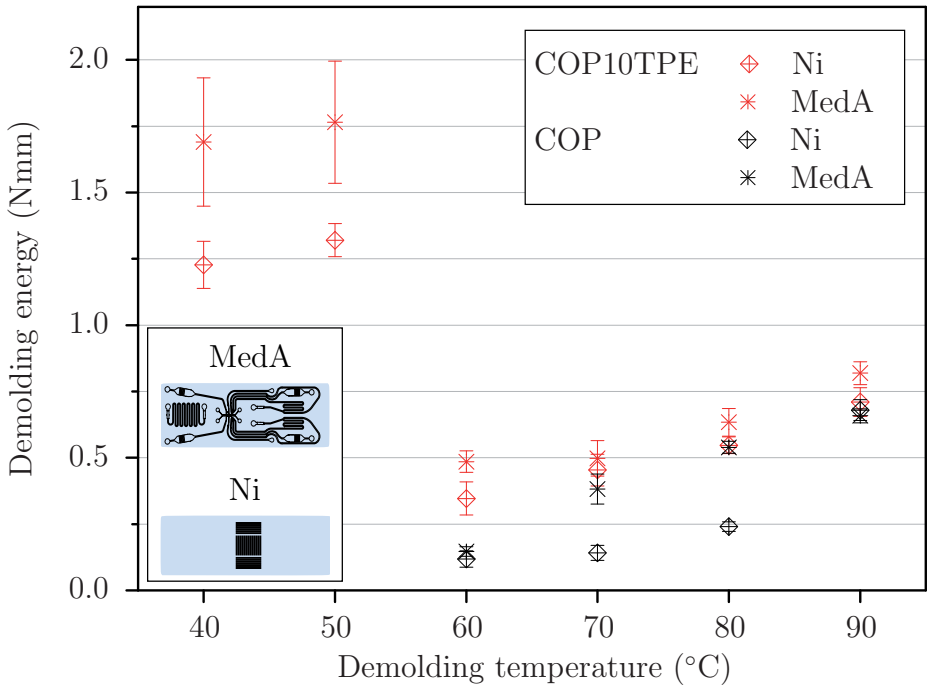

Figure 5.10. Impact of demolding temperature on demolding energies of COP and COP with 10 wt% TPE (COP10TPE) with the medical application (MedA) and nickel testchip (Ni) stamper.

Also, these findings are in accordance with Fu et al. (2008), who investigated the demolding forces at various temperatures for a PIM-feedstock [18].

Similar to what they reported for feedstocks, an according minimum demolding force is found for COP. At this critical demolding temperature (60 °C) the dimensions of the part approximately equal the dimensions of the mold cavity. Due to the thermal expansion and contraction of the polymer, that follows the pvT-curves, an increase in demolding energies occurs towards lower as well as towards higher temperatures from T_{dcr}. Due to the rigidity of native COP, these effects are determined with the addition of 10 wt% COC-TPE. This modification increases the flexibility of the material and hence enables demolding at lower temperatures, although demolding energies increase drastically.

The results from this study were as follows: At lower temperatures the shrinkage of the groundplate is hindered by the micro-cavities. This induces friction between the micro-structures and the surface of the micro-cavity while demolding. As a consequence, the demolding energies increase by approximately 260 % from 60 to 50 °C for the medical application. Likewise the demolding energies increase when applying higher demolding temperatures, which occurred due to the increase in specific volume due to the pressure drop during the demolding stage (compare Chapter 3.2). However, this increment in demolding energies at higher demolding temperatures only constitutes up to 90 % for demolding at 90 °C with the medical application. Overall, these findings are well in accordance with Fu et al. (2008). In addition to T_{dcr}, the strong increase in demolding energies towards lower temperatures and the moderate increase towards higher temperatures agreed with their findings. In accordance to their recommendations, ideal demolding temperatures for COP and COP10TPE are at 60 °C or at temperatures slightly higher than that.

When looking at both stampers, it can be seen, that the testchip displays lower demolding energies compared to the medical application. In this case, which is in contrast to the findings obtained from PP, the medical application shows little variation in demolding energies of both materials. Especially in the ranges of T_m from 70 to 90 °C both materials display similar demolding energies. This convergence of the results with increasing temperature, suggests two simultaneous phenomena: On the one hand the Young's modulus decreases with increasing temperature. Hence, elasticity of the polymer is enhanced, which decreases demolding forces due to lower frictional forces. Since COP10TPE contained material with considerably lower T_g and melting temperature, this decrease at high mold temperatures advanced more severely. This can be seen from the less distinct ascent of COP10TPE at temperatures above 60 °C. On the other hand, increasing temperatures induce stronger forces between polymer and stamper. These seem to result mostly from physical interactions and mechanical interlocking of the 2 sur-

faces. As the elasticity increases, the share of adhesion in demolding energy increases. Due to the increase of demolding energy with increasing temperature the share of adhesion in demolding energies can be derived. This means with increasing temperature surface interaction increases as well.

Additionally, the behavior of PMMA at different mold temperatures was examined. From the set of experiments, successful demolding was achieved for several configurations. The corresponding findings are depicted in Figure 5.11. In contrast to PP and COP, PMMA shows no variation due to demolding temperatures for the medical application compared to the nickel testchip. Furthermore, the medical application does not cause any changes in demolding energies, whereas the demolding energies and even part failure vary strongly for Ni. To explain this phenomenon further investigations were done in another study, since some effects might not have been described accurately by the demolding energy.

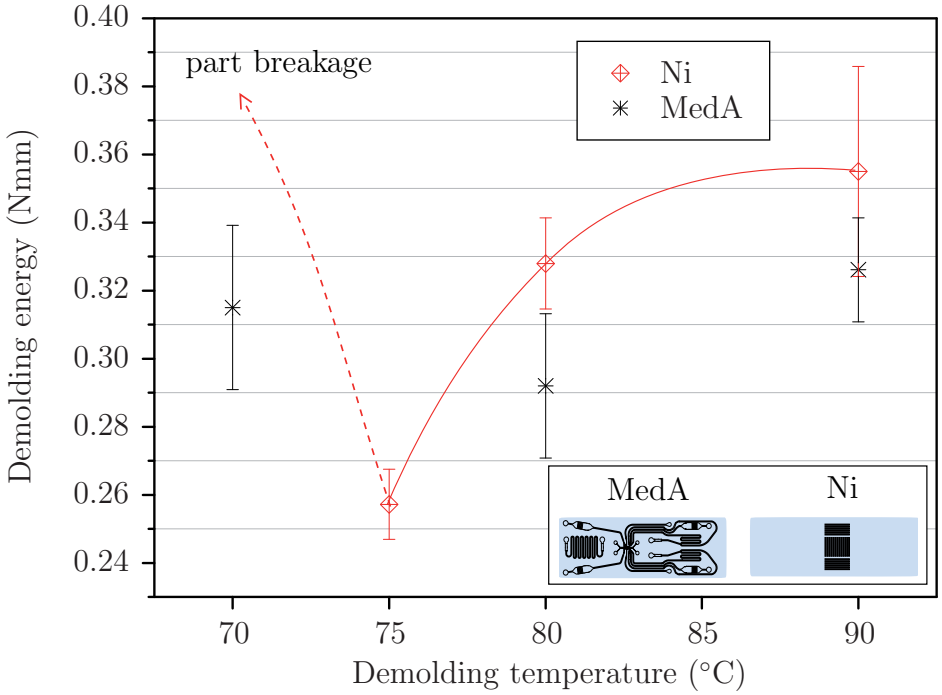

Figure 5.11. Impact of demolding temperature on demolding energies of PMMA with the medical application (MedA) and nickel testchip (Ni) stamper.

At 75 °C the lowest demolding energy for PMMA was obtained, which increased by 30 % when setting the temperature to 80 and 40 % at 90 °C. At the same time, fabricating parts at 70 °C was impossible, since the resulting forces from the demolding process caused the parts to break. This behavior

is emphasized in Figure 5.11 and corresponds to the findings of Trabadelo et al. (2008) [67], who reported minimum demolding forces at approximately 83 °C for the thermal nanoimprint process. Since they used the kink in the demolding force curve (compare Figure 3.15) their absolute values can not be compared to the demolding energies in this work. What is more, the demolding force/energy is found to depend on the demolding velocity as well. In this case the demolding velocity was lower for the injection molding process (but still faster compared to hot embossing), which results in a decrease in demolding forces.

Also, the above findings comply to the findings of Fu et al. (2008) regarding the temperature dependent demolding behavior [18], as well as the results from the tests conducted on COP and COP10TPE within this thesis. It is also interesting to note the narrow processing window for PMMA due to its rigidity. PMMA endured an increase of approximately 40 % in demolding energies before part failure, whereas demolding energies of COP increased by approximately 470 % from 60 to 90 °C with the Ni testchip stamper. The relatively low demolding energies compared to PP and COP are attributed to the specific volume of the part. On the one hand at 75 °C mold temperature the part resembles the mold and thus causes low demolding energy levels. At mold temperatures higher than that, the specific volume of the part increases and causes friction between the polymer micro-structures and the stamper. In accordance with Fu et al. (2008) this phenomenon stagnates with increasing temperature, since expansion occurs to a limited extend. Moreover, the flexibility of the polymer increases with increasing temperature, which in turn lowers the frictional forces. On the other hand at mold temperatures below 75 °C thermal contraction, shrinkage and the decrease in elasticity of the polymer cause part failure during demolding. In addition, the micro-structures act like notches on the polymer, which cause stress concentration in the notch root and consequently part failure along the micro-channels.

Moreover, the impact of variothermal process on the demolding behavior was analyzed. As the application of a variotherm system is a state-of-the-art tool for the fabrication of micro-structured devices, it is important to understand its impact on demolding energies. Equal replication quality has been determined in Section 5.3.1 already. Hence, the influence of variothermal heating on demolding energies is limited to the heat input.

Therefore, Figure 5.12 illustrates the impact of variothermal heating on the demolding energies of COP with 10 wt% TPE. From this data, it can be concluded, that the application of variothermal mold heating lowered demolding energies in a wide temperature range without altering the characteristics of the results. It is also worth noting, that the application of variothermal heating affects the demolding energies similarly for all demolding tempera-

tures.

At 40 °C for instance variothermal heating decreased the demolding energy by 30 %, at 60 °C by 33 % and at 90 °C by 30 %. This reduction occurs due to relaxation mechanisms within the polymer, which are enhanced at elevated temperatures. Since 60 °C yields the lowest demolding energies of all temperature settings for this material, the relatively high decrement as a consequence of the variothermal heating appears even more favorable. However, these findings cannot be confirmed when analyzing PMMA, where part failure was observed due to variothermal heating.

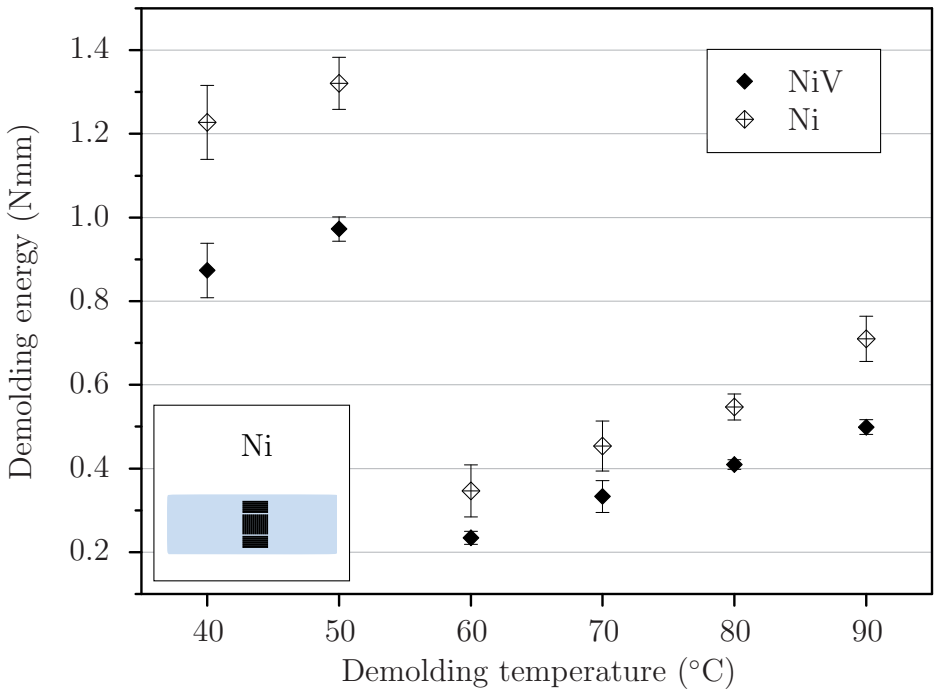

Figure 5.12. Impact of variothermal process on demolding energies of COP with 10 wt% TPE and nickel testchip (Ni).

Apart from PMMA, the same findings are made for all other polymers, except for TPE (compare Figure 5.13). As the impact of variothermal heating is determined not to be temperature dependent, the standard temperature setting is selected to compare demolding energies. PMMA can not be included, since all configurations with variothermal heating broke during the demolding stage. For PP at 40 °C T_m, COP at 80 °C and COP10TPE at 60 °C with the medical application the demolding energies decreased by approximately 30 - 50 %. In contrast to that, the demolding energy for COP40TPE decreased only by 24 %. TPE exhibited the contrary behavior, since variothermal heating increased the demolding energy by 20 %. This be-

havior is attributed to the increasing surface adhesion of TPE to the medical application due to the higher temperatures.

As stated before, for PMMA no parts with variothermal configuration could be demolded successfully. A reason for this could be the one sided application of the ceramic heating to the fixed half of the mold. Due to the thermal disequilibrium that results from this restriction, additional stresses might be induced in the polymer. With the notch effect adding to the micro-channels and the high brittleness of PMMA the maximum stresses exceeded the strength of PMMA, hence causing part failure. This behavior is also observed for COP, although it does occur in fewer occasions.

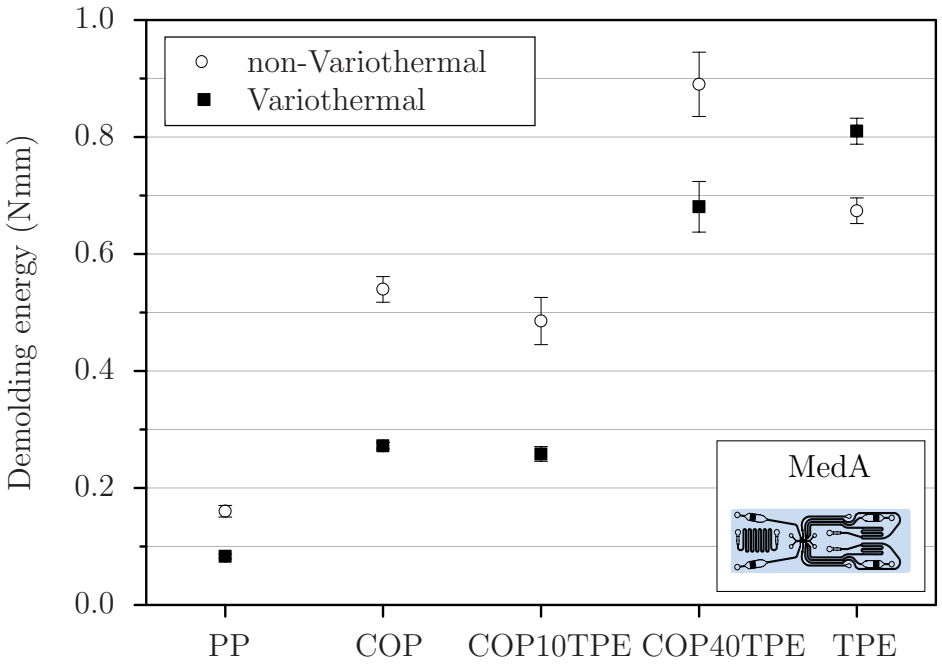

Figure 5.13. Comparison variothermal (V) and non-variothermal process on demolding energies of PP, COP, COP with 10 wt% TPE (COP10TPE), COP with 40 wt% TPE (COP40TPE) and TPE of the medical application (MedA).

5.3.4 Micro-structure design

The impact of the micro-structure design was investigated with two very simple test structures. These were arranged in two configurations, one close to and the other far from the gate. Since Heckele and Schomburg (2004) reported structure placement close to the gate to be the most favorable arrangement [32], case study 6 aimed at analyzing the impact of position relative to the gate as well as the orientation relative to the flow direction.

Thus, Figure 5.14 depicts the impact of feature orientation and placement on PP, COP, COP10TPE and COP40TPE. Due to the relaxation within the polymer as a consequence of variothermal processing, the results are chosen from the non-variothermal test runs to emphasize the results.

Some measurements have to be interpreted with care, due to occuring demolding effects that will be discussed later on. Figure 5.14 for example is lacking demolding energies of PMMA as well as the value of the demolding energy of COP for perpendicular arrangement far from the gate. These parts underwent failure during the demolding stage, which deemed demolding force measurements ineffective. However, even if a part is demolded successfully, demolding defects can occur. Or even worse, the parts experience unwanted effects like peeling off the stamper. In this case the micro-structured parts remain in contact with the micro-structures of the stamper until the measurement range is exceeded. These areas experience the highest friction and adhesion forces due to the sidewalls and the increment in surface area per projected area. This way, the measured demolding force stays below the true value and can only be identified and consequently discarded if the part showes plastic deformation after demolding.

In Figure 5.14, PP is described at 50 °C mold temperature, instead of 40 °C, as part damage occurred for one configuration (perpendicular, far from gate) at this T_m. At 50 °C parts could be fabricated successfully for all configurations. Again, PP displays the lowest overall demolding energies, due to its high elasticity and low tendency for surface adhesion to the stamper. At the same time, COP displays unexpected demolding energies because the low values at arrangements far from the gate contradict the expected behavior. Due to the failure at the configuration perpendicular to flow and far from the gate, it is concluded, that these values result from part failure rather than reflecting the material behavior for this configuration.

Another explanation for this finding could be a flaw in the evaluation based on demolding energies. As explained in Section 3.4 a peak of the demolding force was observed in other works. Since this demolding peak has not been observed for all experiments, which were conducted within this thesis, the demolding energy was chosen as a quantitative value for comparison. However, this method seems to cause adverse behavior of the demolding energy, for those polymers which show such a demolding peak. In this case, the demolding force curve might help for better understanding of the demolding behavior of COP. However, those results cannot be compared to those polymers without a demolding peak.

Additionally, COP with 10 and 40 wt% TPE was included in Figure 5.14. As for the analysis on the impact of the variothermal heating, COP10TPE complies best to the expected results. For this blend the increase in demold-

ing energy due to orientation to the flow direction and placement relative to the gate develops as anticipated. Since blending with 10 wt% TPE induces higher flexibility in COP, all configurations could be demolded and evaluated. Nevertheless, the increase in flexibility by the use of TPE seemed to be connected to the strong increment of adhesion between polymer and stamper. Another effect, which has also been discussed earlier, is again found in case study 6. For COP40TPE the content of TPE seems to lower the impact of friction on the demolding behavior. This confirms the minor impact frictional forces due to thermal stresses in this material, but proves adhesion to be more influential in this case.

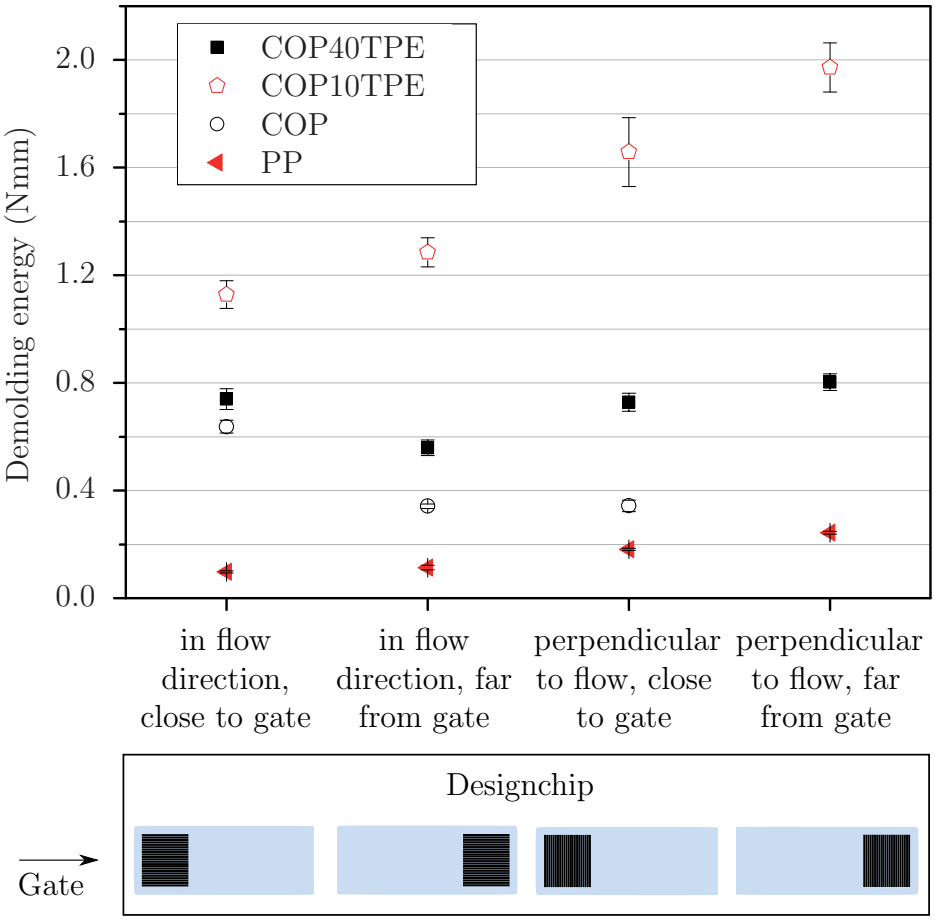

Figure 5.14. Impact of micro-structure design on demolding energies of PP (T_d=50 °C), COP (T_d=80 °C), COP with 10 wt% TPE (T_d=60 °C) and COP with 40 wt% TPE (T_d=60 °C).

5.3.5 Tool surface

At last the impact of a TiN coating in comparison to a nickel stamper was investigated. Figure 5.15 displays the influence of the nickel versus the titanium nitride surface for PP, COP and PMMA. A setting at low temperatures (40 °C for PP, 70 °C for COP and 75 °C for PMMA) and at a high level (70 °C for PP, 90 °C for COP and PMMA) were chosen for discussion. From this it is found, that at low temperatures Ni and TiN yields almost no difference when comparing the results for the same material. At high temperatures however the difference between Ni and TiN stamper grows wider, although no trend that is valid for all polymers can be deduced.

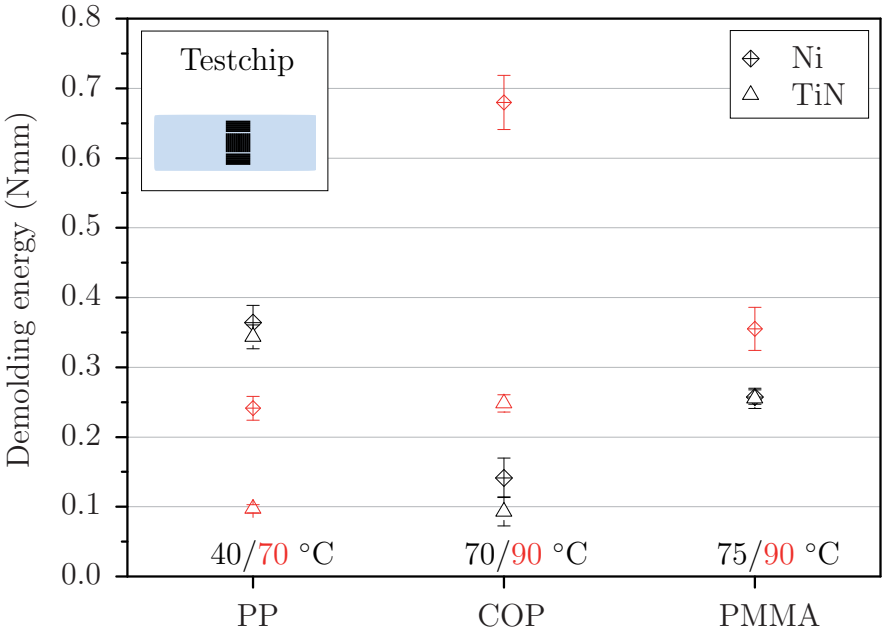

Figure 5.15. Influence of TiN coating on the demolding energies of PP, COP and PMMA at high (marked in red) and low demolding temperatures (marked in black).

Improvements by TiN are achieved for PP and COP at high demolding temperatures. Thereby, demolding energies are lowered by 150 % for PP and by 170 % for COP. Nevertheless, this decrement is only favorable for PP, as the overall demolding energies at higher temperatures are smaller than those at lower demolding temperatures. In case of COP, the decrement in demolding energies at high temperatures due to the TiN coating still exceeds the demolding energy obtained from both stampers at 70 °C. This phenomenon is attributed to the strong surface attraction of COP to Ni and also to TiN, which increases with increasing T_m. Moreover, for PMMA the TiN coating proves inefficient in the ranges studied in this work. In fact, demolding

of parts made from PMMA with the TiN coated stamper was only possible at 75 °C, where the demolding energy was lower compared to the same configuration of nickel.

At last the effect of these tool surfaces on the demolding energies of COP and COP blends was examined (compare Figure 5.16). Apart from higher levels of demolding energies in general, no trend could be deduced from this analysis either. The surfaces of COC-TPE and TiN seem to strongly attract each other, which results in equal or higher demolding energy levels for all configurations with the TiN surface. For COP40TPE and TPE higher demolding temperatures cause higher surface adhesion and thus higher demolding energy levels. As discussed in Section 5.3.2 the introduction of the TPE into the COP seems to suppress the differences of demolding energy levels, since the high elasticity of the material reduces the friction between polymer and stamper.

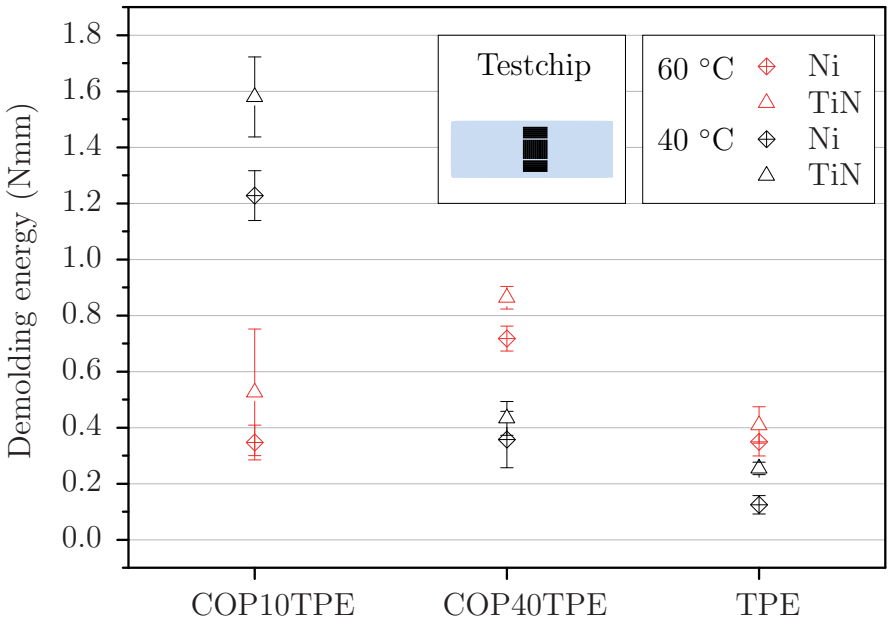

Figure 5.16. Influence of TiN coating on the demolding energies of COP with 10 wt% TPE, COP with 40 wt% TPE and TPE at high (in red) and low demolding temperatures (in black).

Due to that, it was concluded that the TiN coating is only effective if applied in a narrow temperature window, which makes it impractical for adaptations in the process. Nevertheless, TiN was proven to lower demolding forces in several reports [11, 33, 48, 64]. Therefore it is concluded, that the demolding energy is not sufficiently significant for this comparison, since some effects and differences might only be reproduced by the demolding force.

Chapter 6

Conclusion

According to a literature study and theoretical considerations regarding the demolding behavior of micro-structured devices in injection molding, the main influencing factors were grouped into four categories: polymer, machine parameters, micro-structure design and tool surface. Subsequently, a number of factors affecting the demolding energy were attributed to each of those categories and investigated to obtain their relevance. Regarding the polymer the tendency to shrink, the thermal expansion and contraction behavior, the Young's Modulus and the surface energy were selected as the main factors affecting the demolding energy. From the resulting demolding energies of PP, COP and PMMA differences can not be found from a single standard setting. On the one hand this is attributed to the temperature dependent properties of the polymer.

On the other hand it was concluded that the demolding energies were determined by the elasticity of the polymer rather than the shrinkage. However, blends with higher TPE content as well as the native COC-TPE showed contrary behavior due to the strong adhesion to the tool surface especially at higher mold temperatures. Moreover, most configurations of PMMA broke during the demolding step, due to its rigid nature, although the material displays low tendency to shrink. In addition, the shrinkage behavior deduced from the injection molding simulations yielded linear correlations between shrinkage and mold temperature, which do not correlate with the results obtained from the demolding energy measurements. Therefore, to date injection molding simulation is inefficient to predict the demolding behavior.

With regard to the machine parameters the mold temperature and variothermal heating were analyzed, due to their impact on thermal expansion and contraction, Young's modulus and thermally induced stresses as well as relaxation mechanisms. From a study on the impact of demolding temperature on demolding energies, an effect similar to the critical demolding temperature

T_{dcr} was confirmed for amorphous polymers and also for blends of COP with 10 and 40 wt% COC-TPE. The demolding behavior of amorphous polymer and the blends correlates with the expectations deduced from the literature study, whereas the demolding behavior of semi-crystalline PP displays different behavior, which requires further investigation. The COC-TPE seems to reduce the impact of temperature on the demolding energies, due to its high elasticity. When the variothermal heating is applied, the demolding energies of PP, COP and the blends were decreased by up to 50 %, due to enhanced relaxation at elevated temperatures. However, with PMMA the adverse effect was observed, since the variothermal heating induced residual stresses in the material which caused part failure during the demolding stage.

The investigation on the design of the micro-structures confirmed favorable placement close to the gate and in flow direction, although the influence was minor due to the low impact of shrinkage on the demolding energy. However, a number of demolding effects must be considered. For more rigid materials part failure occured for several configurations with micro-structure arrangement perpendicular to the flow direction. Also, a limitation in the evaluation procedure appears, as further modifications are required to adequately describe the demolding of materials with a distinct demolding peak. Additionally, more flexible materials tend to deform. As a consequence, the demolding step takes place after the range of the measurement system is exceeded and the demolding energy describes the demolding stage only partially. This means, an adaptation to the method to compare a wide range of materials with different properties (eg. Young's modulus) remains an important issue.

The efficiency of TiN coatings has been proven in other reports, it was found to lower demolding forces only in a confined temperature range compared to the Ni surface. In general, TiN is advantageous at higher temperatures, although a thorough investigation for a specific polymer-coating-combination is necessary, since the interaction between polymer and coating is strongly temperature dependent on the one hand, and dependent on the polymer on the other.

Summing up, since all relevant factors affecting demolding energies are temperature dependent, the demolding temperature is the most important influencing parameter. Therefore, a comparative study on the effect of demolding temperature on the interaction and interdependence of polymer, machine parameters and tool surface (coatings) is still lacking for better understanding of the demolding phenomenon. Hence, an improvement for the identification system of a set-up for low demolding energies, considering all influencing parameters is required.

References

[1] E. Altendorf, D. Zebert, M. Holl, A. Vannelli, C. Wu, and T. Schulte. Results obtained using a prototype microfluidics-based hematology analyzer. In D. J. Harrison and van den Berg, A., editors, *Micro Total Analysis Systems '98*, pages 73–76. Springer Netherlands, 1998.

[2] U. M. Attia. *Micro-Injection Molding of three dimensional integrated microfluidic devices*. PhD thesis, Cranfield University, 2009.

[3] H. Becker and U. Heim. Hot embossing as a method for the fabrication of polymer high aspect ratio structures. *Sensors and Actuators A: Physical*, 83(1–3):130–135, 2000.

[4] H. Becker and L. E. Locassio. Polymer microfluidic devices. *Talanta*, 56(2):267–287, 2002.

[5] M. Burgsteiner and T. Struklec. Konzepte: Konzepte zur Entformungskraftmessung von Mikrostrukturen, 2011.

[6] C.-M. Chen and C.-K. Sung. Fabricating metallic wire grating inside a polymeric substrate by insertion nanoimprint. *Microelectronic Engineering*, 87(5-8):872–875, 2010.

[7] C.-S. Chen, S.-C. Chen, W.-H. Liao, R.-D. Chien, and S.-H. Lin. Micro injection molding of a micro-fluidic platform. *International Communications in Heat and Mass Transfer*, 37(9):1290–1294, 2010.

[8] S.-C. Chen, Y. Chang, Y.-P. Chang, Y.-C. Chen, and C.-Y. Tseng. Effect of cavity surface coating on mold temperature variation and the quality of injection molded parts. *International Communications in Heat and Mass Transfer*, 36(10):1030–1035, 2009.

[9] R.-D. Chien. Hot embossing of microfluidic platform. *International Communications in Heat and Mass Transfer*, 33(5):645–653, 2006.

[10] R.-D. Chien. Micromolding of biochip devices designed with microchannels. *Sensors and Actuators A: Physical*, 128(2):238–247, 2006.

[11] L. Cunha, M. Andritschky, K. Pischow, Z. Wang, A. Zarychta, A.S Miranda, and A.M Cunha. Performance of chromium nitride and titanium nitride coatings during plastic injection moulding. *Surface and Coatings Technology*, 153(2-3):160–165, 2002.

[12] P. A. Dearnley. Low friction surfaces for plastic injection moulding dies - an experimental case study. *Wear*, 225-229:1109–1113, 1999.

[13] Y. Donggang and K. Byung. Simulation of the filling process in micro channels for polymeric materials. *Journal of Micromechanics and Microengineering*, 12(5):604, 2002.

[14] T. Eriksson and H. K. Rasmussen. The effects of polymer melt rheology on the replication of surface microstructures in isothermal moulding. *Journal of Non-Newtonian Fluid Mechanics*, 127(2-3):191–200, 2005.

[15] G. Fu, N. H. Loh, S. B. Tor, B. Y. Tay, Y. Murakoshi, and R. Maeda. Analysis of demolding in micro metal injection molding. *Microsystem Technologies*, 12(6):554–564, 2006.

[16] G. Fu, S. Tor, N. Loh, B. Tay, and D. E. Hardt. A micro powder injection molding apparatus for high aspect ratio metal micro-structure production. *Journal of Micromechanics and Microengineering*, 17(9):1803–1809, 2007.

[17] G. Fu, S. B. Tor, N. H. Loh, B. Y. Tay, and D. E. Hardt. The demolding of powder injection molded micro-structures: analysis, simulation and experiment. *Journal of Micromechanics and Microengineering*, 18(7):075024, 2008.

[18] M. W. Fu. The application of surface demoldability and moldability to side-core design in die and mold CAD. *Computer-Aided Design*, 40(5):567–575, 2008.

[19] A. Grave, T. Eriksson, and H. N. Hansen. Demouldability of microstructures in polymer moulding. *Proceedings of the 3rd International Conference on multi-material micro manufacturing*, 2007.

[20] P. Gravesen, J. Branebjerg, and Jensen O. S. Microfluidics-a review. *Journal of Micromechanics and Microengineering*, 3(4):168, 1993.

[21] J. Greener and R. Wimberger-Friedl, editors. *Precision Injection Molding*. Carl Hanser Verlag GmbH & Co. KG, München, 2006.

[22] C. A. Griffiths, S. Bigot, E. Brousseau, M. Worgull, M. Heckele, J. Nestler, and J. Auerswald. Investigation of polymer inserts as prototyping tooling for micro injection moulding. *The International Journal of Advanced Manufacturing Technology*, 47(1-4):111–123, 2010.

[23] C. A. Griffiths, S. S. Dimov, E. B. Brousseau, C. Chouquet, J. Gavillet, and S. Bigot. Micro-injection moulding: surface treatment effects on part demolding. *Multi material micro-manufacture*, Whittles Publishing Ltd., Cardiff, 2008.

[24] C. A. Griffiths, S. S. Dimov, E. B. Brousseau, C. Chouquet, J. Gavillet, and S. Bigot. Investigation of surface treatment effects in micro-injection-moulding. *The International Journal of Advanced Manufacturing Technology*, 47(1-4):99–110, 2010.

[25] C. A. Griffiths, S. S. Dimov, E. B. Brousseau, and R. T. Hoyle. The effects of tool surface quality in micro-injection moulding. *Journal of Materials Processing Technology*, 189(1-3):418–427, 2007.

[26] A. E. Guber, M. Heckele, D. Herrmann, A. Muslija, V. Saile, L. Eichhorn, T. Gietzelt, W. Hoffmann, P. C. Hauser, J. Tanyanyiwa, A. Gerlach, N. Gottschlich, and G. Knebel. Microfluidic lab-on-a-chip systems based on polymers - fabrication and application. *Chemical Engineering Journal*, 101(1-3):447–453, 2004.

[27] Y. Guo, G. Liu, Y. Xiong, and Y. Tian. Analysis of the demolding forces during hot embossing. *Microsystem Technologies*, 13(5-6):411–415, 2007.

[28] Y. Guo, G. Liu, Y. Xiong, and Y. Tian. Study of the demolding process - implications for thermal stress, adhesion and friction control. *Journal of Micromechanics and Microengineering*, 17(1):9–19, 2007.

[29] C. A. Harrington, C. Rosenow, and J. Retief. Monitoring gene expression using DNA microarrays. *Current Opinion in Microbiology*, 3(3):285–291, 2000.

[30] D. J. Harrison, K. Fluri, K. Seiler, Z. Fan, C. S. Effenhauser, and A. Manz. Micromachining a miniaturized capillary electrophoresis-based chemical analysis system on a chip. *Science*, 261(5123):895–897, 1993.

[31] S. Haubenwallner, M. Katschnig, U. Fasching, S. Patz, C. Trattnig, N. Andraschek, G Grünbacher, M. Absenger, S. Laske, C. Holzer, W. Balika, M. Wagner, and U. Schäfer. Effects of the polymeric niche on neural stem cell characteristics during primary culturing. *Journal of materials science. Materials in medicine*, 25(5):1339–1355, 2014.

[32] M. Heckele and W. K. Schomburg. Review on micro molding of thermoplastic polymers. *Journal of Micromechanics and Microengineering*, 14(3):R1, 2004.

[33] M. Heinze. Wear resistance of hard coatings in plastics processing. *Surface and Coatings Technology*, 105(1-2):38–44, 1998.

[34] H. Ito, K. Kazama, and T. Kikutani. Effects of process conditions on surface replication and higher-order structure formation in micromolding. *Macromolecular Symposia*, 249-250(1):628–634, 2007.

[35] R. W. Jaszewski, H. Schift, B. Schnyder, A. Schneuwly, and P. Gröning. The deposition of anti-adhesive ultra-thin teflon-like films and their interaction with polymers during hot embossing. *Applied Surface Science*, 143(1-4):301–308, 1999.

[36] W. Kaiser. *Kunststoffchemie für Ingenieure: von der Synthese bis zur Anwendung*. Hanser, München, 2011.

[37] H. Kawata, M. Matsue, K. Kubo, M. Yasuda, and Y. Hirai. Silicon template fabrication for imprint process with good demolding characteristics. *Microelectronic Engineering*, 86(4-6):700–704, 2009.

[38] M. Keil, M. Beck, G. Frennesson, E. Theander, E. Bolmsjö, L. Montelius, and B. Heidari. Process development and characterization of antisticking layers on nickel-based stamps designed for nanoimprint lithography. *Journal of Vacuum Science & Technology B*, 22(6):3283–3287, 2004.

[39] K. Komvopoulos and W. Yan. A fractal analysis of stiction in microelectromechanical systems. *Journal of Tribology*, 119(3):391–400, 1997.

[40] B.-K. Lee and T. H. Kwon. Development of separated micromold system for an efficient replication of high aspect ratio microstructures. *Microsystem Technologies*, 16(8-9):1385–1392, 2010.

[41] G.-B. Lee, S.-H. Chen, G.-R. Huang, W.-C. Sung, and Y.-H. Lin. Microfabricated plastic chips by hot embossing methods and their applications

for DNA separation and detection. *Sensors and Actuators B: Chemical*, 75(1–2):142–148, 2001.

[42] J. G. Lee, B.-K. Lee, T. G. Kang, and T. H. Kwon. Experimental and numerical investigation of injection molding with microrib patterns. *Polymer Engineering & Science*, 50(6):1186–1198, 2010.

[43] A. Manz, N. Graber, and Widmer H.M. Miniaturized total chemical analysis systems: A novel concept for chemical sensing. *Sensors and Actuators B: Chemical*, 1(1–6):244–248, 1990.

[44] A. Manz, D. J. Harrison, Verpoorte, E. M. J., J. C. Fettinger, A. Paulus, H. Lüdi, and H. M. Widmer. Planar chips technology for miniaturization and integration of separation techniques into monitoring systems: Capillary electrophoresis on a chip. *Journal of Chromatography A*, 593(1–2):253–258, 1992.

[45] S. Marson, U. M. Attia, G. Lucchetta, A. Wilson, J. R. Alcock, and D. M. Allen. Flatness optimization of micro-injection moulded parts: the case of a PMMA microfluidic component. *Journal of Micromechanics and Microengineering*, 21(11):115024, 2011.

[46] G. Menges, W. Michaeli, and P. Mohren, editors. *How to Make Injection Molds*. Carl Hanser Verlag GmbH & Co. KG, München, 3. Auflage, 2001.

[47] V. Miikkulainen, M. Suvanto, T. A. Pakkanen, S. Siitonen, P. Karvinen, M. Kuittinen, and H. Kisonen. Thin films of MoN, WN, and perfluorinated silane deposited from dimethylamido precursors as contamination resistant coatings on micro-injection mold inserts. *Surface and Coatings Technology*, 202(21):5103–5109, 2008.

[48] C. Mitterer, F. Holler, D. Reitberger, E. Badisch, M. Stoiber, C. Lugmaier, R. Nöbauer, T. Mueller, and R. Kullmer. Industrial application of PACVD hard coatings. *Surface and Coatings Technology*, (163-164):716–722, 2003.

[49] P. B. Monaghan, A. Manz, and W. W. Nichols. Microbiology on-a-chip. In A. Berg, W. Olthuis, and P. Bergveld, editors, *Micro Total Analysis Systems 2000*, pages 111–114. Springer Netherlands, 2000.

[50] K. Mönkkönen, J. Hietala, P. Pääkkönen, E. J. Pääkkönen, T. Kaikuranta, T. T. Pakkanen, and T. Jääskeläinten. Replication of sub-micron features using amorphous thermoplastics. *Polymer Engineering & Science*, (42):1600–1606, 2002.

[51] K. Mori, Y. Sasaki, H. Hirahara, and Y. Oishi. Development of polymer-molding-releasing metal mold surfaces with perfluorinated-group-containing polymer plating. *Journal of Applied Polymer Science*, pages 2549–2556, 2003.

[52] P. S. Nunes, P. D. Ohlsson, O. Ordeig, and J. P. Kutter. Cyclic olefin polymers: emerging materials for lab-on-a-chip applications. *Microfluidics and Nanofluidics*, 9(2-3):145–161, 2010.

[53] P. O'Leary and M. Harker. An algebraic framework for discrete basis functions in computer vision. In *Image Processing (ICVGIP)*, pages 150–157.

[54] Z. Peng, L. Gang, T. Yangchao, and T. Xuehong. The properties of demoulding of Ni and Ni-ptfe moulding inserts. *Sensors and Actuators A: Physical*, 118(2):338–341, 2005.

[55] R. Pethig, Burt, J. P. H., A. Parton, N. Rizvi, M. S. Talary, and J. A. Tame. Development of biofactory-on-a-chip technology using excimer laser micromachining. *Journal of Micromechanics and Microengineering*, 8(2):57–63, 1998.

[56] H. M. Pollock, D. Maugis, and M. Barquins. The force of adhesion between solid surfaces in contact. *Applied Physics Letters*, 33(9):798–799, 1978.

[57] A. S. Pouzada, E. C. Ferreira, and A. J. Pontes. Friction properties of moulding thermoplastics. *Polymer Testing*, 25(8):1017–1023, 2006.

[58] R. Ruprecht, G. Finnah, and V. Piotter. Microinjection molding - principles and challenges. In H. Brand, O. Brand, G. K. Fedder, C. Hierold, J. G. Korvink, O. Tabata, D. Löhe, and J. Haußelt, editors, *Microengineering of Metals and Ceramics*, pages 253–287. Wiley-VCH Verlag GmbH, 2008.

[59] W. G. Sawyer, K. D. Freudenberg, P. Bhimaraj, and L. S. Schadler. A study on the friction and wear behavior of PTFE filled with alumina nanoparticles. *Wear*, 254(5-6):573–580, 2003.

[60] W. Schinkoethe and T. Walther. Zykluszeiten verringern: Eine alternative Werkzeugtemperierung beim Mikrospritzgießen. *KU Kunststoffe*, 90(5):62–68, 2000.

[61] B. Sha, S. Dimov, C. Griffiths, and M. S. Packianather. Investigation of micro-injection moulding: Factors affecting the replication quality. *Journal of Materials Processing Technology*, 183(2-3):284–296, 2007.

[62] Z. Song, J. Choi, B. H. You, J. Lee, and S. Park. Simulation study on stress and deformation of polymeric patterns during the demolding process in thermal imprint lithography. *Journal of Vacuum Science & Technology B: Microelectronics and Nanometer Structures*, 26(2):598–605, 2008.

[63] M. Stappen, K. Vandierendonck, C. Mol, E. Beeckman, and E. de Clerq. Practice vs. laboratory tests for plastic injection molding. *Surface and Coatings Technology*, (142-144):143–145, 2001.

[64] T. Struklec. *Demolding of micro-structured surfaces in the injection molding process*. PhD thesis, Montanuniversität Leoben, Leoben, 2015.

[65] S. Takayama, J. C. McDonald, E. Ostuni, M. N. Liang, Kenis, P. J. A., R. F. Ismagilov, and G. M. Whitesides. Patterning cells and their environments using multiple laminar fluid flows in capillary networks. *Proceedings of the National Academy of Sciences*, 96(10):5545–5548, 1999.

[66] U. A. Theilade and H. N. Hansen. Surface microstructure replication in injection molding. *The International Journal of Advanced Manufacturing Technology*, 33(1-2):157–166, 2007.

[67] V. Trabadelo, H. Schift, S. Merino, S. Bellini, and J. Gobrecht. Measurement of demolding forces in full wafer thermal nanoimprint. *Microelectronic Engineering*, 85(5-6):907–909, 2008.

[68] C.-W. Tsao and D. L. DeVoe. Bonding of thermoplastic polymer microfluidics. *Microfluidics and Nanofluidics*, 6(1):1–16, 2009.

[69] Watlow. Ultramic advanced ceramic heaters, 2007.

[70] B. H. Weigl and P. Yager. Microfluidic diffusion-based separation and detection. *Science*, 283(5400):346–347, 1999.

[71] M. Worgull, M. Heckele, and W. K. Schomburg. Large-scale hot embossing. *Microsyst. Technol.*, 12(1-2):110–115, 2005.

[72] L. Yi, W. Xiaodong, and Y. Fan. Microfluidic chip made of COP (cyclo-olefin polymer) and comparison to PMMA (polymethylmethacrylate) microfluidic chip. *Journal of Materials Processing Technology*, 208(1-3):63–69, 2008.

[73] S.-H. Yoon, N.-G. Cha, J. S. Lee, J.-G. Park, D. J. Carter, J. L. Mead, and Barry, C. M. F. Effect of processing parameters, antistiction coatings, and polymer type when injection molding microfeatures. *Polymer Engineering & Science*, 50(2):411–419, 2010.